UNIVERSITY OF CALIFORNIA,
IRVINE

# Heme Enzymes: Structure – Function Relationship and Novel Applications

DISSERTATION

submitted in partial satisfaction of the requirements
for the degree of

DOCTOR OF PHILOSOPHY

in Biological Sciences

by

Vidhi C. Murarka

Dissertation Committee:
Distinguished Professor Thomas L. Poulos, Chair
Professor Celia W. Goulding
Associate Professor Katrine L. Whiteson

2023

# DEDICATION

To my parents

and

my dearest brother, Rohit,

for everything.

# TABLE OF CONTENTS

# LIST OF FIGURES

# LIST OF TABLES

# ACKNOWLEDGEMENTS

*Guru (गुरु Sanskrit)– The one who eliminates ignorance.*

I would like to acknowledge my guru, Prof. Thomas L. Poulos. He is a true mentor who understands, enlightens, supports, inspires, and instills a clear goal. His creativity, optimism, curiosity, humility, and patience are qualities to imbibe. I will always be indebted to him for giving me an opportunity of a lifetime to learn and acquire knowledge from him and to make me a better scientist/person.

Prof. Celia Goulding, thank you for your constant support and guidance, especially, during the first half of 2022. Prof. Katrine Whiteson, thank you for your microbiology expertise, encouragement, and kind words. I am grateful to the rest of my advancement committee – Profs. Mike Green and Elizabeth Bess, for their scientific inputs.

Dr. Huiying Li, thank you for patiently teaching me all about X-ray crystallography and NOS. Dr. Irina Sevrioukova, you taught me all the tricks of the P450 trade and imparted your insightful biochemistry knowledge. You both are the true pillars of the Poulos lab, and I'll be ever grateful to you both.

Special mention to Dipanwita Batabyal for the rigorous lab techniques boot-camp when I joined the lab. I'll be grateful to you for teaching me how to handle the ITC instrument delicately and efficiently. José Amaya, thank you for teaching me the stopped-flow instrument, and letting me collaborate on few of your projects. It was a great learning experience.

I would like to acknowledge my collaborators, Prof. Richard Silverman from Northwestern University and Prof. David Lamb from Swansea University, UK.

To my hardworking undergrads – Jenny Kim, Penghao Song, Xiaoping Zhao and Hugo Mendez, your dedication to research was pivotal and it helped me become a better mentor each day. To my graduate school friends, Oanh Tran and Jacob Wolff, graduate school wouldn't have been the same without you both.

My parents, you both are my backbone. Thank you for always being the wind under my wings. Rohit, there are no words to describe the kind of support you have provided throughout my life, especially in California. You are truly my guardian. Thank you for investing a good part of your 20s on me. Shubham, thank you for being my cheerleader and for providing your constant support.

The text of chapter 4 of this dissertation is a reprint of the material as it appears in Murarka, V. C.; Batabyal, D.; Amaya, J. A.; Sevrioukova, I. F.; Poulos, T. L., Unexpected differences between two closely related bacterial P450 camphor monooxygenases, *Biochemistry* **2020,** *59* (29), 2743-2750, used with permission from American Chemical Society. The research was financially supported by National Institutes of Health (NIH) grant GM131920 (to T.L.P). Finally, I would like to acknowledge beamline staff at Stanford Synchrotron and Radiation Laboratory (SSRL) and Advanced Light Source (ALS) for assistance during X-ray diffraction data collections.

# VITA
# Vidhi C. Murarka

## EDUCATION

Ph.D., Biological Sciences — December 2023
University of California, Irvine
Advisor: Distinguished Professor Thomas L. Poulos

M.S., Biotechnology — June 2019
University of California, Irvine

B.S., Pharmacy — May 2017
Institute of Chemical Technology, Mumbai, India

## PUBLICATIONS

1. Amaya JA, Lamb DC, Kelly SL, Caffrey P, Murarka VC, Poulos TL. Structural analysis of P450 AmphL from *Streptomyces nodosus* provides insights into substrate selectivity of polyene macrolide antibiotic biosynthetic P450s. *Journal of Biological Chemistry*. 2022 Apr 1; 298(4).
2. Poulos TL, Kim JS, Murarka VC. Computational analysis of the tryptophan cation radical energetics in peroxidase Compound I. *JBIC Journal of Biological Inorganic Chemistry*. 2022 Mar; 27(2):229-37.
3. Pant T, Murarka V, Jain R, Dandekar P. Chitosan based microcarriers for cellular growth and biologics production. *Carbohydrate Polymer Technologies and Applications*. 2021 Dec 25; 2:100154.
4. Murarka VC, Batabyal D, Amaya JA, Sevrioukova IF, Poulos TL. Unexpected differences between two closely related bacterial P450 camphor monooxygenases. *Biochemistry*. 2020 Jun 17; 59(29):2743-50.

## AWARDS

Krishna and Sujata Tewari Scholar Award — 2022
University of California, Irvine

Graduate Fellowship — 2018
University of California, Irvine

Mrs. Kamala Krishnan Award — 2018
Institute of Chemical Technology, Mumbai, India

Dr. T. N. Vasudevan Pharmacognosy Award — 2018
Institute of Chemical Technology, Mumbai, India

Sir Ratan Tata Scholarship — 2015, 2016, 2017
Institute of Chemical Technology, Mumbai, India

RESEARCH EXPERIENCE

Graduate Student Researcher, Poulos lab April 2018 – December 2023
University of California, Irvine
-Bacterial Nitric Oxide Synthase: A Target for Drug-Resistant Bacteria
Screened various small molecules to determine inhibition of nitric oxide synthase *via* biochemistry and X-ray crystallography.

-Structural And Functional Analysis of Cytochrome P450 In Natural Product Biosynthesis
Characterized cytochrome P450s involved in natural product biosynthesis to understand their regio- and stereo- selective chemistry using X-ray crystallography.

-Structural And Functional Analysis of Closely Related Cytochrome P450 Camphor Monooxygenases
Optimized expression and purification of cytochrome P450 and ferredoxin partner. Characterized them using UV-visible spectrophotometer, stopped-flow kinetics, ITC, and X-ray crystallography.

Undergraduate Researcher, Dr. Ratnesh D. Jain lab July 2016 – May 2017
Institute of Chemical Technology, Mumbai, India
Developed and optimized protocol to synthesize chitosan based microcarriers to enhance cellular growth and biologics production.

Summer Intern June 2016
Ajanta Pharma Ltd., Mumbai, India
Developed solid dosage forms. Carried out stability testing and quality analysis to check the product's compliance with ICH guidelines.

Undergraduate Researcher, Prof. Purnima D. Amin lab July 2015 – May 2016
Institute of Chemical Technology, Mumbai, India
Conducted a detailed literature review on diverse solubility & dissolution techniques of BCS Class II drugs.

TECHNICAL SKILLS

Molecular Biology – Primer design, sub-cloning, site-directed mutagenesis, polymerase chain reaction (PCR), agarose gel electrophoresis.

Recombinant Protein Expression – Optimized heterologous protein expression in *E. coli* BL21(DE3) and C41(DE3) cells.

Protein Purification – Developed protocols to purify proteins using techniques such as affinity, ion exchange, hydrophobic interaction, and size exclusion chromatography (using FPLC GE ÄKTA and Bio-Rad systems). SDS-PAGE gel electrophoresis and Western blot analysis.

X-Ray Crystallography – Sample preparation, high-throughput protein crystallization screening using SPTLabTech Mosquito, hanging drop and sitting drop vapor diffusion optimization tray

setup. Synchrotron data collection, X-ray data processing, refinement, structure solution using molecular replacement for phasing.

Biochemistry, Enzymology, and Proteomics – Protein-ligand, protein-protein interaction/ binding affinity using isothermal titration calorimeter (ITC), UV-vis and fluorescence spectrophotometer. Enzyme inhibition assay, steady-state kinetics, stopped-flow enzyme kinetics. Mass spectrometry techniques such as GC-MS, LC-MS-MS and MALDI-TOF.

CONFERENCE PRESENTATIONS

1. Cytochrome P450AmphL: Structural analysis and insights into its substrate selectivity.
   International Conference on Cytochrome P450, Washington D.C., July 2022
   [talk and poster presentation]
2. How can two structurally similar cytochrome P450s behave differently?
   24th West Coast Structural Biology Workshop, Monterey, CA, March 2019
   [talk and poster presentation]

RELEVANT EXPERIENCES

1. Graduate Teaching Assistant
   University of California, Irvine

| | |
|---|---|
| Biotechnology lab – Nucleic Acid | Fall 2018 |
| Biotechnology lab – Proteins | Winter 2019 |
| Biochemistry lecture | Winter 2019 |
| Biotechnology Management lab | Spring 2019 |
| Molecular Biology lab | Fall 2019 |
| Protein Structure and Function lecture | Fall 2019 |
| Biochemistry lecture | Winter 2020 |
| Microbiology lab | Winter 2020 |

2. Environmental Health and Safety Officer, Poulos lab — January 2020 – December 2023
   University of California, Irvine

3. Student Assistant Supervisor – Evening Proctor — February 2018 – June 2018
   Disability Services Center
   University of California, Irvine

# ABSTRACT OF THE DISSERTATION

Heme Enzymes: Structure – Function Relationship and Novel Applications

By

Vidhi C. Murarka

Doctor of Philosophy in Biological Sciences

University of California, Irvine, 2023

Distinguished Professor Thomas L. Poulos, Chair

Heme enzymes are ubiquitous in nature with several biological functions encompassing cytoprotection, neuronal signaling, biosynthesis of natural products and xenobiotic detoxification. This unique functionality of each heme enzyme is because of its structure. Thus, the aim of this dissertation is to probe structure-function relationships of these enzymes, understand the active site chemistry and employ this information for pharmaceutical applications. This is achieved by studying two different heme enzyme systems – nitric oxide synthase (NOS) and a few cytochromes P450.

NOS is involved in the production of NO which provides antibiotic resistance to various Gram-positive bacteria (bNOS) like methicillin-resistant *Staphylococcus aureus* (MRSA) and acts as a signaling molecule in mammals (mNOS). Inhibition of bNOS decreases NO and makes MRSA more susceptible to antibiotics and host-induced oxidative stress. A collaborative work to design efficient and bNOS selective small molecules to treat MRSA infection is described here.

Various natural products have antibiotic properties and require cytochromes P450 for their biosynthesis. The aim is to structurally and functionally characterize two P450s from *Streptomyces* involved in biosynthesis of antibiotics. This will help to understand protein-substrate interactions

involved in the biosynthesis of these antibiotics. Eventually, this will assist in engineering enzymes to generate novel antibiotics with greater efficacy and specificity.

P450cam (CYP101A1) is one of the most studied P450s and consumes camphor as a source of carbon/energy. This dissertation concludes with a study to better understand structural and functional aspects of another camphor degrading P450 from *Pseudomonas* sp. strain TCU-HL1 which shares about 86% sequence identity with P450cam.

# INTRODUCTION

## 1.1 INTRODUCTION TO HEME ENZYMES

Iron protoporphyrin IX, commonly known as heme, is one of the most profusely used metalloporphyrin in the ecosystem (Gaia). Heme containing enzymes are famously known for their myriad diverse functions, especially in the transport and storage of $O_2$ by the globins, electron transport by cytochrome c, and oxygenase activity of cytochrome P450s and nitric oxide synthases (NOS)[1]. This diversity in functionality by the same cofactor highlights the importance of structure-function of heme enzymes. Thus, it is important to understand the subtle changes in the heme environment that lead to different outputs. This dissertation centers around understanding the structural and functional relationship of two heme enzyme systems: NOS and cytochrome P450s.

## 1.2 NITRIC OXIDE SYNTHASE

Nitric oxide (NO) is a small, lipophilic, highly reactive, free radical gas. Its paramagnetic nature causes it to covalently or non-covalently interact with protein and non-protein targets to induce various biological effects.[2, 3] NO binds to heme iron with a high binding affinity and forms nitrosyl-heme adducts.[2] It irreversibly binds to the heme of guanyl cyclase[4] activating the conversion of magnesium guanosine 5'-triphosphate (GTP) to cyclic guanosine 3',5'- monophosphate (cGMP)[2, 5] thus, causing signal transduction.[5, 6]

NO is produced either by chemical reduction of $NO_2^-$ or by NOS and diffuses to the target site in surrounding cells.[5] NOS is a heme-thiolate enzyme and converts L-arginine and $O_2$ to NO and L-

citrulline (Figure I.1).[1] It requires NADPH, a reduced pterin co-factor and redox partners to enable catalysis.

NOS is hailed as a foster child of cytochrome P450 family because it has quite a resemblance with P450s.[7] It displays the characteristic 450 nm absorption spectra of P450s upon reduction and CO binding, carry out similar chemistries with the help of heme-thiol group, and requires redox partners to transfer electrons from NAD(P)H to the heme active site.[7]

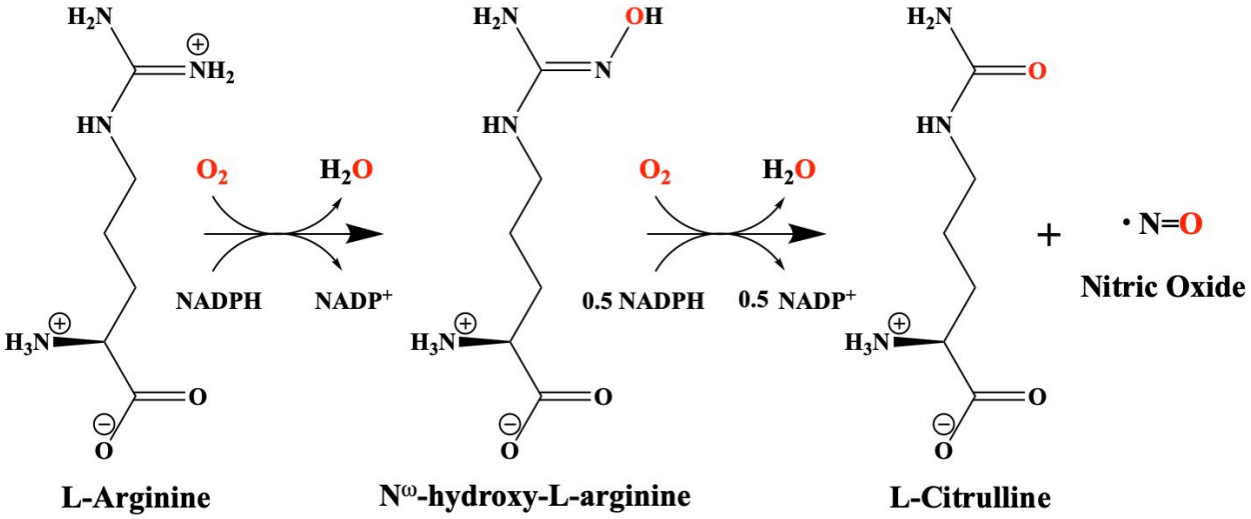


**Figure I.1** NOS catalyzed two-step oxidation of L-arginine to form L-citrulline and nitric oxide *via* an intermediate Nω-hydroxyl-L-arginine (L-NHA).

### *Biological Function*

Even though NO is extensively produced by several organisms, NOS is found only in finite species such as bacteria,[8] myxomycetes[9] and the animal kingdom.[1, 10] In mammals, three different NOS isoforms are expressed in different tissues. Two of them are constitutive: neuronal NOS (nNOS, NOS1), endothelial NOS (eNOS, NOS3), and a third is an inducible NOS (iNOS, NOS2).

nNOS, expressed in central and peripheral neurons, is involved in synaptic plasticity and neuronal signaling in the central nervous system (CNS).[11, 12] It centrally regulates blood pressure, blood vasodilation *via* peripheral nitrergic nerves and smooth muscle relaxation.[11, 12] eNOS produces NO

in vascular endothelial cells and controls blood pressure by promoting vasodilation.[11, 12] It also has vasoprotective and anti-atherosclerotic effects.[11, 12] iNOS is expressed in most nucleated cells and produces NO as a response to cytokines, lipopolysaccharide, or other agents.[11, 12] NO has cytotoxic or cytostatic effect on invading pathogens (including viruses)[13] or cancer cells.[11, 12, 14] It also adds to the pathophysiology of septic shock and inflammatory diseases.[11, 12]

Abnormal functioning of any of the above three NOS isoforms has an adverse effect on normal functioning of the body. Overproduction of NO by nNOS is associated with several neurodegenerative disorders like multiple sclerosis, amyotrophic lateral sclerosis, stroke, Alzheimer's, and Parkinson's disease.[11] Defective eNOS contributes to several vascular diseases such as hypertension, atherosclerosis, and ischemic heart disease to name a few.[12] Overexpression of iNOS is not only toxic to invading pathogens and tumor cells but also harms healthy cells when released at the wrong site.[11] Additionally, it has been linked to tumor promoting effects.[14]

NO produced by NOS is present in a few Gram-positive bacteria. The biological function of NO differs for each bacterial organism. It nitrosylates macromolecules to modulate them,[15, 16] acts as a commensal molecule,[17] provides protection against oxidative stress,[18] and detoxifies antimicrobials.[19] NO acts as a cytoprotective agent in two bacterial species that are of particular interest to human health– *Staphylococcus aureus* and *Bacillus anthracis*.[19, 20]

Methicillin-resistant *Staphylococcus aureus* (MRSA) is a potent pathogen and causes thousands of deaths each year.[21] NO from bacterial NOS (bNOS) has several different roles in MRSA. It protects the bacteria against oxidative and antibiotic induced stress (Figure I.2) by suppression of damaging Fenton chemistry, direct activation of catalase, and induction of superoxide dismutase expression.[19] It also causes direct chemical modification of antibiotics or toxins leading to their detoxification.[19]

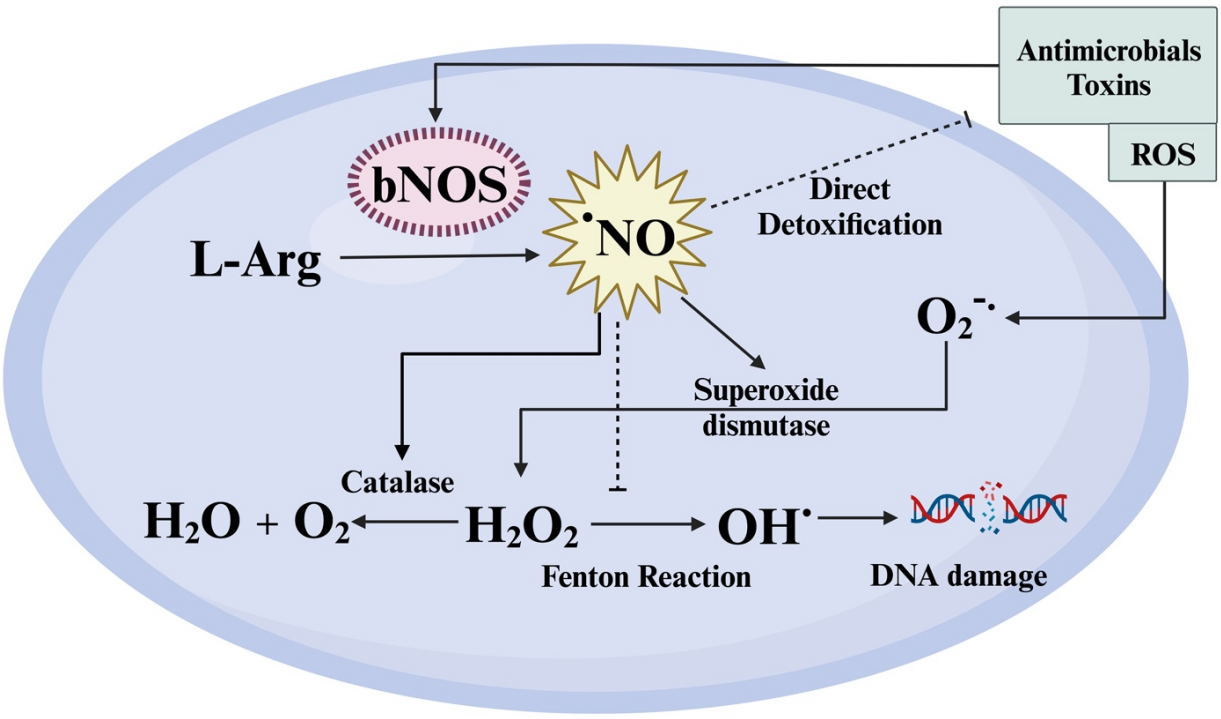


**Figure I.2** Defense mechanism of bNOS generated NO against oxidative stress and antibiotic/ toxin induced stress in MRSA. It achieves it by - (a) direct chemical modification of antibiotics or toxins leading detoxification of them and (b) decreasing oxidative stress by induction of superoxide dismutase, activation of catalase and suppression of Fenton chemistry. I believe this catalase activation is nonsense, but it has been published. (Figure created with BioRender.com)

NO along with NO metabolizing flavohemoprotein (hmp) is essential for MRSA colonization of the mammalian host.[22] Under micro- and anaerobic conditions, NO reversibly binds to heme-containing cytochrome oxidases $aa_3$ and bd and inhibits aerobic respiration (Figure I.3). Additionally, generation and consumption of NO by bNOS and Hmp, respectively, are oxygen dependent. This regulates the electron transfer depending on oxygen availability and ultimately maintains the membrane potential.[22] This also gears MRSA to be resistant to membrane-targeting antibiotics like daptomycin.[22]

All these data suggest that bNOS inhibition will weaken the bacteria to survive against antibiotics and host induced oxidative stress. Therefore, bNOS is a potential druggable target for treatment of a life-threatening infection. The major challenge is to target bNOS without inhibiting mNOS

(all mammalian isoforms). So, specific bNOS inhibitors are required to overcome these limitations. To achieve this, we need to understand the structure of bNOS and all isoforms of mNOS.

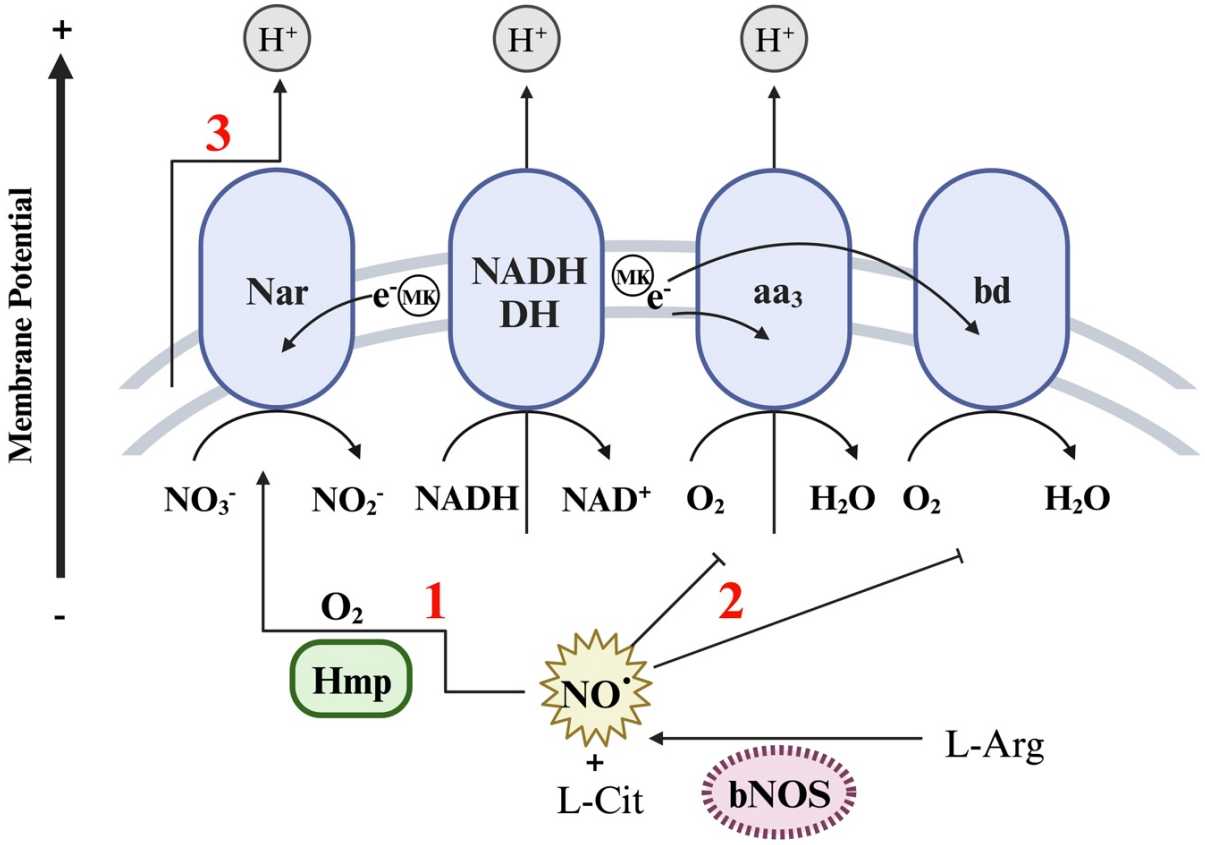


**Figure I.3** bNOS along with Hmp maintains membrane potential in MRSA under microaerobic conditions. Consumption of NO by Hmp (1) increases with an increase in $O_2$ availability. This causes NO levels inversely proportional to $O_2$ availability. Under microaerobic conditions, consumption of NO by Hmp decreases (1). NO reversibly binds to cytochrome oxidase $aa_3$ and bd and inhibits them (2). This diverts electrons from menaquinone (MK) pool to the nitrate reductase (Nar) complex (3) which reduces nitrate to nitrite and maintains the membrane potential. Adapted from Kinkel et al.[22] (Figure created with BioRender.com)

### *Structure of NOS*

Like in the P450s, the heme is axially coordinated to a cysteine residue.[1] In the resting state, the sixth coordination position is either empty or coordinated by a feebly bound aqua ligand.[23] NOS is a homodimer with the heme surrounded by beta structures whereas the P450s are defined by helices.[1] The heme is more solvent exposed with the substrate access channel extending from the

active site to the dimer interface.[23] This allows the substrate to easily enter the active site and NO to diffuse out.[1] The substrate, L-arginine, binds above the heme and H-bonds with guanidinium group and a conserved glutamate to stabilize the binding.[1]

At the dimer interface, a second pterin co-factor binding pocket is formed. The co-factor that binds in this pocket in mNOS is identified as (6*R*)-5,6,7,8-tetrahydrobiopterin ($H_4B$). $H_4B$ is permanently bound in the pterin pocket (Figure 1.4) and acts as an electron donor during catalysis.[1, 23] The identity of this cofactor in bNOS is yet to be established because bacteria[23] lack the biosynthetic machinery required to synthesize $H_4B$. Current findings show pterin tetrahydrofolate suitable for bNOS activity.[24]

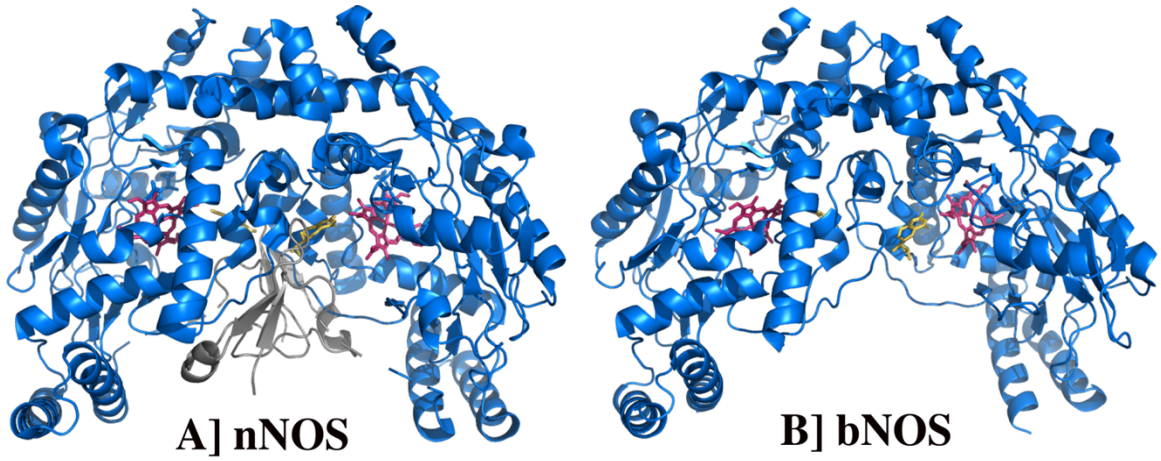


**Figure I.4** Comparison of oxygenase domains of A] rat nNOS with $Zn^{2+}$ binding motif in gray (PDB: 2G6K), and B] *B. subtilis* bNOS (PDB: 2FC1). Heme (red) and $H_4B$ (yellow).

mNOS isoforms dimers are formed of two long polypeptides with multiple domains. Each polypeptide contains a heme-containing oxygenase domain, a reductase domain comprised of FAD and FMN binding sites, and a calmodulin binding domain linking the two domains.[23, 25] As mentioned earlier, the dimer interface contains the pterin binding pocket and also a $Zn^{2+}$ binding motif which binds $Zn^{2+}$ and helps facilitate the dimerization (Figure I.4).[25-27]

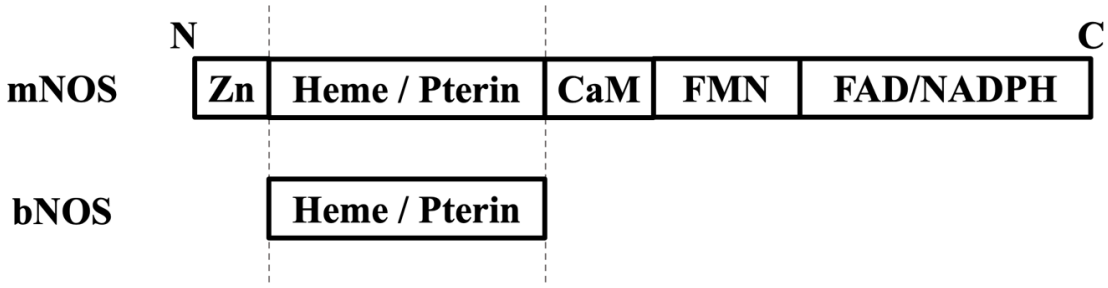


**Figure I.5** mNOS and bNOS protein architecture. mNOS consists of an oxygenase and a reductase domain. On the contrary, bNOS consists only of the oxygenase domain. CaM – calmodulin binding domain, Zn – $Zn^{2+}$ binding motif.

Regardless of structural similarities between mNOS and bNOS, bNOS is unique and contains only the oxygenase domain (Figure I.5) and depends on redox active enzymes to acquire electrons.[25] It lacks and doesn't require the calmodulin binding domain for its activity. The $Zn^{2+}$ binding domain is absent as well.[23, 25, 28, 29] Upon a closer investigation of the active site shows conservation of key residues. This suggests that NO is produced *via* the same mechanism.[25, 28]

### *NOS mechanism*

NOS produces NO by a two-step process.[30] The first step coverts L-arginine to $N^{\omega}$-hydroxy-L-arginine (L-NHA)[31], an enzyme-bound intermediate, and proceeds like a traditional P450 reaction.[32] The second step, oxidation of L-NHA to L-citrulline and NO, is more complex. Two main mechanisms have been proposed and the more plausible one is described in Figure I.6. It starts with $H_4B$ donating an electron[33] and reducing the oxycomplex[34] to peroxy species.[33] Nucleophilic attack of peroxy species on L-NHA forms a cyclic intermediate.[35] The proximal oxygen of this intermediate, abstracts a proton from the nitrogen atom of L-NHA and collapses to give $NO^-$ and L-citrulline.[35] Finally, $NO^-$ reduces the cationic $H_4B$ radical to give $H_4B$ and NO.[33, 35]

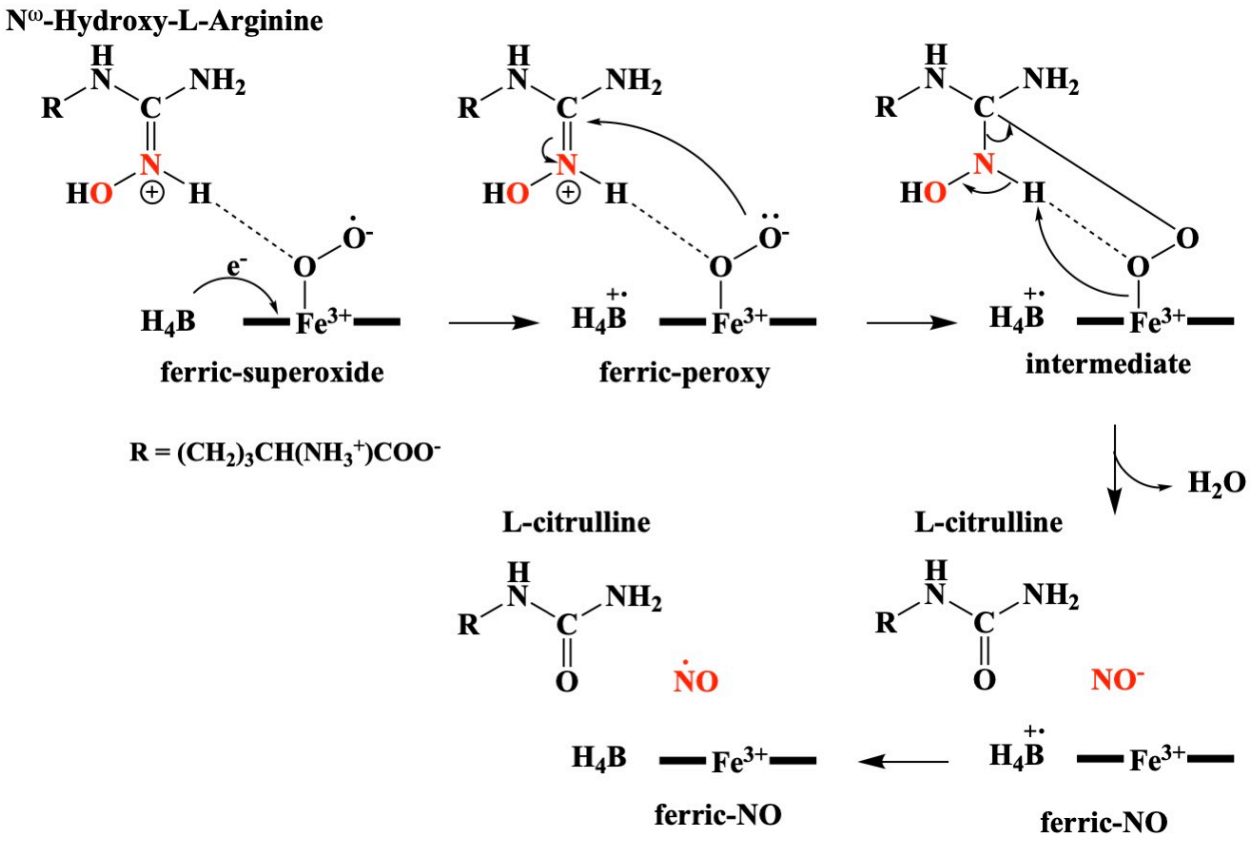


**Figure I.6** Proposed mechanism of conversion of L-NHA to L-citrulline and NO.

### *NOS inhibitors*

The aim is to design and develop bNOS selective inhibitors which requires taking advantage of subtle structural differences from mNOS isoforms. As mentioned earlier, bNOS lacks the $Zn^{2+}$ binding motif which makes the pterin binding pocket more solvent exposed.[25] This decreases the pterin binding affinity to the pterin pocket and results in a large cavity right next to the bNOS active site.[25] Another key difference is the presence of an Asn in bNOS compared to Asp in nNOS.[36] This leads to key electrostatic differences in the active site. Unfortunately, this residue in eNOS also is Asn.[36] So, designing inhibitors only to target this feature can be challenging. An ideal inhibitor would be the one which combines and exploits the above two differences at the same time.

Previous studies from our lab yielded two chemical moieties, aminoquinoline[37] and aminopyridine,[36] that bind to the active and the pterin site by displacing the pterin cofactor.[36] These molecules were shown to be bNOS selective. Based on this information, our collaborators, the Silverman lab at Northwestern University, designed compounds with these two moieties connected with a flexible linker to bind to both sites. These compounds were screened using X-ray crystallography and biochemical studies to understand their selectivity.

## 1.3 CYTOCHROME P450

Cytochromes P450 form a superfamily of heme-thiolate enzymes that are prevalent in all biological kingdoms, including humans, animals, plants, protists, fungi, archaea, bacteria, and viruses.[1, 38, 39] P450s play a key role in drug metabolism, xenobiotic detoxification, and natural product biosynthesis.[1, 38] P450s were first discovered in the early 1950s and display a distinct absorption spectrum at 450 nm upon CO binding to ferrous heme.[6, 40-42] Hence, the name P450 (P = pigment).[6] P450s are famously known as monooxygenases, for insertion of one oxygen atom from $O_2$ into an unactivated C-H hydrocarbon bond to give the corresponding alcohol. The typical hydroxylation reaction is shown in equation (1)

$$R - H + O_2 + 2H^+ + 2e^- \rightarrow R - OH + H_2O \ldots (1)$$

### *Classification of Cytochrome P450*

Evident from equation (1), two electrons are required for the completion of the reaction.[38] NAD(P)H supplies these electrons *via* redox active protein partners.[1, 38] The P450 redox systems are classified into two main classes: class I and II.[1] The bacterial and mitochondrial soluble P450s form class I, and class II comprise of eukaryotic microsomal membrane bound P450s. Class I is a

three-component system where electrons are transferred from NAD(P)H → FAD reductase → [2Fe-2S] ferredoxin → P450. While class II is a two- component system, and the electrons are transferred from NAD(P)H → FAD-FMN containing reductase → P450. There are a few exceptions to this classification, like $P450_{BM3}$ from Gram-positive *Bacillus megaterium*[43] and $P450_{RhF}$ from *Rhodococcus* sp.,[44] in which all the redox active components are fused into a multi-domain single polypeptide chain.

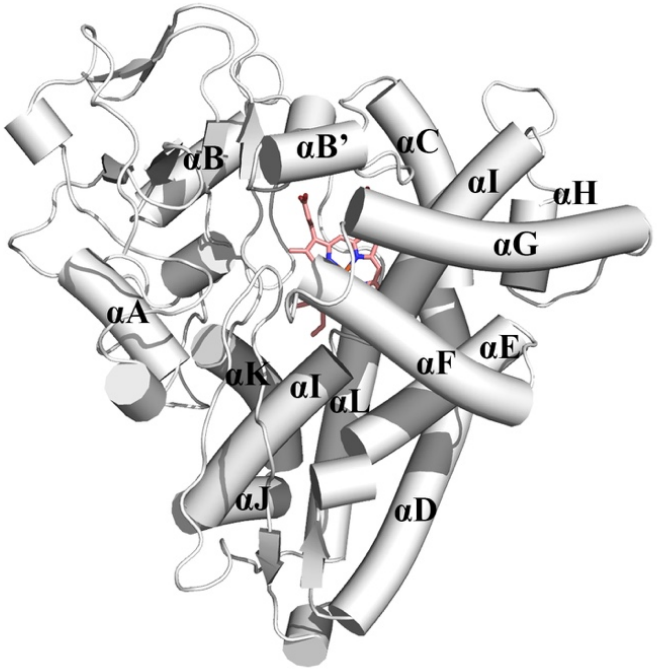


**Figure I.7** Structure of cytochrome P450 displaying the tradition triangular P450-fold (PDB: 5CP4). The α-helices (cylinders) are labeled alphabetically according to the naming tradition.

### *Structure of Cytochrome P450*

Up until now, all P450s exhibit a highly conserved triangular P450 fold (Figure I.7) and are generally between 40-50 kDa in size.[1] On comparison with soluble P450s, membrane-bound P450s contain a non-polar N-terminal tail as an anchor to the membrane but the removal of this N-terminal has an insignificant effect on the core structure.[1] As a consequence of the conserved

structure, an alphabetical nomenclature is adopted by the P450 community to describe the secondary structures of P450 (Figure I.7).[45]

Right above the heme surface, runs a very long I helix which contains residues that interact with substrate and dioxygen.[45] The proximal side of heme has an axially ligating conserved cysteine residue that is situated at the beginning of L helix. The local structure around the cysteine ligand is highly conserved and contributes to the sulfur's electron donating character.[46] This in-turn modulates the iron redox potential to perform P450-type chemistry.[46]

P450s are dynamic and exhibit two extreme structural forms: substrate-free (open) and substrate-bound (closed). The F and G helices and the connecting FG loop display a large movement between the two open and closed forms and regulates the access of substrate to the active site.[1, 47, 48] This motion is essential in introducing structural changes that are necessary for initiation of P450 catalytic cycle.[47, 48]

### *Cytochrome P450 mechanism*

A generalized P450 reaction mechanism is illustrated in Figure I.8. It begins with the enzyme in the resting state with heme iron in low-spin ($S$=1/2), hexacoordinate state.[49] A water is bound to the heme iron in the sixth axial position. This water molecule along with others occupying the active site pocket are displaced when the substrate binds in the active site. The heme iron shifts to a high-spin ($S$=5/2) pentacoordinate state[49] and results in an increase in its redox potential.[50] This permits the electron transfer from NAD(P)H *via* redox partner protein(s) only to the substrate bound enzyme.[51] This enables reduction of the heme ferric to ferrous, and enables $O_2$ to bind and form the oxy-complex (ferric-superoxide/superoxo).[52] The next step is a proton coupled electron transfer, where the electron transfer event produces the peroxy intermediate and upon protonation

forms the hydroperoxy complex (compound 0).[52] Additional protonation forms a dihydroperoxy complex which undergoes heterolytic cleavage of the O-O bond. This results in the loss of a water molecule and formation of compound I, the active hydroxylating agent.[53] This is followed by hydrogen atom abstraction from the substrate and formation of a substrate radical and compound II.[54] The substrate radical combines with the hydroxyl of compound II and forms hydroxylated substrate (or product). The newly formed molecule is released, water coordinates to the heme and restores the enzyme to the resting state.[52]

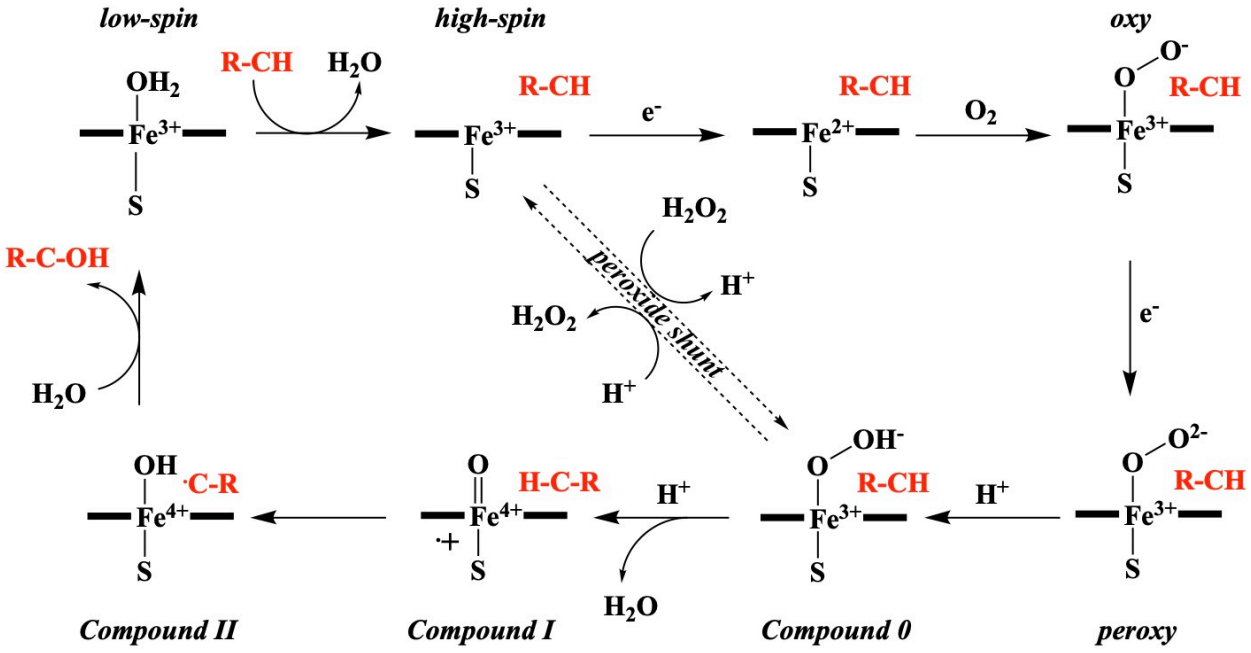


**Figure I.8** Cytochrome P450 reaction mechanism.

### *Cytochrome P450 in natural product synthesis*

Natural products are an assortment of small molecules with a conspicuously broad variety of biological activities.[55] To date, these still remain the best wellspring for new drug or lead molecules and molecular probes to understand biological functions.[55-57] They are structurally and chemically complex molecules built from simple building blocks by an array of enzymes in Nature. Multiple

methods can be used to accomplish the biosynthesis of these complex molecules, but the mainstream way is the construction of an inert scaffold accompanied by a chain of reactions that functionalize the molecule. The newly added groups serve a variety of chemical properties necessary for target interaction, substrate recognition, or linkers for other moieties to name a few.[58] Among all the enzymes, P450s are the most exploited to functionalize unactive C-H bonds of the scaffold, a crucial reaction to produce biologically active natural products. Due to the complexity and variety of natural product structures, P450s involved in natural product biosynthetic pathways exhibit diversity in sequence, structure, function, and mechanism.[58] This opens up a whole new aspect of biotechnological applications of P450s in natural product biosynthesis.

### *Cytochrome P450 in Streptomyces*

Actinomycetes are a marvelous reservoir of bioactive natural products of pharmaceutical importance.[59] Among them, *Streptomyces* are a source of two-thirds of clinically relevant molecules, especially antibiotics.[60] Therefore, *Streptomyces* maintain a remarkable number of P450s with catalytically unique and efficient functions. About 184 functionally characterized P450s of *Streptomyces* origin are tabulated by Rudolph et al.[58]

Many P450s from *Streptomyces* show flexibility in accepting electrons from non-native redox partners.[58] They easily accept redox partners from other *Streptomyces* species,[61-63] [2Fe-2S] binding putidaredoxin (Pdx) and FAD binding putidaredoxin reductase (PdR) from the P450cam system,[64] flavodoxin and flavodoxin reductase from *E. coli*,[65, 66] as well as commercially available spinach ferredoxins.[67, 68] Fusion of *Streptomyces* P450 with the reductase domain of CYP102D1[69] or $P450_{RhF}$[70] to form a self-sufficient P450 were successful as well. Few P450s are able to turnover upon addition of $H_2O_2$ *via* the peroxide shunt pathway in the P450 catalytic cycle.[67] All this makes

P450s from *Streptomyces* very capable and qualify them to be great biocatalysts.[58] Understanding the structure-function relationship of these P450s along with substrate interactions and chemistry would help us engineer biocatalysts to create new molecules with better efficacy and lower toxicity. In collaboration with Prof. David Lamb from Swansea University, UK, and Dr. Patrick Caffrey from University College Dublin, Ireland, we studied two P450s from *Streptomyces* involved in production of nystatin and a newfound, oxyskyllamycin A.

### *CYP101A1 (P450cam)*

Among all the P450s, the most studied is a soluble P450 from *Pseudomonas putida* named P450cam (CYP101A1)[71]. It is the first P450 to be sequenced,[72, 73] crystallized,[45] and biochemically characterized.[71]

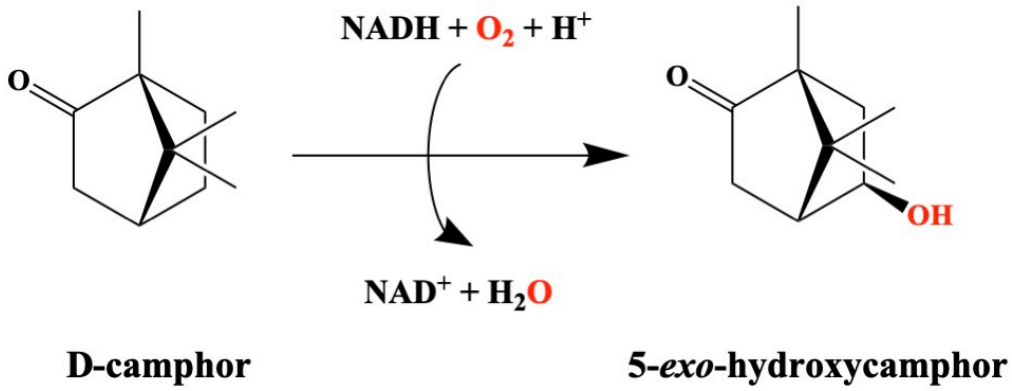


**Figure I.9** P450cam hydroxylation reaction.

It is responsible for regio- and stereo-selective hydroxylation of camphor to 5-*exo*-hydroxycamphor (Figure I.9), to assimilate camphor as a sole carbon source.[71] P450cam belongs to class I type of P450s and utilizes two redox active partner to transfer electrons - Pdx and PdR.[74] More recently, a new camphor monooxygenase P450tcu was discovered.[75] Structural and biochemical studies were undertaken to understand the structure-function relationship between the two P450s.[76]

**REFERENCES**


1. Poulos, T. L., Heme enzyme structure and function. *Chem Rev* **2014,** *114* (7), 3919-62.

2. Ignarro, L., Nitric oxide. A novel signal transduction mechanism for transcellular communication. *Hypertension* **1990,** *16* (5), 477-483.

3. Giovinazzo, D.; Dawson, V.; Dawson, T., Nitric oxide. In *Encyclopedia of the Neurological Sciences*, Elsevier Inc.: 2014; pp 597-600.

4. Martin, E.; Berka, V.; Sharina, I.; Tsai, A. L., Mechanism of binding of NO to soluble guanylyl cyclase: implication for the second NO binding to the heme proximal site. *Biochemistry* **2012,** *51* (13), 2737-46.

5. Donald, J. A.; Cameron, M. S., Subchapter 134A - Nitric oxide. In *Handbook of Hormones (Second Edition)*, Ando, H.; Ukena, K.; Nagata, S., Eds. Academic Press: San Diego, 2021; pp 1083-1086.

6. Omura, T.; Sato, R., A new cytochrome in liver microsomes. *The Journal of biological chemistry* **1962,** *237*, 1375-1376.

7. Gorren, A. C.; Mayer, B., Nitric-oxide synthase: a cytochrome P450 family foster child. *Biochim Biophys Acta* **2007,** *1770* (3), 432-45.

8. Sudhamsu, J.; Crane, B. R., Bacterial nitric oxide synthases: what are they good for? *Trends Microbiol* **2009,** *17* (5), 212-8.

9. Messner, S.; Leitner, S.; Bommassar, C.; Golderer, G.; Grobner, P.; Werner, E. R.; Werner-Felmayer, G., Physarum nitric oxide synthases: genomic structures and enzymology of recombinant proteins. *Biochem J* **2009,** *418* (3), 691-700.

10. Trimmer, B. A.; Aprille, J. R.; Dudzinski, D. M.; Lagace, C. J.; Lewis, S. M.; Michel, T.; Qazi, S.; Zayas, R. M., Nitric oxide and the control of firefly flashing. *Science* **2001,** *292* (5526), 2486-2488.

11. Forstermann, U.; Sessa, W. C., Nitric oxide synthases: regulation and function. *Eur Heart J* **2012,** *33* (7), 829-37, 837a-837d.

12. Krol, M.; Kepinska, M., Human Nitric Oxide Synthase-Its Functions, Polymorphisms, and Inhibitors in the Context of Inflammation, Diabetes and Cardiovascular Diseases. *Int J Mol Sci* **2020,** *22* (1).

13. Karupiah, G.; Xie, Q.-w.; Buller, R. M. L.; Nathan, C.; Duarte, C.; MacMicking, J. D., Inhibition of Viral Replication by Interferon-γ-Induced Nitric Oxide Synthase. *Science* **1993,** *261* (5127), 1445-1448.

14. Lechner, M.; Lirk, P.; Rieder, J., Inducible nitric oxide synthase (iNOS) in tumor biology: The two sides of the same coin. *Seminars in Cancer Biology* **2005,** *15* (4), 277-289.

15. Buddha, M. R.; Tao, T.; Parry, R. J.; Crane, B. R., Regioselective Nitration of Tryptophan by a Complex between Bacterial Nitric-oxide Synthase and Tryptophanyl-tRNA Synthetase. *Journal of Biological Chemistry* **2004,** *279* (48), 49567-49570.

16. Kers, J. A.; Wach, M. J.; Krasnoff, S. B.; Widom, J.; Cameron, K. D.; Bukhalid, R. A.; Gibson, D. M.; Crane, B. R.; Loria, R., Nitration of a peptide phytotoxin by bacterial nitric oxide synthase. *Nature* **2004,** *429* (6987), 79-82.

17. Gusarov, I.; Gautier, L.; Smolentseva, O.; Shamovsky, I.; Eremina, S.; Mironov, A.; Nudler, E., Bacterial Nitric Oxide Extends the Lifespan of C.elegans. *Cell* **2013,** *152* (4), 818-830.

18. Gusarov, I.; Nudler, E., NO-mediated cytoprotection: Instant adaptation to oxidative stress in bacteria. *Proceedings of the National Academy of Sciences* **2005,** *102* (39), 13855-13860.

19. Gusarov, I.; Shatalin, K.; Starodubtseva, M.; Nudler, E., Endogenous Nitric Oxide Protects Bacteria Against a Wide Spectrum of Antibiotics. *Science* **2009,** *325* (5946), 1380-1384.

20. Shatalin, K.; Gusarov, I.; Avetissova, E.; Shatalina, Y.; McQuade, L. E.; Lippard, S. J.; Nudler, E., Bacillus anthracis-derived nitric oxide is essential for pathogen virulence and survival in macrophages. *Proceedings of the National Academy of Sciences* **2008,** *105* (3), 1009-1013.

21. CDC Methicillin-resistant Staphylococcus aureus (MRSA). https://www.cdc.gov/mrsa/.

22. Kinkel, T. L.; Ramos-Montanez, S.; Pando, J. M.; Tadeo, D. V.; Strom, E. N.; Libby, S. J.; Fang, F. C., An essential role for bacterial nitric oxide synthase in Staphylococcus aureus electron transfer and colonization. *Nat Microbiol* **2016,** *2*, 16224.

23. Daff, S., NO synthase: Structures and mechanisms. *Nitric Oxide* **2010,** *23* (1), 1-11.

24. Adak, S.; Aulak, K. S.; Stuehr, D. J., Direct evidence for nitric oxide production by a nitric-oxide synthase-like protein from Bacillus subtilis. *J Biol Chem* **2002,** *277* (18), 16167-71.

25. Crane, B. R.; Sudhamsu, J.; Patel, B. A., Bacterial nitric oxide synthases. *Annu Rev Biochem* **2010,** *79*, 445-70.

26. Li, H.; Raman, C. S.; Glaser, C. B.; Blasko, E.; Young, T. A.; Parkinson, J. F.; Whitlow, M.; Poulos, T. L., Crystal Structures of Zinc-free and -bound Heme Domain of Human Inducible Nitric-oxide Synthase: IMPLICATIONS FOR DIMER STABILITY AND COMPARISON WITH ENDOTHELIAL NITRIC-OXIDE SYNTHASE. *Journal of Biological Chemistry* **1999,** *274* (30), 21276-21284.

27. Raman, C. S.; Li, H.; Martásek, P.; Král, V.; Masters, B. S. S.; Poulos, T. L., Crystal Structure of Constitutive Endothelial Nitric Oxide Synthase: A Paradigm for Pterin Function Involving a Novel Metal Center. *Cell* **1998,** *95* (7), 939-950.

28. Pant, K.; Crane, B. R., Nitrosyl−Heme Structures of Bacillus subtilis Nitric Oxide Synthase Have Implications for Understanding Substrate Oxidation. *Biochemistry* **2006,** *45* (8), 2537-2544.

29. Pant, K.; Bilwes, A. M.; Adak, S.; Stuehr, D. J.; Crane, B. R., Structure of a Nitric Oxide Synthase Heme Protein from Bacillus subtilis. *Biochemistry* **2002,** *41* (37), 11071-11079.

30. Marletta, M. A.; Hurshman, A. R.; Rusche, K. M., Catalysis by nitric oxide synthase. *Current opinion in chemical biology* **1998,** *2* (5), 656-663.

31. Stuehr, D. J.; Kwon, N. S.; Nathan, C. F.; Griffith, O. W.; Feldman, P.; Wiseman, J., N omega-hydroxy-L-arginine is an intermediate in the biosynthesis of nitric oxide from L-arginine. *Journal of Biological Chemistry* **1991,** *266* (10), 6259-6263.

32. Davydov, R.; Ledbetter-Rogers, A.; Martasek, P.; Larukhin, M.; Sono, M.; Dawson, J. H.; Masters, B. S.; Hoffman, B. M., EPR and ENDOR characterization of intermediates in the cryoreduced oxy-nitric oxide synthase heme domain with bound L-arginine or N(G)-hydroxyarginine. *Biochemistry* **2002,** *41* (33), 10375-81.

33. Wei, C. C.; Wang, Z. Q.; Hemann, C.; Hille, R.; Stuehr, D. J., A tetrahydrobiopterin radical forms and then becomes reduced during Nomega-hydroxyarginine oxidation by nitric-oxide synthase. *J Biol Chem* **2003,** *278* (47), 46668-73.

34. Abu-Soud, H. M.; Gachhui, R.; Raushel, F. M.; Stuehr, D. J., The ferrous-dioxy complex of neuronal nitric oxide synthase: divergent effects of L-arginine and tetrahydrobiopterin on its stability. *Journal of Biological Chemistry* **1997,** *272* (28), 17349-17353.

35. Woodward, J. J.; Nejatyjahromy, Y.; Britt, R. D.; Marletta, M. A., Pterin-centered radical as a mechanistic probe of the second step of nitric oxide synthase. *J Am Chem Soc* **2010,** *132* (14), 5105-13.

36. Holden, J. K.; Li, H.; Jing, Q.; Kang, S.; Richo, J.; Silverman, R. B.; Poulos, T. L., Structural and biological studies on bacterial nitric oxide synthase inhibitors. *Proceedings of the National Academy of Sciences* **2013,** *110* (45), 18127-18131.

37. Holden, J. K.; Lewis, M. C.; Cinelli, M. A.; Abdullatif, Z.; Pensa, A. V.; Silverman, R. B.; Poulos, T. L., Targeting Bacterial Nitric Oxide Synthase with Aminoquinoline-Based Inhibitors. *Biochemistry* **2016,** *55* (39), 5587-5594.

38. De Montellano, P. R. O., *Cytochrome P450: structure, mechanism, and biochemistry*. Springer: 2005; Vol. 3.

39. Lamb, D. C.; Lei, L.; Warrilow, A. G.; Lepesheva, G. I.; Mullins, J. G.; Waterman, M. R.; Kelly, S. L., The first virally encoded cytochrome p450. *J Virol* **2009,** *83* (16), 8266-9.

40. Klingenberg, M., Pigments of rat liver microsomes. *Archives of biochemistry and biophysics* **1958,** *75* (2), 376-386.

41. Garfinkel, D., Studies on pig liver microsomes. I. Enzymic and pigment composition of different microsomal fractions. *Archives of biochemistry and biophysics* **1958,** *77* (2), 493-509.

42. Omura, T.; Sato, R., The carbon monoxide-binding pigment of liver microsomes. I. Evidence for its hemoprotein nature. *J biol Chem* **1964,** *239* (7), 2370-2378.

43. Narhi, L.; Fulco, A. J., Phenobarbital induction of a soluble cytochrome P-450-dependent fatty acid monooxygenase in Bacillus megaterium. *Journal of Biological Chemistry* **1982,** *257* (5), 2147-2150.

44. Roberts, G. A.; Grogan, G.; Greter, A.; Flitsch, S. L.; Turner, N. J., Identification of a new class of cytochrome P450 from a Rhodococcus sp. *J Bacteriol* **2002,** *184* (14), 3898-908.

45. Poulos, T. L.; Finzel, B. C.; Howard, A. J., High-resolution crystal structure of cytochrome P450cam. *Journal of molecular biology* **1987,** *195* (3), 687-700.

46. Green, M. T., C-H bond activation in heme proteins: the role of thiolate ligation in cytochrome P450. *Curr Opin Chem Biol* **2009,** *13* (1), 84-8.

47. Tripathi, S.; Li, H.; Poulos, T. L., Structural basis for effector control and redox partner recognition in cytochrome P450. *Science* **2013,** *340* (6137), 1227-30.

48. Follmer, A. H.; Tripathi, S.; Poulos, T. L., Ligand and Redox Partner Binding Generates a New Conformational State in Cytochrome P450cam (CYP101A1). *J Am Chem Soc* **2019,** *141* (6), 2678-2683.

49. Tsai, R.; Yu, C. A.; Gunsalus, I. C.; Peisach, J.; Blumberg, W.; Orme-Johnson, W. H.; Beinert, H., Spin-state changes in cytochrome P-450cam on binding of specific substrates. *Proc Natl Acad Sci U S A* **1970,** *66* (4), 1157-63.

50. Sligar, S. G., Coupling of spin, substrate, and redox equilibriums in cytochrome P450. *Biochemistry* **1976,** *15* (24), 5399-5406.

51. Daff, S. N.; Chapman, S. K.; Turner, K. L.; Holt, R. A.; Govindaraj, S.; Poulos, T. L.; Munro, A. W., Redox control of the catalytic cycle of flavocytochrome P-450 BM3. *Biochemistry* **1997,** *36* (45), 13816-23.

52. Luthra, A.; Denisov, I. G.; Sligar, S. G., Spectroscopic features of cytochrome P450 reaction intermediates. *Arch Biochem Biophys* **2011,** *507* (1), 26-35.

53. Rittle, J.; Green, M. T., Cytochrome P450 compound I: capture, characterization, and C-H bond activation kinetics. *Science* **2010,** *330* (6006), 933-7.

54. Yosca, T. H.; Rittle, J.; Krest, C. M.; Onderko, E. L.; Silakov, A.; Calixto, J. C.; Behan, R. K.; Green, M. T., Iron(IV)hydroxide pK(a) and the role of thiolate ligation in C-H bond activation by cytochrome P450. *Science* **2013,** *342* (6160), 825-9.

55. Newman, D. J.; Cragg, G. M., Natural Products as Sources of New Drugs from 1981 to 2014. *J Nat Prod* **2016,** *79* (3), 629-61.

56. Xie, P.; Ma, M.; Rateb, M. E.; Shaaban, K. A.; Yu, Z.; Huang, S. X.; Zhao, L. X.; Zhu, X.; Yan, Y.; Peterson, R. M.; Lohman, J. R.; Yang, D.; Yin, M.; Rudolf, J. D.; Jiang, Y.; Duan, Y.; Shen, B., Biosynthetic potential-based strain prioritization for natural product discovery: a showcase for diterpenoid-producing actinomycetes. *J Nat Prod* **2014,** *77* (2), 377-87.

57. Schmitt, E. K.; Moore, C. M.; Krastel, P.; Petersen, F., Natural products as catalysts for innovation: a pharmaceutical industry perspective. *Curr Opin Chem Biol* **2011,** *15* (4), 497-504.

58. Rudolf, J. D.; Chang, C. Y.; Ma, M.; Shen, B., Cytochromes P450 for natural product biosynthesis in Streptomyces: sequence, structure, and function. *Nat Prod Rep* **2017,** *34* (9), 1141-1172.

59. Nett, M.; Ikeda, H.; Moore, B. S., Genomic basis for natural product biosynthetic diversity in the actinomycetes. *Nat Prod Rep* **2009,** *26* (11), 1362-84.

60. Yagüe, P.; Gonzalez-Quiñonez, N.; Fernández-García, G.; Alonso-Fernández, S.; Manteca, A., New Strategies to Activate Secondary Metabolism in Streptomyces. In *Natural Products from Actinomycetes: Diversity, Ecology and Drug Discovery*, Springer: 2022; pp 185-198.

61. Hussain, H. A.; Ward, J. M., Enhanced heterologous expression of two Streptomyces griseolus cytochrome P450s and Streptomyces coelicolor ferredoxin reductase as potentially efficient hydroxylation catalysts. *Appl Environ Microbiol* **2003,** *69* (1), 373-82.

62. Hussain, H. A.; Ward, J. M., Ferredoxin reductase enhances heterologously expressed cytochrome CYP105D1 in Escherichia coli and Streptomyces lividans. *Enzyme and microbial technology* **2003,** *32* (7), 790-800.

63. Wang, W.; Wang, F. Q.; Wei, D. Z., Characterization of P450 FcpC, the enzyme responsible for bioconversion of diosgenone to isonuatigenone in Streptomyces virginiae IBL-14. *Appl Environ Microbiol* **2009,** *75* (12), 4202-5.

64. Niraula, N. P.; Bhattarai, S.; Lee, N. R.; Sohng, J. K.; Oh, T. J., Biotransformation of flavone by CYP105P2 from Streptomyces peucetius. *J Microbiol Biotechnol* **2012,** *22* (8), 1059-65.

65. Taylor, M.; Lamb, D. C.; Cannell, R.; Dawson, M.; Kelly, S. L., Cytochrome P450105D1 (CYP105D1) from Streptomyces griseus: heterologous expression, activity, and activation effects of multiple xenobiotics. *Biochem Biophys Res Commun* **1999,** *263* (3), 838-42.

66. Zhao, B.; Lamb, D. C.; Lei, L.; Kelly, S. L.; Yuan, H.; Hachey, D. L.; Waterman, M. R., Different binding modes of two flaviolin substrate molecules in cytochrome P450 158A1 (CYP158A1) compared to CYP158A2. *Biochemistry* **2007,** *46* (30), 8725-33.

67. Kells, P. M.; Ouellet, H.; Santos-Aberturas, J.; Aparicio, J. F.; Podust, L. M., Structure of cytochrome P450 PimD suggests epoxidation of the polyene macrolide pimaricin occurs *via* a hydroperoxoferric intermediate. *Chem Biol* **2010,** *17* (8), 841-51.

68. Jungmann, V.; Molnar, I.; Hammer, P. E.; Hill, D. S.; Zirkle, R.; Buckel, T. G.; Buckel, D.; Ligon, J. M.; Pachlatko, J. P., Biocatalytic conversion of avermectin to 4"-oxo-avermectin: characterization of biocatalytically active bacterial strains and of cytochrome p450 monooxygenase enzymes and their genes. *Appl Environ Microbiol* **2005,** *71* (11), 6968-76.

69. Choi, K. Y.; Jung, E.; Jung, D. H.; An, B. R.; Pandey, B. P.; Yun, H.; Sung, C.; Park, H. Y.; Kim, B. G., Engineering of daidzein 3'-hydroxylase P450 enzyme into catalytically self-sufficient cytochrome P450. *Microb Cell Fact* **2012,** *11*, 81.

70. Makino, T.; Katsuyama, Y.; Otomatsu, T.; Misawa, N.; Ohnishi, Y., Regio- and stereospecific hydroxylation of various steroids at the 16alpha position of the D ring by the Streptomyces griseus cytochrome P450 CYP154C3. *Appl Environ Microbiol* **2014,** *80* (4), 1371-9.

71. Katagiri, M.; Ganguli, B.; Gunsalus, I., A soluble cytochrome P-450 functional in methylene hydroxylation. *Journal of Biological Chemistry* **1968,** *243* (12), 3543-3546.

72. Haniu, M.; Armes, L.; Yasunobu, K.; Shastry, B.; Gunsalus, I., Amino acid sequence of the Pseudomonas putida cytochrome P-450. II. Cyanogen bromide peptides, acid cleavage peptides, and the complete sequence. *Journal of Biological Chemistry* **1982,** *257* (21), 12664-12671.

73. Haniu, M.; Tanaka, M.; Yasunobu, K.; Gunsalus, I., Amino acid sequence of the Pseudomonas putida cytochrome P-450. I. Sequences of tryptic and clostripain peptides. *Journal of Biological Chemistry* **1982,** *257* (21), 12657-12663.

74. Peterson, J. A.; Lorence, M. C.; Amarneh, B., Putidaredoxin reductase and putidaredoxin. Cloning, sequence determination, and heterologous expression of the proteins. *Journal of Biological Chemistry* **1990,** *265* (11), 6066-6073.

75. Tsang, H. L.; Huang, J. L.; Lin, Y. H.; Huang, K. F.; Lu, P. L.; Lin, G. H.; Khine, A. A.; Hu, A.; Chen, H. P., Borneol Dehydrogenase from Pseudomonas sp. Strain TCU-HL1 Catalyzes the Oxidation of (+)-Borneol and Its Isomers to Camphor. *Appl Environ Microbiol* **2016,** *82* (21), 6378-6385.

76. Murarka, V. C.; Batabyal, D.; Amaya, J. A.; Sevrioukova, I. F.; Poulos, T. L., Unexpected Differences between Two Closely Related Bacterial P450 Camphor Monooxygenases. *Biochemistry* **2020,** *59* (29), 2743-2750.

# Chapter 1

# Novel Double-Headed Inhibitors Against Bacterial Nitric Oxide Synthase


## SUMMARY

There is a dire need for novel therapeutic strategies to fight antibiotic resistant pathogens like MRSA. In MRSA, NO generated by bNOS assists the pathogen to overcome antibiotic and host induced oxidative stress. Previous studies demonstrated that inhibition of bNOS is effective in improving the efficacy of antibacterial agents. Since humans also produce NOS-generated NO critical for both the immune response and the cardiovascular system, it is important to avoid inhibition of human mNOS isoforms. Previous efforts from our lab have shown that certain NOS inhibitors preferentially bind to the pterin cofactor site in bNOS compared to mNOS isoforms. Our collaborators, the Silverman lab from Northwestern University, designed and synthesized a novel set of inhibitors targeting the bNOS pterin site which we have structurally and biochemically characterized them.


## INTRODUCTION

The emergence of antibiotic resistant bacteria along with the lack of development of newer antibiotics has resulted in an antibiotic resistance crisis.[1] The Centers for Disease Control and Prevention (CDC) states that MRSA is one of the most serious threats.[2] It causes a variety of clinical diseases ranging from skin infection to endocarditis[3] and is resistant to several first-line antibiotics, killing about 10,600 people each year.[2] In view of this, novel therapeutic strategies for these difficult and resistant bacteria are the need of the hour.

bNOS generated NO in MRSA is known to protect the bacteria from antibiotic and host induced oxidative stress.[4, 5] It prepares the bacteria for anerobic respiration and maintains the membrane potential.[6] This is essential for the bacterial colonization of a mammalian host and establishing infection.[6] Therefore, bNOS is a potential drug target for a life-threatening infection. Three isoforms of NOS are also present in humans - eNOS, nNOS, and iNOS.[7] NO produced from these acts as an important signaling molecule.[7] Hence, it is important to selectively target bNOS over all isoforms of mNOS.

In previous studies, a large number of novel NOS inhibitors designed to selectively inhibit nNOS[7, 8] were screened for inhibition of bNOS. It was found that some of these inhibitors synergistically work with antibiotic- and $H_2O_2$-induced oxidative stress to kill *B. subtilis* and MRSA.[9, 10] Many of these compounds inhibited not only various mNOS isoforms but also bNOS. An abundance of crystal structures[9-12] shed light upon potentially important structural differences that can be leveraged to develop highly selective bNOS inhibitors.

$H_4B$[13, 14] is a required cofactor for activity in all mNOS isoforms. bNOS can also use $H_4B$ but the cofactor that is utilized *in vivo* is unknown. $H_4B$ binds in a pocket near one of the heme propionates. Since bNOS has a missing $Zn^{2+}$ binding motif compared to mNOS, the pterin pocket of bNOS is much larger and more exposed (Figure 1.1). This causes a weaker affinity of pterins in bNOS. Previous crystallographic studies suggest that various inhibitors can more readily displace $H_4B$ from bNOS than mNOS.[9-12] This is because of weaker binding affinity of $H_4B$ to bNOS than mNOS. Based on these observations, our collaborators, the Silverman lab at Northwestern University, has synthesized a series of inhibitors that specifically target the bNOS pterin binding pocket. We, at the Poulos lab, have solved crystal structures and determined spectral binding constants for these series of inhibitors.

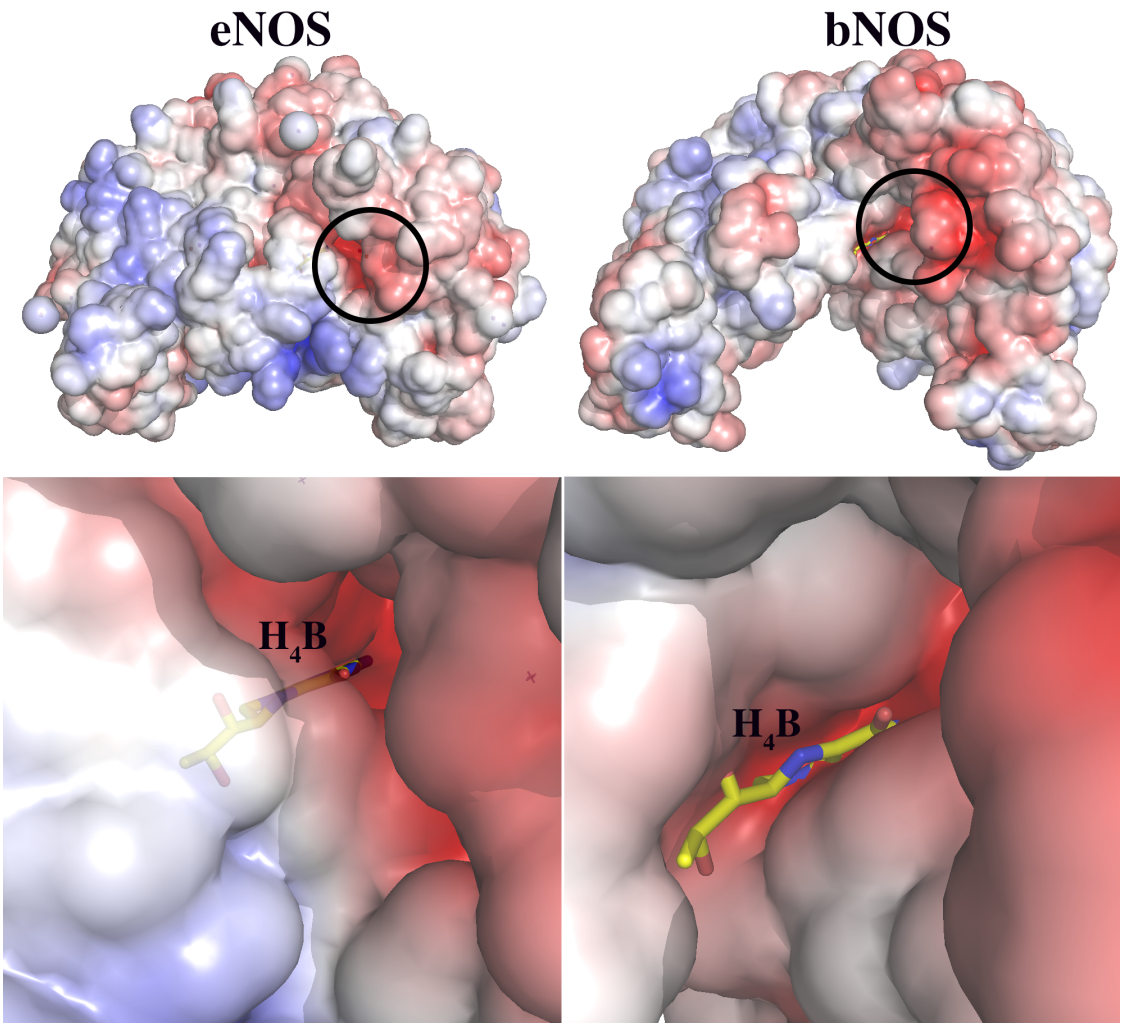


**Figure 1.1** Structures of eNOS and bNOS showing the electrostatic surface potential contoured at ±5kt (red=negative, blue=positive). Magnified view of the pterin binding pocket illustrate that the pocket in bNOS is larger and more exposed than in eNOS.

## EXPERIMENTAL PROCEDURE

### *Chemical Synthesis of inhibitors*

The inhibitors were synthesized by Silverman lab at Northwestern University.

### *Cloning and Mutagenesis*

Even though the therapeutic target is bNOS from MRSA, NOS from *Bacillus subtilis* (bsNOS) is used as a suitable model for our studies. This is because bsNOS crystals diffracts to a desired high resolution and have about 98% sequence identity compared to MRSA bNOS.

Surface entropy reduced mutant (E24A/E25A/E316A) of bsNOS gene in pET28a plasmid was used.[9] These mutations improve crystal quality.[9]

Site directed mutagenesis was carried out to introduce N248D mutation on bsNOS gene using PrimeSTAR® Max DNA polymerase kit (Takara Bio USA, Inc.). Primers N248D-Fw- 5'-GGCACCGAAATCGGCGCGCGATCTGGCCGACGAAAAACGTTAC-3' and N248D-Rv-5'-GTAACGTTTTTCGTCGGCCAGATCGCGCGCCGATTTCGGTGCC-3' were used.

***Protein expression and purification***

bsNOS and bsNOS_N248D were overexpressed in *Escherichia coli* BL21(DE3) cells and purified as described earlier[9, 15, 16] in the absence of added $H_4B$ and L-Arg.[16] Heme domains of human nNOS (hnNOS_HD) and eNOS (heNOS_HD), a gift from Dr. Huiying Li, were expressed and purified as previously reported.[17, 18]

***Imidazole displacement assay***

The optical spectra were recorded using a Cary 300 UV-visible spectrophotometer at room temperature. In the resting state, NOS is largely in a high-spin state due to weakly bound aqua ligand. This causes an insignificant change from low-spin to high-spin state upon addition of inhibitors or type I ligand. Therefore, imidazole, a type II ligand, is used to fully convert NOS to the low-spin heme-iron(III)-imidazole complex. About 2 μM of appropriate NOS was added to a cuvette (1-cm pathlength) containing 50 mM Tris pH 7.6 and 100 μM imidazole and incubated for 15 minutes at room temperature to ensure complete low-spin conversion. Increasing concentration of inhibitors was titrated into the cuvette and optical spectra were recorded.

Apparent dissociation constants ($K_{S,app}$) were determined by plotting the absorbance changes between imidazole bound low-spin Soret peak and inhibitor bound high-spin Soret peak as a function of the inhibitor concentration. Data were fitted to a non-linear regression analysis in

GraphPad Prism using equation 2, $A_{high-spin} - A_{low-spin} = \frac{B_{max.}\,[I]}{K_{S,app} + [I]}$. The spectral binding constant ($K_S$) for each inhibitor was then calculated from $K_{S,app}$, using equation 3, $K_{S,app} = K_S(1 + \frac{[imidazole]}{K_{d,imidazole}})$.[19] The dissociation constants ($K_d$) of imidazole for bsNOS = 36 μM, bsNOS_N248D = 26 μM, heNOS_HD = 40 μM, and hnNOS_HD = 70 μM were experimentally determined and employed.

***Crystallization***

Crystals of bsNOS were grown using the hanging drop vapor diffusion method at room temperature. The reservoir solution contained 60 mM Bis-Tris/40 mM citric acid pH 7.6, 15 % (w/v) PEG 3350 and 1.9 % (v/v) 1-propanol. bsNOS was exchanged into 25 mM Bis-Tris pH 7.6, 150 mM sodium chloride, 1 % (v/v) glycerol, 1 % (w/v) PEG 3350, 1 mM DTT, and 0.5 mM imidazole. Drops of 20 mg/mL bsNOS was mixed with an equal volume of reservoir solution and equilibrated against 800 μL of reservoir solution. Crystals were soaked in the reservoir solution containing 23% (v/v) glycerol as a cryoprotectant, 7-10 mM of inhibitor and 2 mM of $H_4B$ for 3 hours. Co-crystals of bsNOS-103 were formed by the above method except 5 mM of 103 was mixed with bsNOS before crystallization. Crystals were flash-frozen using liquid nitrogen.

Diffraction data were collected at the Advanced Light Source beamline 5.0.2 or 8.2.1. XDS[20] was used to index and integrate the raw data. Aimless was used to for scaling the datasets.[21] The structure was determined by molecular replacement with Phaser[22] and bsNOS (PDB: 4D3J) as the search model. Phenix[23] was used to carry out further refinements.

## RESULTS AND DISCUSSION

### *Inhibitor Design*

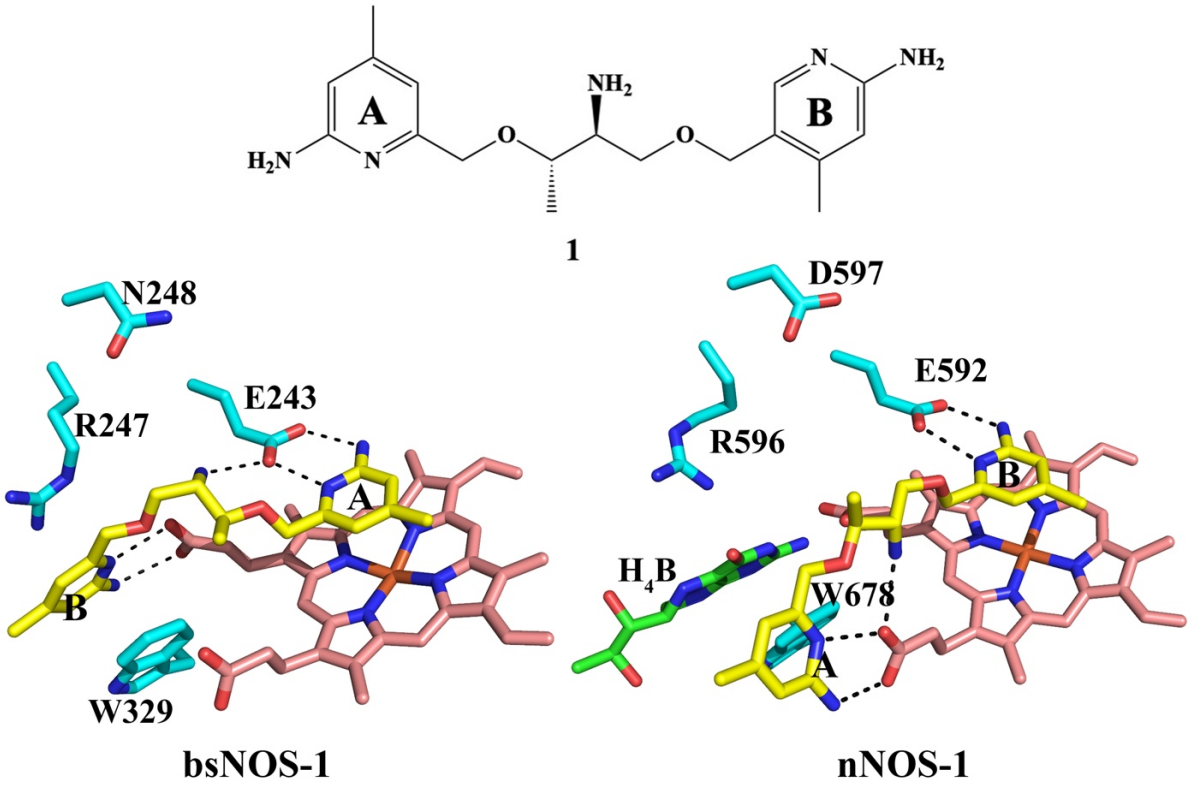


**Figure 1.2** Crystal structures of bsNOS (PDB: 4LWA) and rat nNOS (PDB: 4K5G) with **1** bound. In bsNOS the **A** aminopyridine ring binds over the heme while the **B** ring binds in the pterin binding pocket displacing $H_4B$. In rat nNOS, it is the opposite where the **B** ring binds over the heme and the **A** ring extends out of the active site to interact with one of the heme propionates and is unable to displace $H_4B$.

The crystal structure of **1** bound to bsNOS was the first to indicate that $H_4B$ can be displaced in bsNOS while the same inhibitor bound to rat nNOS has the $H_4B$ still in place (Figure 1.2).[9, 24] Therefore, $H_4B$ can be more readily displaced in bNOS even though $H_4B$ was included in the crystallization medium[9] most likely because $H_4B$ binds more tightly to nNOS. **1** also exhibited excellent bacterial killing activity with a spectral binding constant ($K_S$) = 1.1 μM.[9] However, **1** also binds tightly to eNOS and nNOS, $K_S$ = 1.7 μM and 0.4 μM, respectively.[9]

A series of crystal structures of bNOS complexed with various aminopyridine and aminoquinoline inhibitors showed that the larger aminoquinoline ring favors binding in the active site to form H-bonds with Glu243.[11, 25] In addition, those inhibitors that were able to displace $H_4B$ had the aminopyridine in the pterin pocket. These studies also indicated that a subtle difference in the active site favors the binding of aminoquinolines in bNOS over mNOS. Ile218 in bNOS is replaced by Val in mNOS, and mutagenesis studies indicate that Ile as opposed to Val favors binding of the larger aminoquinoline in the active site.[25] This is because the slightly larger Ile provides more extensive non-bonded contacts with the larger aminoquinoline. A wealth of crystallographic data on both bNOS and the various mNOS isoforms shows that using nitrogen in the linker provides an opportunity for strong H-bonding interactions between the inhibitor linker amine and heme propionates.

Lessons learned from **1** and other crystal structures were used to improve bNOS selectivity by designing double-headed inhibitors. These inhibitors contain an aminoquinoline on one end, which should bind in the active site heme pocket, and an aminopyridine at the other end, which should bind in the pterin pocket. The main variable in the inhibitor design is the linker length and type of hetero atom, oxygen or nitrogen, used in the linker. These possibilities, together with molecular modeling and synthetic feasibility, were used to design seven new inhibitors (Figure 1.3).

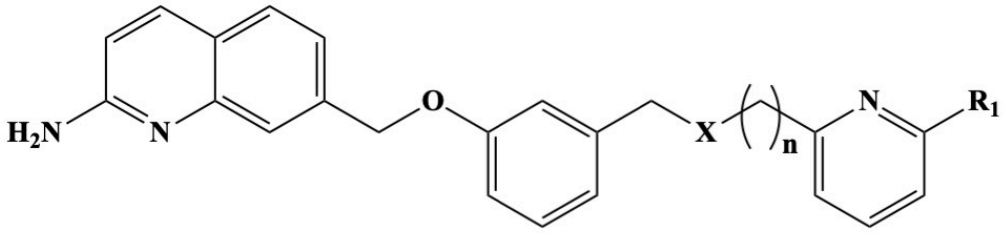

2. X = $CH_2$ , $R_1$ = $NH_2$ , n = 0

3. X = NH , $R_1$ = H , n = 1

4. X = NH , $R_1$ = $NH_2$ , n = 1

5. X = NH , $R_1$ = H , n = 2

6. X = NH , $R_1$ = $NH_2$ , n = 4

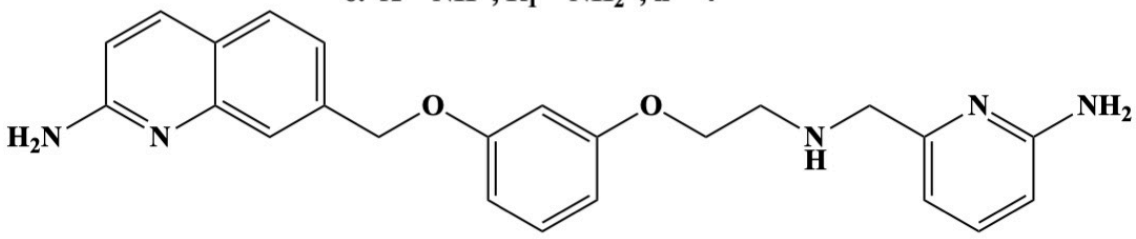

7

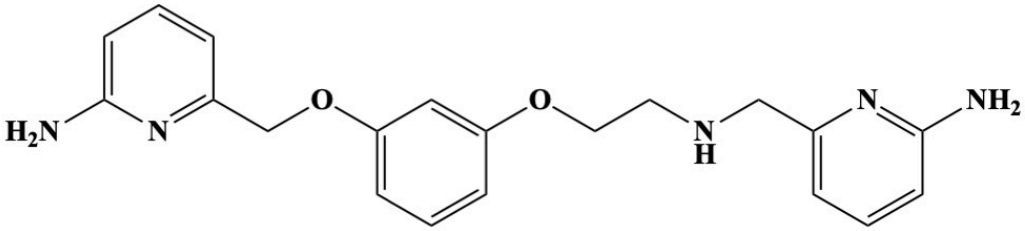

8

**Figure 1.3** Chemical structure of synthesized bNOS inhibitors for this study.

***Spectral binding***

The binding of inhibitors to NOS results in an easily detected low- to high- spin shift in the UV/Vis spectrum that provides the basis for obtaining the $K_S$, shown in Table 1.1. Weak binders tend to give poor spectral titration data. We included human eNOS given that this human isoform is most likely to be affected by bNOS inhibitors. We also screened these inhibitors for nNOS activity, and these inhibitors bind extremely well to the nNOS isoforms. This is less of a concern since these highly charged inhibitors are not very effective at crossing the blood brain barrier and thus are

unlikely to have much of an effect on nNOS. We also made a nNOS like mutant of bNOS where Asn248 is mutated to an Asp. Both eNOS and bNOS have an Asn whereas nNOS has an Asp. This causes changes in electrostatic interactions in the active site resulting in different binding affinities.

**Table 1.1** Spectral binding constants of double-headed inhibitors

| Inhibitor | bsNOS (μM) | bsNOS_N248D (μM) | heNOSHD (μM) | hnNOSHD (μM) |
|---|---|---|---|---|
| **2 (PWA150)** | 1.8 | 0.8 | 0.7 | 0.9 |
| **3 (PWA101)** | 4.7 | 0.9 | 12.2 | 1.3 |
| **4 (PWA207)** | 3.6 | 0.9 | 4.5 | 1.2 |
| **5 (PWA138)** | 2.3 | 0.5 | 6.3 | 0.5 |
| **6 (PWA103)** | 0.8 | 0.5 | 0.6 | 0.6 |
| **7 (PWA206)** | 1.5 | 0.5 | 5.4 | 0.6 |
| **8 (PWA325)** | 62.5 | 12.1 | 94.0 | 2.7 |

Out of all the compounds, **6** shows the strongest binding affinity, in mid-nanomolar range, to all four NOSs while **8** is the weakest. Each of the inhibitors exhibit similar binding affinities for both bsNOS and eNOS. Not too surprisingly, the inhibitors show stronger binding affinity for nNOS and the nNOS-like bsNOS_N248D mutant. The addition of one more negative charge in the active site confers tighter binding to these positively charged inhibitors. These data also suggests that these inhibitors can have an alternative application as nNOS inhibitors in the treatment of neurodegenerative disorders.

*Crystal Structures*

We were able to obtain crystal structures of all the compounds complexed to bsNOS. The crystal structure of **6** and **8** were recently solved (Table 1.2). The other crystal structures were previously solved in our lab by Dr. Matt Lewis (unpublished data). The $2F_o$-$F_c$ electron density maps contoured at 1.0 σ for bsNOS-**6** and bsNOS-**8** are shown in Figure 1.4.

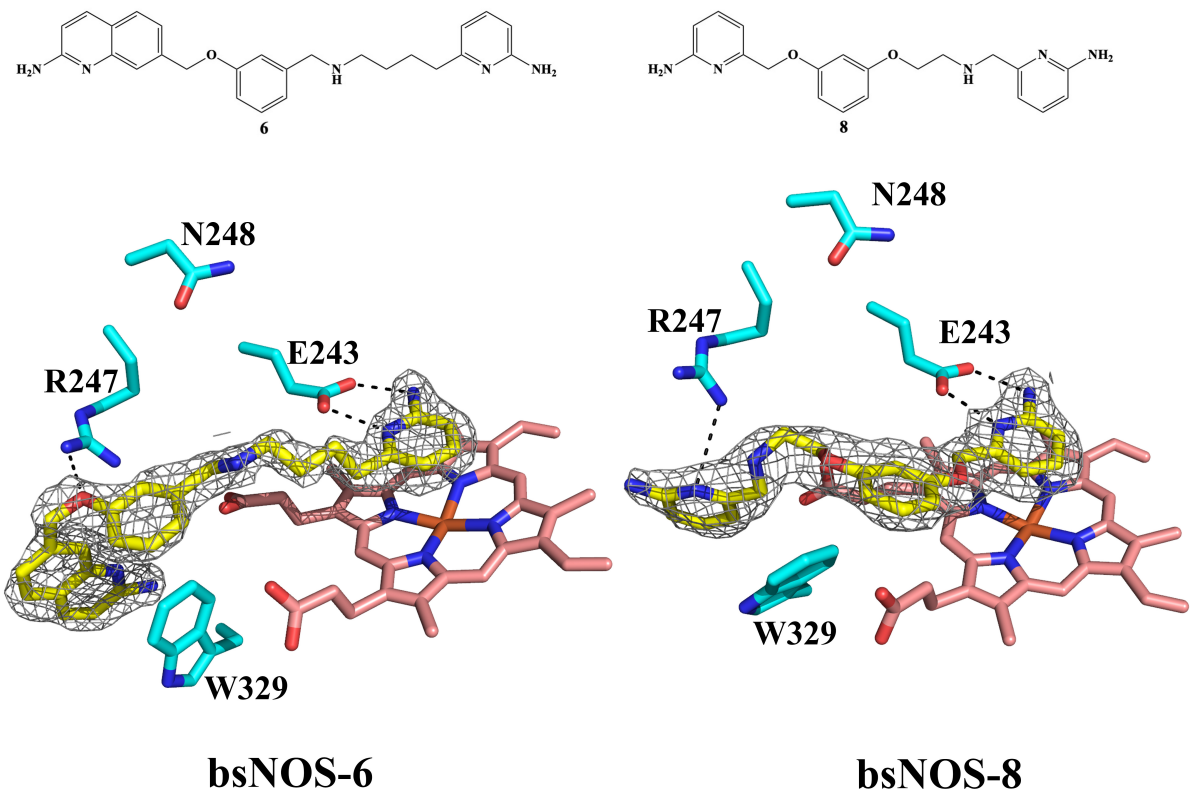


**Figure 1.4** $2F_o$-$F_c$ electron density maps contoured at 1.0 σ for inhibitors **6** and **8** bound to bsNOS. The pterin binding pocket is bracketed by Trp329 and Arg247. In both the structures the density of inhibitors is well defined. Unexpectedly in bsNOS-**6**, the aminopyridine binds over heme and H-bonds with Glu243 whereas the aminoquinoline binds in the pterin binding pocket forming π-stacking interaction with Trp329. In bsNOS-**8**, one aminopyridine heads binds over the heme and the other in the pterin binding pocket. There is the expected H-bonding interaction with Glu243. Arg247 is close enough to the amino pyridine in the pterin pocket for potential H-bonding.

In all the bsNOS-inhibitor complex structures previously solved (unpublished data from Dr. Matt Lewis), the aminoquinoline of the inhibitor, as predicted, is positioned over the heme, enabling the inhibitor to H-bond with the active site Glu243. The tail end of the inhibitor, pyridine or aminopyridine, is positioned in the pterin binding pocket displacing $H_4B$ even though $H_4B$ was included in the crystallization medium.

In bsNOS-**6**, the binding of **6** is completely opposite to what was expected. The aminopyridine occupies the active site and H-bonds with the active site Glu243. The aminoquinoline binds in the pterin pocket displacing $H_4B$. It has a π–stacking interaction with Trp329 which forms part of the

pterin pocket. Trp329 also has a T-shaped π–stacking interaction with the central phenyl ring. The linker oxygen atom forms H-bonds with Arg247 whereas the linker amine H-bonds with the heme propionates. All these interactions combined lead to a stronger binding of **6** to bsNOS compared to the other inhibitors. Similar interactions are expected in the other three NOSs as well because of similar binding affinities.

**8** is an exception in the inhibitor library with two aminopyridine heads. It binds weakly to bsNOS with one aminopyridine in the active site and the other in the pterin pocket displacing the $H_4B$. As expected, Glu243 H-bonds with the aminopyridine in the active site while unlike with the other inhibitors, the aminopyridine in the pterin binding pocket is oriented such that it cannot H-bond with the heme propionate. This very likely accounts for the weaker affinity of **8**. Even though a weak binder for bNOS, **8** shows greater selectivity for nNOS over eNOS. This can make **8** a good starting scaffold to make nNOS selective inhibitors for treatment of neurodegenerative disorders.

**Table 1.2** X-ray crystallography data collection and refinement statistics

| **Parameter** | **bNOS-6** | **bNOS-8** |
|---|---|---|
| Wavelength (Å) | 1.00004 | 1.00000 |
| Resolution range (Å) | 44.04 - 1.86 (1.926 - 1.86) | 46.25 - 2.1 (2.175 - 2.1) |
| Space group | P 21 21 2 | P 21 21 2 |
| Unit cell | 81.174 94.657 62.966 90 90 90 | 80.161 92.498 58.302 90 90 90 |
| Total reflections | 82217 (8117) | 51605 (5107) |
| Unique reflections | 41379 (4066) | 25907 (2554) |
| Multiplicity | 2.0 (2.0) | 2.0 (2.0) |
| Completeness (%) | 99.73 (99.95) | 99.61 (99.80) |
| Mean I/sigma(I) | 15.07 (5.04) | 23.77 (7.60) |
| Wilson B-factor | 28.88 | 37.12 |
| R-merge | 0.02124 (0.1072) | 0.01553 (0.07497) |
| R-meas | 0.03003 (0.1517) | 0.02196 (0.106) |
| R-pim | 0.02124 (0.1072) | 0.01553 (0.07497) |
| CC1/2 | 0.999 (0.978) | 1 (0.991) |
| CC* | 1 (0.995) | 1 (0.998) |

| | | |
|---|---|---|
| Reflections used in refinement | 41353 (4065) | 25888 (2551) |
| Reflections used for R-free | 498 (49) | 942 (93) |
| R-work | 0.1635 (0.1898) | 0.1591 (0.1877) |
| R-free | 0.1966 (0.2270) | 0.1972 (0.2234) |
| CC(work) | 0.971 (0.949) | 0.970 (0.965) |
| CC(free) | 0.943 (0.942) | 0.959 (0.951) |
| Number of non-hydrogen atoms | 3564 | 3362 |
| macromolecules | 3035 | 3005 |
| Ligands | 115 | 109 |
| Solvent | 414 | 248 |
| Protein residues | 364 | 366 |
| RMS(bonds) | 0.007 | 0.006 |
| RMS(angles) | 0.92 | 0.93 |
| Ramachandran favored (%) | 97.51 | 97.80 |
| Ramachandran allowed (%) | 2.22 | 2.20 |
| Ramachandran outliers (%) | 0.28 | 0.00 |
| Rotamer outliers (%) | 1.54 | 0.94 |
| Clashscore | 2.73 | 4.23 |
| Average B-factor | 38.74 | 46.47 |
| macromolecules | 37.81 | 46.12 |
| Ligands | 36.41 | 46.06 |
| Solvent | 46.18 | 50.83 |

Value in () are the statistics for highest resolution shell. Statistics generated by using the "Table 1" utility in Phenix.

## CONCLUSION

The design of the new bNOS inhibitors in this study was based on the hypothesis that the aminoquinoline head group would bind over the heme while the tail aminopyridine/pyridine would displace the $H_4B$ and bind in the pterin pocket. In all the crystal structures except **6**, the aminoquinoline binds over the heme while the aminopyridine is positioned in the pterin binding

pocket and H-bonds with the heme propionate. Since **8** has two aminopyridines, one binds in the active site and the other in the pterin binding pocket. Preference for the larger aminoquinoline in the active site is because of Ile218 in bNOS. It provides a more non-polar surface area to interact with the aminoquinoline than Val in mNOS. Therefore, the preference for the larger aminoquinoline in the bNOS active sites is tied to the preference for aminopyridines in the pterin site.

We also found that these inhibitors bind to eNOS as well as bNOS so these are not selective for bNOS. However, these inhibitors have the strongest interactions to nNOS suggesting that these inhibitors can be repurposed as nNOS inhibitors to treat neurodegenerative disorders. **8** is 35-fold more selective for nNOS over eNOS which is quite low compared to the current nNOS inhibitors.[26] Even so **8** can serve as a starting scaffold to develop better and highly selective nNOS inhibitors. Despite these binding affinity complexities, these double-headed inhibitors are able to bind to both the active site and the pterin site and readily displace $H_4B$ in bNOS but not mNOS although targeting the H4B site with these double-headed inhibitors is insufficient for selectivity. This is very likely because H-bonding interactions between the aminopyridine or the aminoquinoline with the active site Glu and similar interactions between the linker and heme propionates are quite strong in all NOS isoforms. This suggests that it might be best to focus on designing inhibitors that target just the $H_4B$ site in bNOS. Despite this lack of selectivity, some of these inhibitors do exhibit bacterial killing activity and thus are worth further biological *in vitro* and possibly, *in vivo* testing.

**REFERENCES**


1. Ventola, C. L., The antibiotic resistance crisis: part 1: causes and threats. *Pharmacy and therapeutics* **2015,** *40* (4), 277.

2. CDC Methicillin-resistant Staphylococcus aureus (MRSA). https://www.cdc.gov/mrsa/.

3. DeLeo, F. R.; Otto, M.; Kreiswirth, B. N.; Chambers, H. F., Community-associated meticillin-resistant Staphylococcus aureus. *Lancet* **2010,** *375* (9725), 1557-68.

4. Gusarov, I.; Nudler, E., NO-mediated cytoprotection: instant adaptation to oxidative stress in bacteria. *Proc Natl Acad Sci U S A* **2005,** *102* (39), 13855-60.

5. Gusarov, I.; Shatalin, K.; Starodubtseva, M.; Nudler, E., Endogenous nitric oxide protects bacteria against a wide spectrum of antibiotics. *Science* **2009,** *325* (5946), 1380-4.

6. Kinkel, T. L.; Ramos-Montanez, S.; Pando, J. M.; Tadeo, D. V.; Strom, E. N.; Libby, S. J.; Fang, F. C., An essential role for bacterial nitric oxide synthase in Staphylococcus aureus electron transfer and colonization. *Nat Microbiol* **2016,** *2*, 16224.

7. Poulos, T. L.; Li, H., Structural basis for isoform-selective inhibition in nitric oxide synthase. *Acc Chem Res* **2013,** *46* (2), 390-8.

8. Silverman, R. B., Design of selective neuronal nitric oxide synthase inhibitors for the prevention and treatment of neurodegenerative diseases. *Acc Chem Res* **2009,** *42* (3), 439-51.

9. Holden, J. K.; Li, H.; Jing, Q.; Kang, S.; Richo, J.; Silverman, R. B.; Poulos, T. L., Structural and biological studies on bacterial nitric oxide synthase inhibitors. *Proc Natl Acad Sci U S A* **2013,** *110* (45), 18127-31.

10. Holden, J. K.; Kang, S.; Beasley, F. C.; Cinelli, M. A.; Li, H.; Roy, S. G.; Dejam, D.; Edinger, A. L.; Nizet, V.; Silverman, R. B.; Poulos, T. L., Nitric Oxide Synthase as a Target for Methicillin-Resistant Staphylococcus aureus. *Chem Biol* **2015,** *22* (6), 785-92.

11. Holden, J. K.; Dejam, D.; Lewis, M. C.; Huang, H.; Kang, S.; Jing, Q.; Xue, F.; Silverman, R. B.; Poulos, T. L., Inhibitor Bound Crystal Structures of Bacterial Nitric Oxide Synthase. *Biochemistry* **2015,** *54* (26), 4075-82.

12. Holden, J. K.; Kang, S.; Hollingsworth, S. A.; Li, H.; Lim, N.; Chen, S.; Huang, H.; Xue, F.; Tang, W.; Silverman, R. B.; Poulos, T. L., Structure-based design of bacterial nitric oxide synthase inhibitors. *J Med Chem* **2015,** *58* (2), 994-1004.

13. Hevel, J. M.; Marletta, M. A., Macrophage nitric oxide synthase: relationship between enzyme-bound tetrahydrobiopterin and synthase activity. *Biochemistry* **1992,** *31* (31), 7160-7165.

14. Mayer, B.; John, M.; Heinzel, B.; Werner, E. R.; Wachter, H.; Schultz, G.; Böhme, E., Brain nitric oxide synthase is a biopterin-and flavin-containing multi-functional oxido-reductase. *FEBS letters* **1991,** *288* (1-2), 187-191.

15. Pant, K.; Bilwes, A. M.; Adak, S.; Stuehr, D. J.; Crane, B. R., Structure of a nitric oxide synthase heme protein from Bacillus subtilis. *Biochemistry* **2002,** *41* (37), 11071-9.

16. Salard-Arnaud, I.; Stuehr, D.; Boucher, J. L.; Mansuy, D., Spectroscopic, catalytic and binding properties of Bacillus subtilis NO synthase-like protein: comparison with other bacterial and mammalian NO synthases. *J Inorg Biochem* **2012,** *106* (1), 164-71.

17. Li, H.; Shimizu, H.; Flinspach, M.; Jamal, J.; Yang, W.; Xian, M.; Cai, T.; Wen, E. Z.; Jia, Q.; Wang, P. G.; Poulos, T. L., The novel binding mode of N-alkyl-N'-hydroxyguanidine to neuronal nitric oxide synthase provides mechanistic insights into NO biosynthesis. *Biochemistry* **2002,** *41* (47), 13868-75.

18. Raman, C. S.; Li, H.; Martasek, P.; Kral, V.; Masters, B. S.; Poulos, T. L., Crystal structure of constitutive endothelial nitric oxide synthase: a paradigm for pterin function involving a novel metal center. *Cell* **1998,** *95* (7), 939-50.

19. Roman, L. J.; Sheta, E. A.; Martasek, P.; Gross, S. S.; Liu, Q.; Masters, B., High-level expression of functional rat neuronal nitric oxide synthase in Escherichia coli. *Proceedings of the National Academy of Sciences* **1995,** *92* (18), 8428-8432.

20. Kabsch, W., Xds. *Acta Crystallogr D Biol Crystallogr* **2010,** *66* (Pt 2), 125-32.

21. Winn, M. D.; Ballard, C. C.; Cowtan, K. D.; Dodson, E. J.; Emsley, P.; Evans, P. R.; Keegan, R. M.; Krissinel, E. B.; Leslie, A. G.; McCoy, A.; McNicholas, S. J.; Murshudov, G. N.; Pannu, N. S.; Potterton, E. A.; Powell, H. R.; Read, R. J.; Vagin, A.; Wilson, K. S., Overview of the CCP4 suite and current developments. *Acta Crystallogr D Biol Crystallogr* **2011,** *67* (Pt 4), 235-42.

22. McCoy, A. J.; Grosse-Kunstleve, R. W.; Adams, P. D.; Winn, M. D.; Storoni, L. C.; Read, R. J., Phaser crystallographic software. *J Appl Crystallogr* **2007,** *40* (Pt 4), 658-674.

23. Adams, P. D.; Afonine, P. V.; Bunkoczi, G.; Chen, V. B.; Echols, N.; Headd, J. J.; Hung, L. W.; Jain, S.; Kapral, G. J.; Grosse Kunstleve, R. W.; McCoy, A. J.; Moriarty, N. W.; Oeffner, R. D.; Read, R. J.; Richardson, D. C.; Richardson, J. S.; Terwilliger, T. C.; Zwart, P. H., The Phenix software for automated determination of macromolecular structures. *Methods* **2011,** *55* (1), 94-106.

24. Jing, Q.; Li, H.; Chreifi, G.; Roman, L. J.; Martásek, P.; Poulos, T. L.; Silverman, R. B., Chiral linkers to improve selectivity of double-headed neuronal nitric oxide synthase inhibitors. *Bioorganic & Medicinal Chemistry Letters* **2013,** *23* (20), 5674-5679.

25. Holden, J. K.; Lewis, M. C.; Cinelli, M. A.; Abdullatif, Z.; Pensa, A. V.; Silverman, R. B.; Poulos, T. L., Targeting Bacterial Nitric Oxide Synthase with Aminoquinoline-Based Inhibitors. *Biochemistry* **2016,** *55* (39), 5587-5594.

26. Vasu, D.; Do, H. T.; Li, H.; Hardy, C. D.; Awasthi, A.; Poulos, T. L.; Silverman, R. B., Potent, Selective, and Membrane Permeable 2-Amino-4-Substituted Pyridine-Based Neuronal Nitric Oxide Synthase Inhibitors. *Journal of Medicinal Chemistry* **2023,** *66* (14), 9934-9953.

# Chapter 2

# Structural Analysis of Cytochrome P450 NysI Involved in Nystatin Biosynthesis


## SUMMARY

NysL, a cytochrome P450 monooxygenase from *Streptomyces noursei*, is involved in the biosynthesis of the polyene macrolide antifungal, nystatin. It catalyzes the final step, hydroxylation of 10-deoxynystain, in the production of nystatin. In this study, we present a 2 Å resolution crystal structure of NysL bound to nystatin to understand the substrate regio- and stereo-selectivity. Furthermore, a detailed structural comparison was made with AmphL and PimD, two closely related P450s, to advance our knowledge about the structural basis of substrate selectivity. These comparisons provide important structural information that can contribute in accelerating the development of a new generation of antibiotics with enhanced pharmacological properties.


## INTRODUCTION

Polyene macrolide antibiotics, produced by *Streptomyces spp.*, are an indispensable class of highly effective antifungal agents with a broad spectrum of activity.[1, 2] They are amphipathic rod-shaped molecules consisting of a large hydroxylated, polyene macrolactone ring with a six-membered hemi-ketal ring attached to the macrolactone *via* a glycosidic bond.[3] A major mode of action is interaction with ergosterol in fungal cytoplasmic membranes which creates hydrophilic transmembrane channels resulting in leakage of ions and small molecules, ultimately causing cell death.[4, 5] However, they also have affinity for cholesterol in mammalian cytoplasmic membranes which can cause nephrotoxicity.[2, 5, 6] The biosynthetic gene clusters of polyene macrolides encode

for modular polyketide synthases responsible for the macrolactone core assembly, including cytochrome P450 enzymes to functionalize/modify the macrolactone core, and enzymes for attachment of the hemiketal ring.[2, 3]

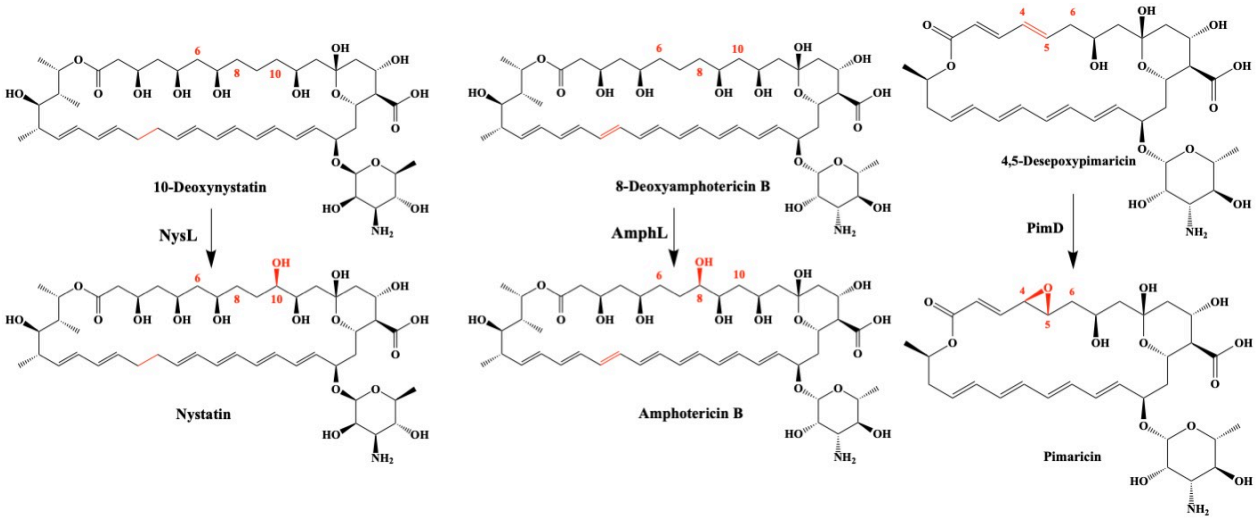


**Figure 2.1** Reactions catalyzed by three closely related macrolide oxidizing P450s. NysL hydroxylates 10-deoxynystatin at the C10 position. AmphL hydroxylates 8-deoxyamphotericin B at the C8 position. PimD epoxidates 4,5-desepoxypimaricin across C4=C5.

*Streptomyces noursei* produces a complex mixture of nystatins which are used for the treatment of superficial mycoses. Nystatin $A_1$, a 38-membered macrolactone ring, forms a major component of the complex.[7, 8] The macrolactone core is assembled by six polyketide synthase proteins[9] which is further modified by monooxygenases (NysN and NysL) and glycosyltransferases (NysDI) to form nystatin.[7] The last step is carried out by a cytochrome P450, NysL, which hydroxylates at C-10.[7, 8] The reaction is described in Figure 2.1. A 2 Å crystal structure of NysL bound to nystatin, the final product, is described in this work. The structure was subjected to a detailed comparison with two closely related macrolide oxidizing P450s, AmphL[10] and PimD,[11] which share 71 % and 57 % sequence identity, respectively, with NysL (Figure 2.2). AmphL catalyzes the C8 hydroxylation of 8-deoxyamphotericin B to form a 38-membered ring, amphotericin B.[10] PimD epoxidates C4-C5 of 4,5-desepoxypimaricin to form a 26-memebered ring, pimaricin.[11] Amphotericin B and nystatin

both share the same macrolactone core with slight differences in conjugated bonds and hydroxylation pattern (Figure. 2.1). It will be very interesting to understand the structural nuances that lead to substrate specific stereo- and regio-selective oxidation. This will enhance our knowledge on the substrate selectivity and help in combinatorial biosynthesis of novel pharmaceuticals and of products for other applications.

```
PimD            MTAASHDLPCLNLEPPKMLKLSPLLRALQDRGPIHRVRTPAGDEAWLVTRHAELKQLLHD
NysL            -MSTPTAPPSLKAEVPPVLRLSPLLRELQSRAPVCKVRTPAGDEGWLVTRHTELKQLLHD
AmphL           -MVNPTPPPSLEDAAPSVLRLSPLLRELQMRAPVTKIRTPAGDEGWLVTRHAELKQLLHD
                     .   *.*:   * :*.****** ** *.*: .:*******.******:********

PimD            ERIGRTHPDPPSAAQYVRSPFLDLLISDADAESGRRQHAETRRLLTPLFSARRVLEMQPK
NysL            DRLARAHADPANAPRYVHNPFLDLLVVD-DFDLARTLHAEMRSLFTPQFSARRVMDLTPR
AmphL           ERLARAHADPANAPRYVKSPLMDLLIMD-DVEAARAAHAELRTLLTPQFSARRVLNMMPM
                :*:.*:*.**..*..**..*::***: * * : .*  *** * *:** ******::: *

PimD            VEEAADTLLDAFIAQGPPGDLHGELTVPFALTVLCEVIGVPPQRRAELTTLLAGIAKLDD
NysL            VEALAEGVLAHFVAQGPPADLHNDFSLPFSLSVLCALIGVPAEEQGKLIAALTKLGELDD
AmphL           VEGIAEQILNGFAAQEQPADLRGNFSLPYSLTVLCALIGIPLQEQGQLLAVLGEMATLND
                **  *: :*  * **  *.**..::::*::*:*** :**:* : ..:* : *  :. *:*

PimD            REGAVRAQDDLFGYVAGLVEHKRAEPGPDIISRLNDGELTEDRVAHLAMGLLFAGLDSVA
NysL            PARVQEGQDELFGLLSGLARRKRITPEDDVISRLCLKVPSDERIGPIASGLLFAGLDSVA
AmphL           AESVARSQAKLFGLLTDLAGRKRAEPGDDVISRLCETVPEDERIGPIAASLLFAGLDSVA
                   .  .* .*** ::.*. .**  *  *:****      ::*:. :* .**********

PimD            SIMDNGVVLLAAHPDQRAAALADPDVMARAVEEVLRTARAGGS-VLPPRYASEDMEFGGV
NysL            SHIDLGTVLFIQHPDQLAAALADEKLMRGAVEEILRSAKAGGS--VLPRYATADVPIGDV
AmphL           THVDLGVVLFTQYPDQLKEALADEKLMRSGVEEILRAAKAGGSGAALPRYATDDIEIADV
                : :* *.**:  :***   **** .:*  .***:**:*.****    ****: *: :..*

PimD            TIRAGDLVLFDLGLPNFDERAFTGPEEFDAARTPNPHLTFGHGIWHCIGAPLARLELRTM
NysL            TIRAGDLVLLDFTLVNFDRTVFDEPELFDIRRAPNPHLTFGHGMWHCIGAPLARVNLRTA
AmphL           TIRTGDLVLLDFTLVNFDEAVFDDADLFDIRRSPNEHLTFGHGMWHCIGAPLARMMLKTA
                ***:*****:*: * ***  .*  .: **  *:** *******:**********: *.*

PimD            FTKLFTRLPELRPELPVEQLRLKEGQLSGGFAELRVVW
NysL            YTLLFTRLPGLRLVRPVEELRVLSGQLSAGLTELPVTW
AmphL           YTQLFTRLPGLKLASSVEELQVTSGQLNGGLTELPVTW
                :* ****** *.   .**:*.: .***..*::** *.*
```

**Figure 2.2** Sequence alignment of PimD, NysL and AmphL. Generated using MUSCLE.[12]

## EXPERIMENTAL PROCEDURE

### *Protein Expression and Purification*

UniProt database was used to obtain the gene sequence that encodes NysL (accession# Q9L4X0). A synthetic gene encoding NysL was codon optimized to express in *Escherichia coli* (GenScript USA Inc.). The gene was subcloned into pET28a (NdeI and BamHI) with a thrombin-cleavable N-terminal six-His tag.

The plasmid was transformed into *E. coli* BL21(DE3) cells. A single-plated colony of transformed bacteria was used to inoculate 5 mL of Luria-Bertani (LB) media containing 50 μg/mL of kanamycin and incubated overnight at 37°C and 200 rpm. About 500 μL of overnight culture was then added to 1 L Terrific Broth (TB) media containing 50 μg/mL of kanamycin. Cultures were grown at 37°C and 200 rpm. When $A_{600}$ reached 0.8 - 1.0, the cells were induced with 1 mM isopropyl 1-thio-D-galactopyranoside (IPTG). To improve heme synthesis for formation of heme-bound NysL, 30 μg/mL of δ- aminolevulinic acid was added. The cells were incubated for additional 36 hours at 25°C and 120 rpm before they were harvested by centrifugation.

Cell pellets were suspended in lysis buffer containing 50 mM KPi (pH 7.4), 100 mM NaCl and 5 mM imidazole and lysed *via* sonication. The lysate was centrifuged at 4°C and 15,000 rpm for 1 hour. The resulting supernatant was loaded onto a $Ni^{2+}$-nitrilotriacetate agarose column equilibrated with lysis buffer. The column was washed with lysis buffer containing 15 mM imidazole. The protein was eluted using lysis buffer containing 200 mM imidazole. Thrombin was added to the eluted protein to cleave the N-terminal six-His tag from the protein and then was dialyzed overnight against 50 mM KPi (pH 7.4) at 4°C. NysL was further purified by DEAE column chromatography previously equilibrated with 50 mM KPi (pH 7.4). The protein

was eluted using a gradient of 0 to 300 mM KCl. The protein fractions were pooled, and buffer exchanged into 50 mM KPi (pH 7.4) and concentrated. The protein concentration was calculated using an extinction coefficient ($\varepsilon_{415nm}$)=115 $mM^{-1}.cm^{-1}$.

***Crystallization***

NysL crystals were grown at room temperature using the hanging drop vapor diffusion method. The reservoir solution contained 100 mM Bis-tris propane (pH 7) and 1.5 M lithium sulfate.

About 20 mg/mL of NysL (in 50 mM KPi (pH 7.4) and nystatin) was mixed with the reservoir solution in a 1:1 ratio and equilibrated against 700 μL of reservoir solution. Crystals were flash frozen using liquid nitrogen with ParatonN (Hampton Research) as a cryoprotectant. Diffraction data were collected at the Stanford Synchrotron Radiation Lightsource beamline 12-2. XDS was used to index, integrate, and scale the raw data.[13] Phaser[14] was used to carry out molecular replacement and PimD (PDB: 2XBK) was used as the search model. Refinements were carried out using phenix.refine.[15] Data collection and refinement statistics are summarized in Table 2.1.

## RESULTS AND DISCUSSION

***Overall Structural Analysis of NysL***

Due to the unavailability of the substrate, 10-deoxynystatin, we were unable to solve a crystal structure of NysL bound to its substrate. We were able to solve and refine a 2 Å crystal structure of NysL bound to its product, nystatin. NysL crystal belongs to space group P $3_1$ 2 1 with a dimer in the asymmetric unit. The rms difference in Cα atoms of the two molecules is 0.269 Å and the two nystatin molecules bound to NysL is 0.493 Å. NysL exhibits the traditional triangular P450

fold (Figure 2.3) with the heme iron coordinated to the protein *via* a conserved cysteine (Cys343) present on the L helix. NysL hydroxylates the C10 of 10-deoxynystatin to form nystatin. In Figure 2.3, the C10-hydroxyl group is located 3.3 Å from the heme iron indicating the C10 is accurately placed for regio- and stereo-selective hydroxylation. Hence, the NysL-product complex is a true representation of NysL-substrate complex.

**Table 2.1** Crystallographic data collection and refinement statistics.

| **Parameter** | **NysL** |
|---|---|
| Wavelength (Å) | 0.9795 |
| Resolution range (Å) | 37.79 - 2.0 (2.072 - 2.0) |
| Space group | P $3_1$ 2 1 |
| Unit cell | 136.29 136.29 135.6 90 90 120 |
| Total reflections | 196494 (19470) |
| Unique reflections | 98252 (9735) |
| Multiplicity | 2.0 (2.0) |
| Completeness (%) | 99.65 (98.89) |
| Mean I/sigma(I) | 9.52 (2.41) |
| Wilson B-factor | 30.5 |
| R-merge | 0.02727 (0.2294) |
| R-meas | 0.03856 (0.3245) |
| R-pim | 0.02727 (0.2294) |
| CC1/2 | 0.999 (0.961) |
| CC* | 1 (0.99) |
| Reflections used in refinement | 97951 (9628) |
| Reflections used for R-free | 632 (62) |
| R-work | 0.1730 (0.2555) |
| R-free | 0.2054 (0.2316) |
| CC(work) | 0.968 (0.918) |
| CC(free) | 0.948 (0.950) |
| Number of non-hydrogen atoms | 7137 |
| macromolecules | 6103 |
| Ligands | 266 |
| Solvent | 768 |
| Protein residues | 782 |
| RMS(bonds, Å) | 0.007 |
| RMS(angles, degrees) | 1.14 |

| | |
|---|---|
| Ramachandran favored (%) | 97.42 |
| Ramachandran allowed (%) | 2.06 |
| Ramachandran outliers (%) | 0.52 |
| Rotamer outliers (%) | 2.74 |
| Clashscore | 3.63 |
| Average B-factor | 43.6 |
| macromolecules | 43.31 |
| Ligands | 42.12 |
| Solvent | 46.45 |

Values in () are for the highest resolution shell. Statistics generated by using the "Table 1" utility in Phenix.

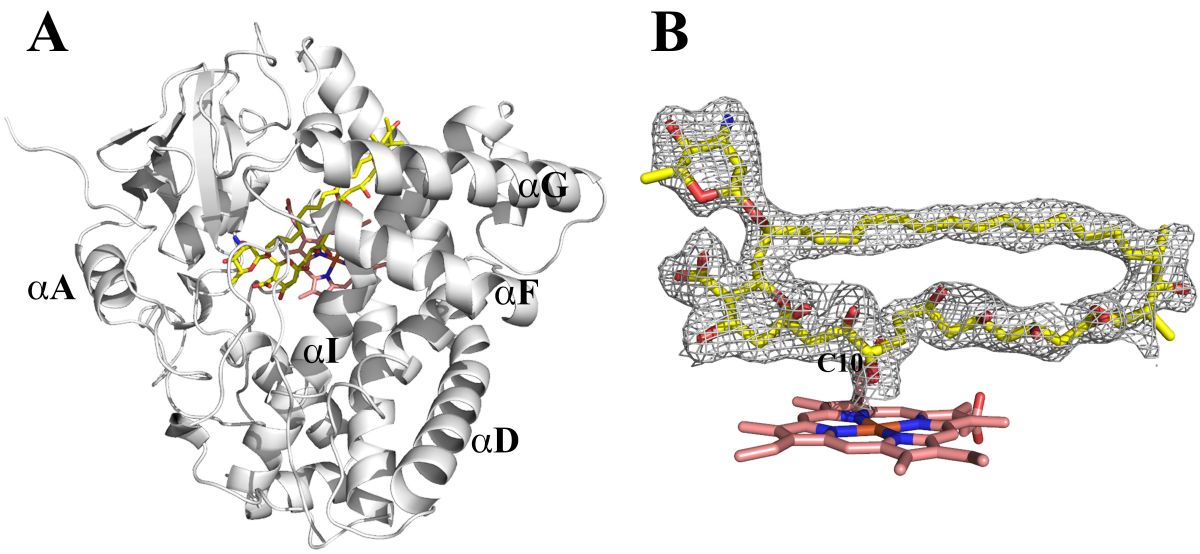


**Figure 2.3** Structure of NysL. A] NysL exhibits the traditional triangular P450 fold. B] $2F_o$-$F_c$ electron density map contoured at 1.0 σ with nystatin, the product of NysL. The C10 hydroxyl points towards the heme-iron at a distance of 3.3 Å.

***Substrate Access Channel***

Structurally, AmphL[10] and PimD[11] are very similar to NysL with a rms difference in Cα atoms being 0.664 Å and 0.880 Å, respectively. Similar to AmphL and PimD, NysL may use another channel that runs parallel to the I helix (channel 2, Figure 2.4)[10, 11] and not the entry near the F/G loop (channel 1) that is used by a majority of P450s.[16] Channel 2 has a wider opening and allows for the substrate to enter the active site along its elongated/long axis. This requires less

conformational changes/reorientation of the substrate compared to entry *via* channel 1.[10, 11] Hence, channel 2 is a more plausible substrate access channel.

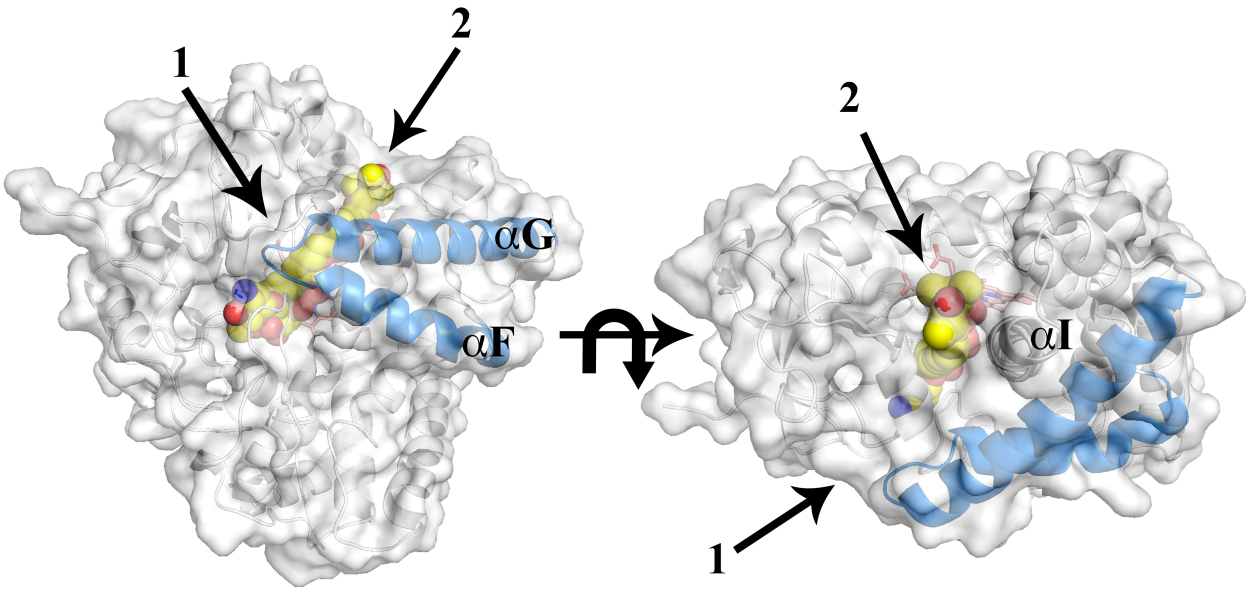


**Figure 2.4** Possible substrate access channels of NysL. Channel 1 is located near the F/G loop and is used by majority of P450s. This channel requires the large substrate to undergo large conformational changes to enter the active site. Channel 2, parallel to I helix, is used by NysL, AmphL and PimD. This channel helps the substrate to enter along the long axis without requiring much change in substrate orientation or protein conformation.

***Substrate-protein interactions***

Upon closer investigation of the active site, we can understand the interaction between NysL and its substrate. As in AmphL and PimD, the "back wall" of the binding cavity in NysL determines how deep the substrate can be buried in the active site pocket.[10, 11] This helps to precisely position the substrate over heme iron for catalysis. The mycosamine ring of nystatin H-bonds with the nearby Tyr85 whereas the hemiketal ring interacts with Lys277, Ser239, Ser281 and Ser384 (Figure 2.5). On the opposite end of the hemiketal and mycosamine rings, hydroxyl and methyl group on the macrolactone interacts with Arg221 (H-bond) and Ile225 (hydrophobic), respectively. The rest of the macroloactone core interacts with hydrophobic Phe (80, 103 and 231), Leu (81, 84 and 383) and Ala232 in the active site.

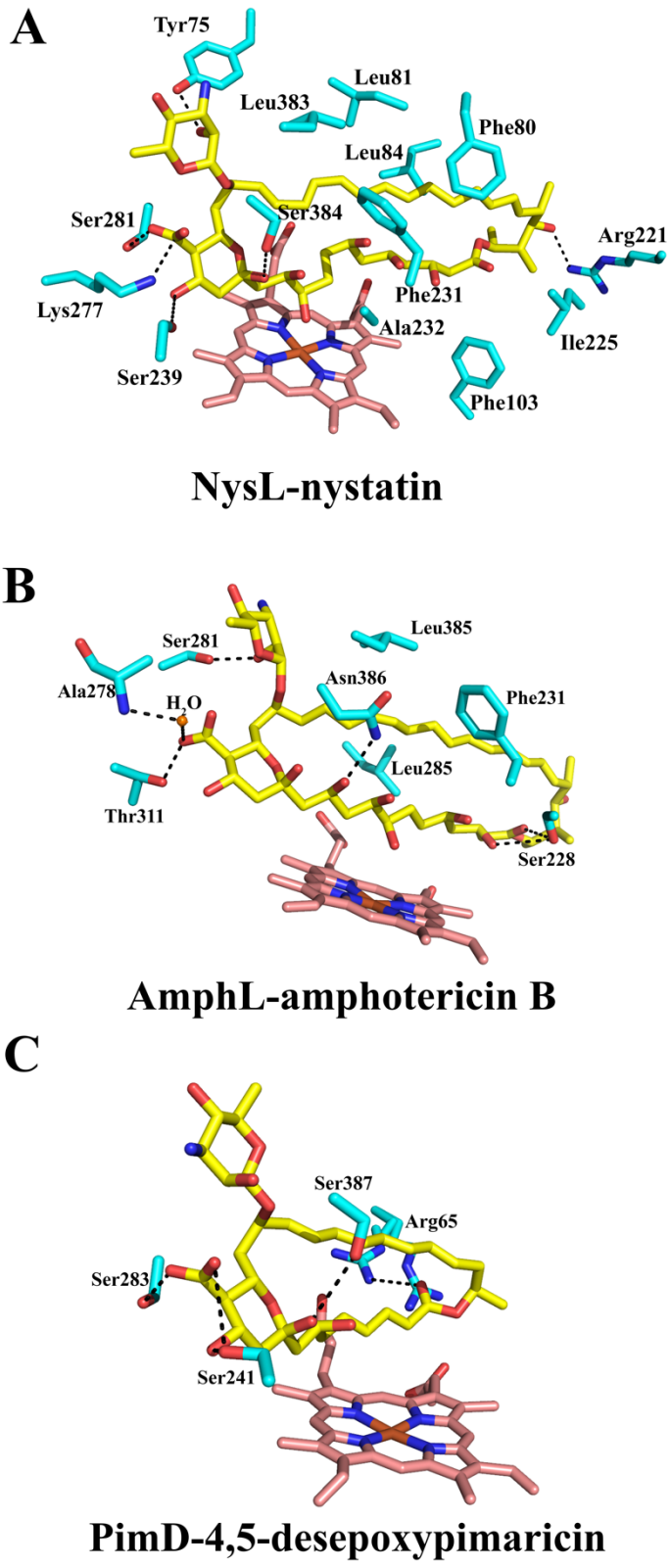


**Figure 2.5** Substrate-protein interactions in three closely related macrolide oxidizing P450s. The key residues involved in substrate interaction are shown in sticks and H-bonds are shown as black dashed lines. A] In NysL, Tyr75 interacts with the mycosamine while Lys277, Ser239, Ser281and Ser384 interacts with the hemiketal of nystatin. Other residues form hydrophobic interactions with the macrolactone ring. B] In AmphL (PDB: 7SHI), Ala278 forms a water bridge with the carboxyl group of the hemiketal. This less bulky residue (compared to Lys277 in NysL) enables the substrate, 8-deoxyamphotericin B, to be buried deeper into the active site positioning the C8 above heme iron. C] In PimD (PDB: 2XBK), interactions with substrate are similar to the one in NysL. Ser241 and Ser283 interacts with the hemiketal and. Ser387 and Arg65 interacts with macrolactone hydroxyls. Residues responsible for hydrophobic interaction with substrate aren't shown.

In AmphL, Ser281 of AmphL interacts with mycosamine moiety (Figure 2.5) of the substrate whereas Ser281 of NysL interacts with the hemiketal ring. A functionally equivalent Thr311 (Ser281 in NysL) interacts with the hemiketal in AmphL. Ser228 and Asn386 H-bonds with the hydroxyl groups on the macrolactone ring. The hydrophobic macrolactone ring interacts with hydrophobic Phe231, Leu285 and Leu385. All these interactions help position the substrate, 8-deoxyamphotericin B, in the active site of AmphL. Lys277 of NysL forms a salt bridge with the hemiketal carboxyl group. This residue is Ala278 in AmphL and the peptidyl amine forms a water bridge with the carboxyl group of the hemiketal. The bulkier Lys in NysL leads to a less deep burial of the substrate in the active site compared to AmphL. Therefore, C10 gets hydroxylated in NysL whereas it is C8 in AmphL.

In PimD, Ser241, Ser283 and Ser387 (Ser239, Ser281 and Ser384 in NysL) interact with the hemiketal ring of the substrate (Figure 2.5).[11] Arg65 interacts with carbonyl of the ester of the macrolactone ring on the opposite end of the two rings. This is similar to Arg221 interactions in NysL. Hence, similar interactions govern substrate binding in NysL and PimD. This makes it possible for C6 of 4,5-deseopxypimaricin to position right above the heme-iron in NysL for hydroxylation to form 6-hydroxy-4,5-deseopxypimaricin.[17]

***Catalytic Residues***

Identical to AmphL and PimD, NysL retains critical active site residues required for P450 $O_2$ activation.[10, 11] NysL has a Ser236 (Ser236 in AmphL and Ser238 in PimD) instead of a Thr as in majority of P450s (Thr252 in P450cam)[16] that is adjacent to $O_2$ coordinated to the heme iron. Ser is a good functional alternative to Thr as it would be difficult to accommodate substrate due to steric crowding with the larger Thr (Figure 2.6). Ser236 along with Asp235 (Asp235 in AmphL,

Asp237 in PimD and Asp251 in P450cam) forms part of a proton relay network required for $O_2$ activation.[18] Previous studies prove that NysL is able to catalyze *in vitro* conversion of 10-deoxynystatin to nystatin in the presence of spinach ferredoxin/ferredoxin reductase.[8] Hence, NysL follows the traditional P450 catalytic cycle without a strict requirement of a catalytic partner (unlike P450cam with a strict requirement for the native redox partners)[19].

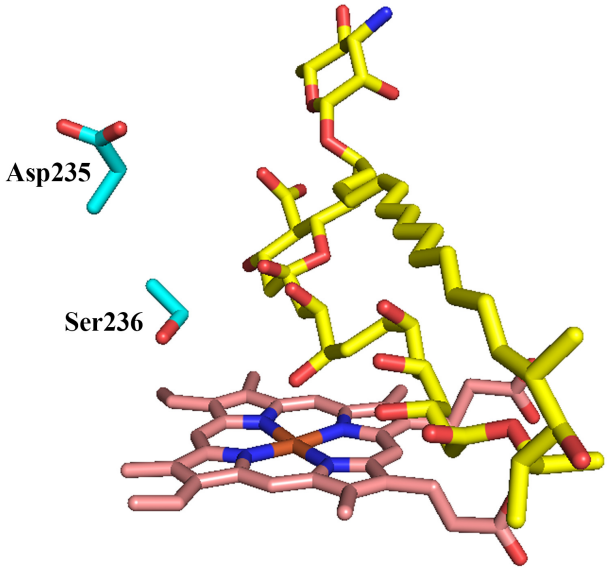


**Figure 2.6** Catalytic residues required for $O_2$ activation in NysL. Ser236 in NysL is functional equivalent of Thr252 in P450cam. Asp235 (Asp251 in P450cam) and Ser236 are responsible for proton relay network in $O_2$ activation.

## CONCLUSION

A detailed comparison of three closely related macrolide oxidizing P450s, NysL, AmphL and PimD, highlights the subtle differences in structure that lead to the precise positioning of substrate in the active site. Overall structural analyses of these three P450s supports the hypothesis that interactions at the back wall of the binding cavity with the two rings of the substrate is responsible for controlling how deeply the substrate will penetrate into the active site which plays a key role in positioning the correct carbon atom for oxidation. Ultimately, this knowledge will help to engineer P450s to produce antibiotics with different oxidation profiles and with different and, possibly, better pharmacological activities.

**REFERENCES**


1. Newman, D. J.; Cragg, G. M., Natural products as sources of new drugs over the last 25 years. *J Nat Prod* **2007,** *70* (3), 461-77.

2. Caffrey, P.; De Poire, E.; Sheehan, J.; Sweeney, P., Polyene macrolide biosynthesis in streptomycetes and related bacteria: recent advances from genome sequencing and experimental studies. *Appl Microbiol Biotechnol* **2016,** *100* (9), 3893-908.

3. Aparicio, J. F.; Caffrey, P.; Gil, J. A.; Zotchev, S. B., Polyene antibiotic biosynthesis gene clusters. *Appl Microbiol Biotechnol* **2003,** *61* (3), 179-88.

4. Bolard, J., How do the polyene macrolide antibiotics affect the cellular membrane properties? *Biochim Biophys Acta* **1986,** *864* (3-4), 257-304.

5. Byrne, B.; Carmody, M.; Gibson, E.; Rawlings, B.; Caffrey, P., Biosynthesis of deoxyamphotericins and deoxyamphoteronolides by engineered strains of Streptomyces nodosus. *Chem Biol* **2003,** *10* (12), 1215-24.

6. Zotchev, S. B., Polyene macrolide antibiotics and their applications in human therapy. *Curr Med Chem* **2003,** *10* (3), 211-23.

7. Bruheim, P.; Borgos, S. E.; Tsan, P.; Sletta, H.; Ellingsen, T. E.; Lancelin, J. M.; Zotchev, S. B., Chemical diversity of polyene macrolides produced by Streptomyces noursei ATCC 11455 and recombinant strain ERD44 with genetically altered polyketide synthase NysC. *Antimicrob Agents Chemother* **2004,** *48* (11), 4120-9.

8. Volokhan, O.; Sletta, H.; Ellingsen, T. E.; Zotchev, S. B., Characterization of the P450 monooxygenase NysL, responsible for C-10 hydroxylation during biosynthesis of the polyene macrolide antibiotic nystatin in Streptomyces noursei. *Appl Environ Microbiol* **2006,** *72* (4), 2514-9.

9. Brautaset, T.; Sekurova, O. N.; Sletta, H.; Ellingsen, T. E.; StrLm, A. R.; Valla, S.; Zotchev, S. B., Biosynthesis of the polyene antifungal antibiotic nystatin in Streptomyces noursei ATCC 11455: analysis of the gene cluster and deduction of the biosynthetic pathway. *Chem Biol* **2000,** *7* (6), 395-403.

10. Amaya, J. A.; Lamb, D. C.; Kelly, S. L.; Caffrey, P.; Murarka, V. C.; Poulos, T. L., Structural analysis of P450 AmphL from Streptomyces nodosus provides insights into substrate selectivity of polyene macrolide antibiotic biosynthetic P450s. *J Biol Chem* **2022,** *298* (4), 101746.

11. Kells, P. M.; Ouellet, H.; Santos-Aberturas, J.; Aparicio, J. F.; Podust, L. M., Structure of cytochrome P450 PimD suggests epoxidation of the polyene macrolide pimaricin occurs *via* a hydroperoxoferric intermediate. *Chem Biol* **2010,** *17* (8), 841-51.

12. Madeira, F.; Pearce, M.; Tivey, A. R. N.; Basutkar, P.; Lee, J.; Edbali, O.; Madhusoodanan, N.; Kolesnikov, A.; Lopez, R., Search and sequence analysis tools services from EMBL-EBI in 2022. *Nucleic Acids Res* **2022,** *50* (W1), W276-W279.

13. Kabsch, W., Xds. *Acta Crystallogr D Biol Crystallogr* **2010,** *66* (Pt 2), 125-32.

14. McCoy, A. J.; Grosse-Kunstleve, R. W.; Adams, P. D.; Winn, M. D.; Storoni, L. C.; Read, R. J., Phaser crystallographic software. *J Appl Crystallogr* **2007,** *40* (Pt 4), 658-674.

15. Adams, P. D.; Afonine, P. V.; Bunkoczi, G.; Chen, V. B.; Echols, N.; Headd, J. J.; Hung, L. W.; Jain, S.; Kapral, G. J.; Grosse Kunstleve, R. W.; McCoy, A. J.; Moriarty, N. W.; Oeffner, R. D.; Read, R. J.; Richardson, D. C.; Richardson, J. S.; Terwilliger, T. C.; Zwart, P. H., The Phenix software for automated determination of macromolecular structures. *Methods* **2011,** *55* (1), 94-106.

16. Poulos, T. L., Heme enzyme structure and function. *Chem Rev* **2014,** *114* (7), 3919-62.

17. Santos-Aberturas, J.; Engel, J.; Dickerhoff, J.; Dörr, M.; Rudroff, F.; Weisz, K.; Bornscheuer, U. T., Exploration of the substrate promiscuity of biosynthetic tailoring enzymes as a new source of structural diversity for polyene macrolide antifungals. *ChemCatChem* **2015,** *7* (3), 490-500.

18. Gerber, N. C.; Sligar, S. G., A role for Asp-251 in cytochrome P-450cam oxygen activation. *Journal of Biological Chemistry* **1994,** *269* (6), 4260-4266.

19. Tripathi, S.; Li, H.; Poulos, T. L., Structural basis for effector control and redox partner recognition in cytochrome P450. *Science* **2013,** *340* (6137), 1227-30.

# Chapter 3

## Biosynthesis of a new skyllamycin analogue in *Streptomyces nodosus*: structure of a cytochrome P450 that forms an epoxide in the cinnamoyl chain


### SUMMARY

Activation of a silent cluster in *Streptomyces nodosus* leads to synthesis of a skyllamycin-like cinnamoyl-containing peptide (CCNP). Our collaborators isolated this novel CCNP and determined its structure using mass spectrometry and nuclear magnetic resonance (NMR) spectroscopy. The isolated compound is an oxidized skyllamycin A with the additional oxygen atom incorporated as an epoxide in the cinnamoyl side-chain. Gene deletion studies indicate that a cytochrome P450 encoding gene located within the *S. nodosus* cluster is responsible for epoxidation. A 1.43 Å crystal structure was solved of this epoxide-forming P450sky2. This is the first structure for a P450 that forms an epoxide in a substituted cinnamoyl chain of a lipopeptide. These results add to knowledge of bioactive CCNP biosynthesis and helps engineer enzymatic synthesis of valuable chiral epoxides that are of pharmaceutical importance.


*[The work described in this chapter is based on Thomas Poulos – David Lamb – Patrick Caffrey collaboration. I'm a co-author on the manuscript in preparation as a result of this collaboration. My contribution includes spectral characterization, solving crystal structure of P450sky2 and modeling skyllamycin A molecule in the active site of P450sky2.]*

### INTRODUCTION

The diversity in biological activities of cinnamoyl acyl chain substituted non-ribosomal lipopeptides (CCNPs) has led to an increase in their scientific interest.[1-9] They have a potential as anticancer drugs,[10] antibiotics[4] and biofilm-dispersing agents.[11] Biosynthesis of the substituted cinnamate requires the following enzymes: a highly reducing type II polyketide synthase (PKS)

composed of discrete acyl carrier proteins (ACPs), ketosynthase, ketoreductase and, dehydratase enzymes. The assembly begins with construction of an acyl chain containing a series of conjugated *trans* double bonds. An isomerase converts one of the *trans* double bonds to the *cis* isomer which enables formation of an aromatic ring *via* an electrocyclization.[9]

After assembly, the completed cinnamoyl chain is transferred from the discrete ACP onto the first module of a non-ribosomal peptide synthetase (NRPS). The cinnamoyl chain is attached to the first activated amino acid and the NRPS assembly line synthesizes a lipopeptidyl thioester that is cyclized to give the final lipopeptide or lipodepsipeptide.

While all CCNPs feature ortho-substituted cinnamates, slight differences between PKS systems give variations in chain length, functionalization, and double bond geometry. The peptide macrocycle and structure of the cinnamoyl chain is said to govern the biological activities of CCNPs.[12] Some recent studies indicate that P450s are responsible for modification of the cinnamoyl chains.[4, 13] This highlights the importance of P450s in the functionalization of natural scaffold for various biological activities.

One of the best-studied CCNPs is a complex propenyl-cinnamoyl-containing cyclodepsipeptide, skyllamycin A (Figure 3.1). It was first isolated from *Streptomyces sp.* KY 117842[10] and later on reisolated from *Streptomyces sp.* Acta 2897.[14] It inhibits platelet-derived growth factor (PGDF) signalling pathway in tumor cells and in turn has an anti-cancer effect.[10] The biosynthetic pathway to produce skyllamycin A has been studied in detail[14] and its structure with absolute configuration of amino acids has been determined.[15] Recently, Giltrap et al. were able to achieve the total synthesis of skyllamycins.[16, 17]

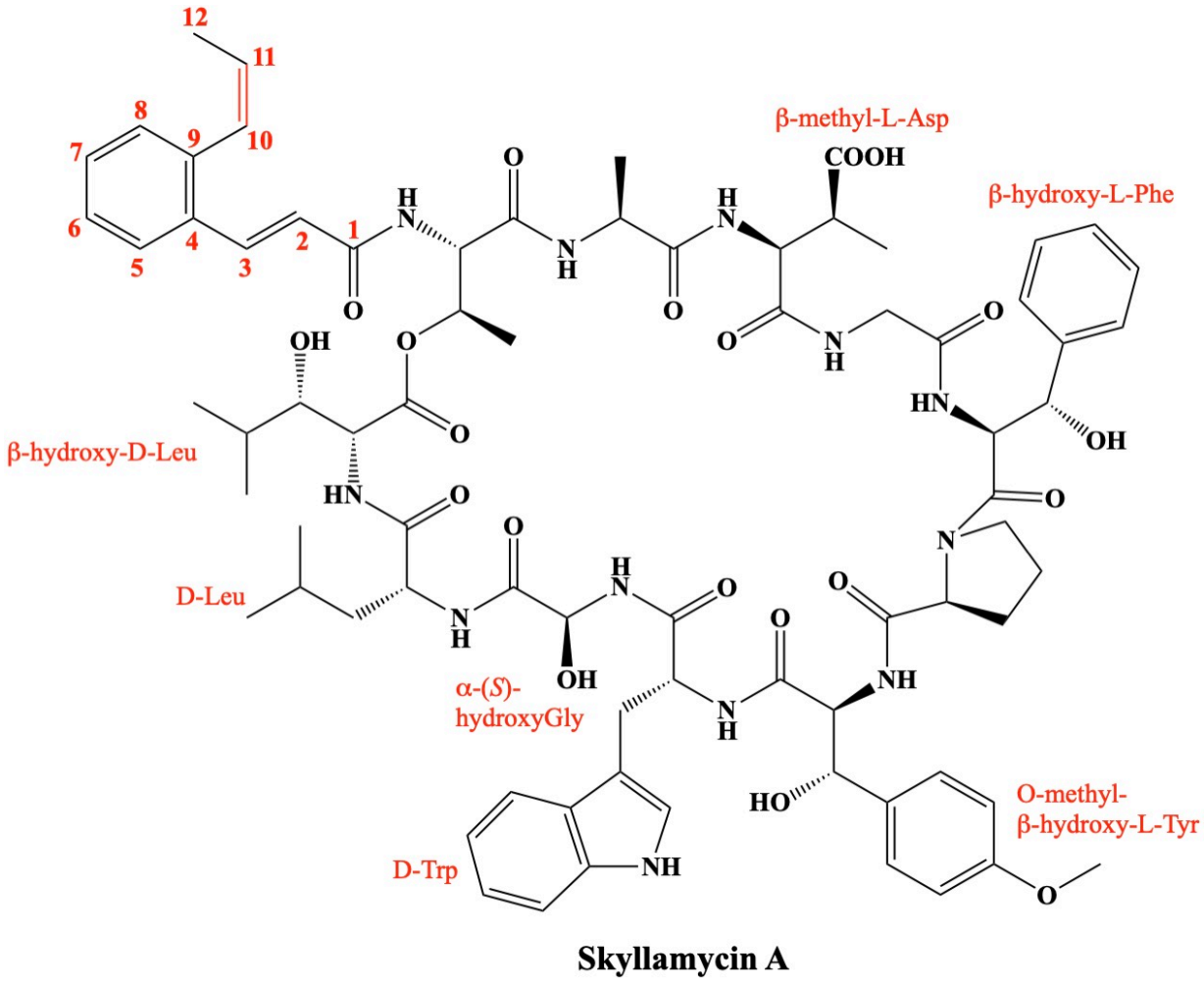


**Figure 3.1** Structure of skyllamycin A. The carbon atoms of the propenyl-cinnamoyl chain are numbered 1 to 12. Non-standard amino acid residues are labelled.

The sequence of peptidyl thioester of skyllamycin A prior to cyclization is: propenylcinnamoyl-L-Thr-L-Ala-β-methyl-L-Asp-Gly-β-hydroxy-L-Phe-L-Pro-O-methyl-β-hydroxy-L-Tyr-D-Trp-α-hydroxy-Gly-D-Leu-β-hydroxy-L-Leu. A glutamate mutase encoded in the BCG forms the β-methyl-L-Asp.[14] The β-hydroxy- L-Phe, O-methyl-β-hydroxy- L-Tyr, and β-hydroxy-L-Leu residues are formed by a single cytochrome P450sky (CYP163B3) that catalyses stereospecific β-hydroxylation of aminoacyl building blocks which are thioester-linked to peptidyl carrier protein domains within the NRPS.[18, 19] A two-component flavin-dependent monooxygenase catalyses the

formation of unusual α-(*S*)-hydroxyglycine residue.[14, 15] Standard epimerase domains which are a part of NRPS modules generate D-Trp and D-Leu residues.[14] The chain terminating bifunctional thioesterase (TE) has both epimerization and cyclization activity.[20] It forms the final β-hydroxy-D-leucine residue from its L-isomer prior to macrolactonization.[20]

*Streptomyces nodosus*, famously known to produce amphotericin B, has a chromosomal region that is almost identical to biosynthetic gene cluster (BGC) for skyllamycin A.[21] It is a silent cluster which upon activation produces a lipopeptide with a molecular mass of 1498.6 g $mol^{-1}$. It is 16 mass units greater than skyllamycin A indicating that the new lipopeptide contains an extra oxygen atom.[21] Closer investigation of the cluster highlighted a gene (SNOD_28885[21] or CP978_29155[22]) that encodes a cytochrome P450sky2 which has no analogue in the well-defined skyllamycin producer *Streptomyces sp* Acta 2897.[14, 21] These observations indicate that P450sky2 inserts an extra oxygen atom as a hydroxyl or epoxide group at an unknown position during biosynthesis of this lipopeptide analogue.[21]

To investigate further, our collaborators carried out purification and further structural analysis of the *S. nodosus* skyllamycin, oxy-skyllamycin. They confirmed that it contains an epoxide in the substituted cinnamoyl side chain (unpublished data). Since we are collaborators on this project, we obtained a high-resolution X-ray crystal structure of P450sky2 to understand the structure-function relationship of the enzyme catalysis. The epoxide-forming P450sky2 has the potential for production of chiral epoxides during chemical synthesis of molecules of pharmaceutical importance.

## EXPERIMENTAL PROCEDURE

### *Purification of oxy-skyllamycin analogue, Mass spectrometry, NMR spectroscopy, P450sky2 gene deletion study and P450sky2 cloning*

Performed by our collaborators.

### *P450sky2 expression, purification, and spectral characterization*

The plasmid containing the gene for P450sky2 was transformed into *E. coli* C41 (DE3) cells. A single transformant colony was used to inoculate Luria-Bertani media containing 50 μg/mL kanamycin and grown overnight at 37 ºC and 220 rpm. About 10 mL of overnight culture was added to 1L Terrific Broth media supplemented with 50 μg/mL kanamycin, 125 μg/mL thiamine and trace metals. Cultures were grown at 37 °C and 200 rpm. When the culture reached $A_{600}$ ~ 1.5, the temperature was reduced to 25 °C and induced with 1 mM isopropyl 1-thio-D-galactopyranoside. To increase synthesis of heme, the prosthetic group for P450sky2, 30 μg/mL δ-aminolevulinic acid was added to each flask. The cells were grown for 48 hours and harvested by centrifugation.

Cell pellets were resuspended in buffer A (50 mM potassium phosphate buffer pH 7.5, 100 mM NaCl and 10 mM imidazole) and lysed using microfluidizer. This lysate was then centrifuged at 15,000 rpm for 1 hour at 4 °C. The supernatant was loaded on a previously equilibrated $Ni^{2+}$-nitrilotriacetic acid agarose column and was washed with buffer A containing 35 mM imidazole. The protein was eluted with buffer A containing 200 mM imidazole. The eluted protein was concentrated, and buffer exchanged into buffer B (50 mM potassium phosphate buffer pH 7.5 and 100 mM NaCl). The protein was further purified using S200 Sephacryl column in buffer B. A Cary 300 UV-visible spectrophotometer was used to record UV-visible spectra at room

temperature. P450sky2 concentration was determined using molar extinction coefficient ($\varepsilon_{418}$) of 115 $mM^{-1}cm^{-1}$ for the low-spin oxidized form.

***P450sky2 crystallization***

To determine crystallization condition, high-throughput crystal screening was done using MCGS2 kit from Anatrace at room temperature. A SPT labtech Mosquito robot was used to dispense 300 nL drops of 30 mg/mL of P450sky2 and screening solution and mixed in a 1:1 ratio. These were then equilibrated against 100 μL of the screening solution at room temperature. Crystals were observed in wells containing 0.2 M ammonium acetate, 0.1 M Tris:HCl buffer pH 8.5 and 25% w/v PEG 3350. Crystals were transferred to cryoprotectant buffer consisting of 0.2 M ammonium acetate, 0.1 M Tris:HCl buffer pH 8.5, 25% w/v PEG 3350 and 25% (v/v). glycerol, mounted on nylon loops and flash frozen using liquid nitrogen.

Diffraction data were collected at the Stanford Synchrotron Radiation beamline 12-2. XDS[23] or iMOSFLM[24] was used to index and integrate the raw data, and Aimless[25] was used for scaling. The structure was determined by molecular replacement with Phaser[26] and cytochrome P450 PksS (PDB: 4YZR) as the search model. Phenix[27] was used to carry out further refinements.

## RESULTS AND DISCUSSION

***Structure of oxy-skyllamycin A (Collaborator's work)***

The structure of oxy-skyllamycin A was determined by our collaborators. It is a skyllamycin A with a the C10-C11 epoxide in the cinnamoyl chain (unpublished data, Figure 3.2). Deletion of gene encoding P450sky2 resulted in skyllamycin A formation. This confirms that P450sky2 is responsible for formation of oxy-skyllamycin A (unpublished data).

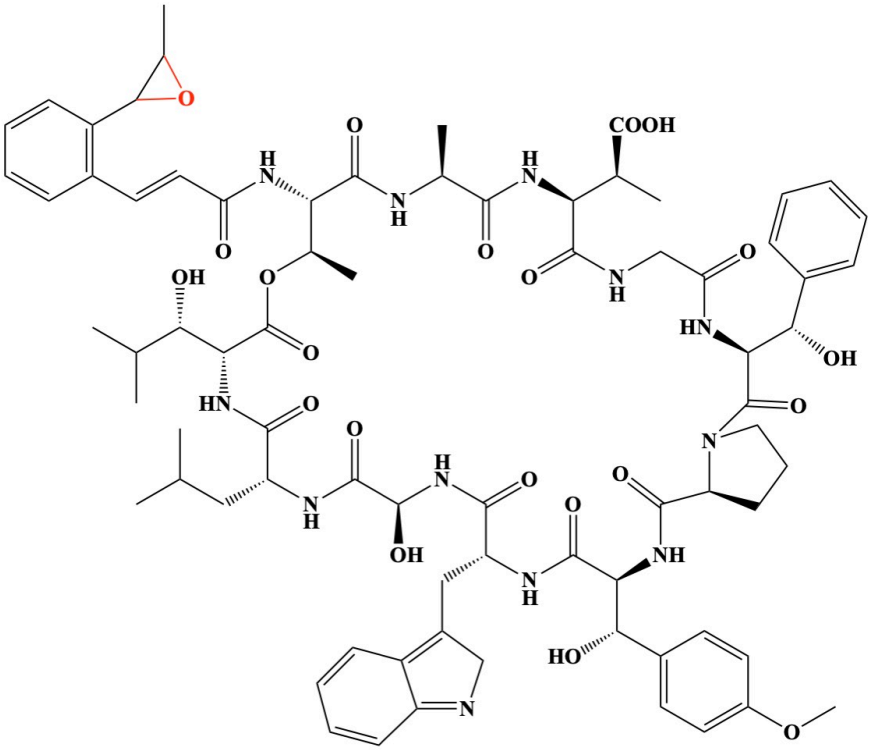


**Figure 3.2** Structure of oxy-skyllamycin from *S. nodosus*. The molecule is identical to skyllamycin A except for the C10-C11 epoxide in the cinnamoyl chain.

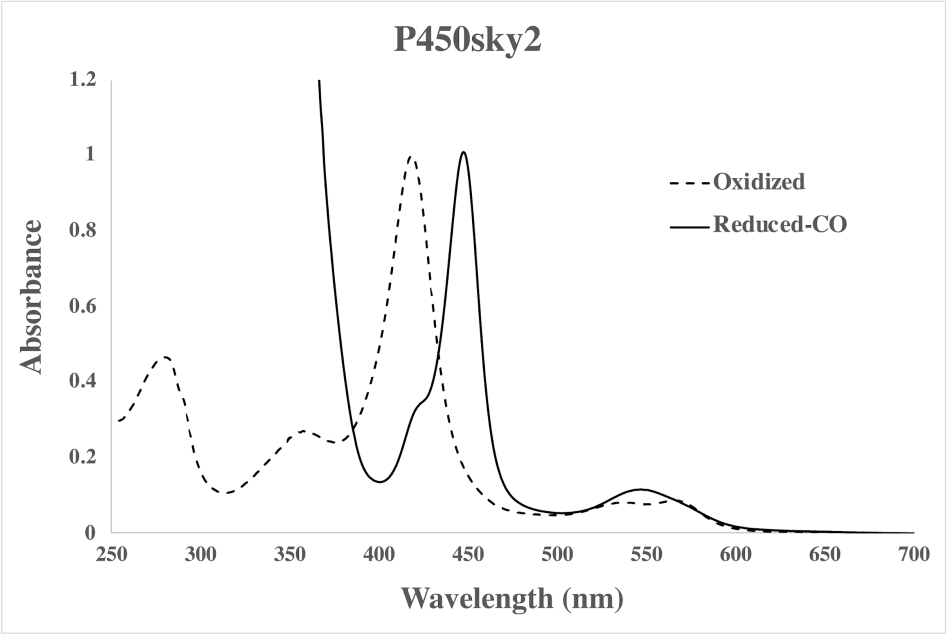


**Figure 3.3** Absolute UV-visible spectra of 8.7 µM substrate-free P450sky2 in 50 mM potassium phosphate buffer pH 7.5. As expected, a low-spin spectrum is observed for oxidized substrate-free protein. Upon bubbling with CO followed by sodium dithionite reduction, characteristic P450 band is formed with a fraction of P420. Formation of P420 in substrate-free P450s is not uncommon.

***P450sky2 overproduction and characterization***

The P450sky2 enzyme was overproduced in *E. coli* and purified as detailed in Experimental Procedures. The UV-visible spectrum of oxidized P450sky2 (Figure 3.3) has a characteristic low-spin Soret absorption at 418 nm, and α- and β- bands at 566 nm and 538 nm, respectively. The reduced-CO spectrum displays a characteristic P450 band with a Soret at 447 nm.

***Overall P450sky2 structural analysis***

The P450sky2 crystal structure was solved and refined at 1.43 Å (Table 1). Crystals belong to space group P 1 $2_1$ 1 with a monomer in the asymmetric unit. P450sky2 exhibits the traditional P450 triangular fold (Figure 3.4A). The heme iron is axially coordinated to the protein with a conserved cysteine (Cys354). The heme is sandwiched between the I and L helices. Right on top of I helix are the F and G helices which are connected by FG loop and form a wide-open active site. This disordered loop has a few missing amino acids.

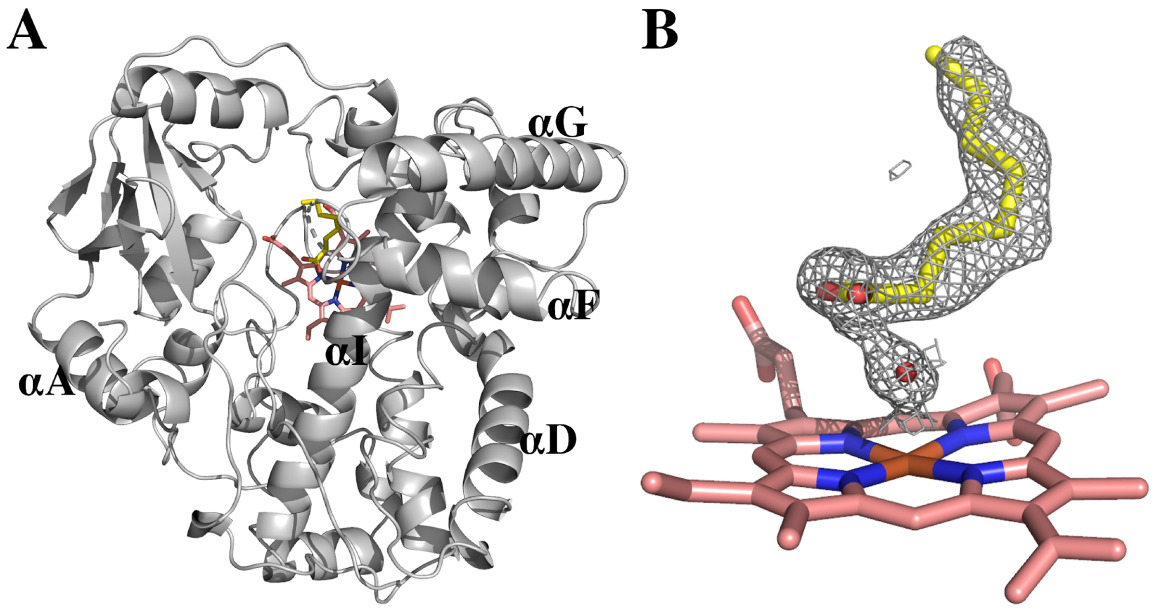


**Figure 3.4** Crystal structure of P450sky2. (A) P450sky2 exhibits the traditional P450 triangular fold consisting of α-helical and β-sheet domains which is observed in other P450s. (B) $2F_o$-$F_c$ electron density map contoured at 1.0σ with water-bound hexacoordinated iron heme and octanoic acid in the active site.

**Table 3.1** P450sky2 X-ray crystallography data collection and refinement statistics.

| **Parameter** | **P450sky2** |
|---|---|
| PDB ID | 8FZ8 |
| Wavelength (Å) | 0.97946 |
| Resolution range (Å) | 35.84 - 1.43 (1.481 - 1.43) |
| Space group | P 1 21 1 |
| Unit cell (Å and degrees) | 35.98 97.8501 52.5 90 95.12 90 |
| Total reflections | 253782 (25702) |
| Unique reflections | 64328 (6466) |
| Multiplicity | 3.9 (4.0) |
| Completeness (%) | 96.44 (97.29) |
| Mean I/sigma(I) | 11.94 (2.90) |
| Wilson B-factor | 15.55 |
| R-merge | 0.05438 (0.366) |
| R-meas | 0.06255 (0.4233) |
| R-pim | 0.0303 (0.209) |
| CC1/2 | 0.998 (0.896) |
| CC* | 1 (0.972) |
| Reflections used in refinement | 64284 (6465) |
| Reflections used for R-free | 2000 (201) |
| R-work | 0.1633 (0.2139) |
| R-free | 0.1826 (0.2532) |
| CC(work) | 0.969 (0.906) |
| CC(free) | 0.973 (0.874) |
| Number of non-hydrogen atoms | 3680 |
| Macromolecules | 3212 |
| Ligands | 54 |
| Solvent | 414 |
| Protein residues | 391 |
| RMS(bonds, Å) | 0.006 |
| RMS(angles, degrees) | 0.9 |
| Ramachandran favored (%) | 97.67 |
| Ramachandran allowed (%) | 1.81 |
| Ramachandran outliers (%) | 0.52 |
| Rotamer outliers (%) | 0.28 |
| Clashscore | 4.08 |
| Average B-factor | 22.33 |
| Macromolecules | 21.2 |

| | |
|---|---|
| Ligands | 16.45 |
| Solvent | 31.9 |

Value in () are the statistics for highest resolution shell. Statistics generated by using the "Table 1" utility in Phenix.

A water molecule, at a distance of 2.3 Å, is coordinated to the heme iron (Figure 3.4B) which is characteristic of a substrate-free P450. Upon closer investigation of the active site, a long continuous Y-shaped electron density above this water molecule was observed. This is clearly a fatty acid molecule from *Escherichia coli* cells[28] with the 16-carbon palmitic acid being the most likely candidate. However, only eight carbons could be modelled so octanoic acid was used in the refinement (Figure 3.4B) with the carboxylate group close to the water coordinated heme iron. The distance between heme iron and carboxylate oxygen of octanoic acid is 4.1 Å. The presence of similarly positioned fatty acid in the active site has been found in other P450 structures.[29, 30] This very likely has no functional significance. Rather, the open mostly hydrophobic substrate access channel can bind a variety of nonpolar molecules and in this case it is a fatty acid.

***Modeling skyllamycin A – P450sky2 complex***

Considerable effort will be required to investigate fully the enzymatic activity of P450sky2 *in vitro*. It is unclear whether the natural substrate is skyllamycin A, or an early intermediate such as propenyl-cinnamoyl-ACP (Figure 3.5). At present these potential substrates are unavailable in sufficient quantity. It was possible to model skyllamycin A into the wide-open active site cavity of P450sky2 (Figure 3.6A) using Pymol (pymol.org). 4,5-De-epoxypimaricin bound PimD[31] (PDB: 2XBK) was used as the starting model because PimD, like P450sky2, epoxidizes its substrate. C10-C11 of skyllamycin A was aligned with C4-C5 of 4,5-de-epoxypimaricin in the active site. The distance between the heme iron and modelled C10-C11 of skyllamycin A is 4 Å and 5 Å,

respectively (Figure 3.6B). As shown in Figure 3.6A, the whole molecule of skyllamycin A (spheres) fits well in the active site of P450sky2 suggesting that skyllamycin A itself can enter the protein and form oxy-skyllamycin upon catalysis. Since the substrate was modelled in the open structure of P450sky2, we cannot say at this time that this is true representation of a protein-substrate complex since P450s can undergo substantial structural changes when substrate binds.

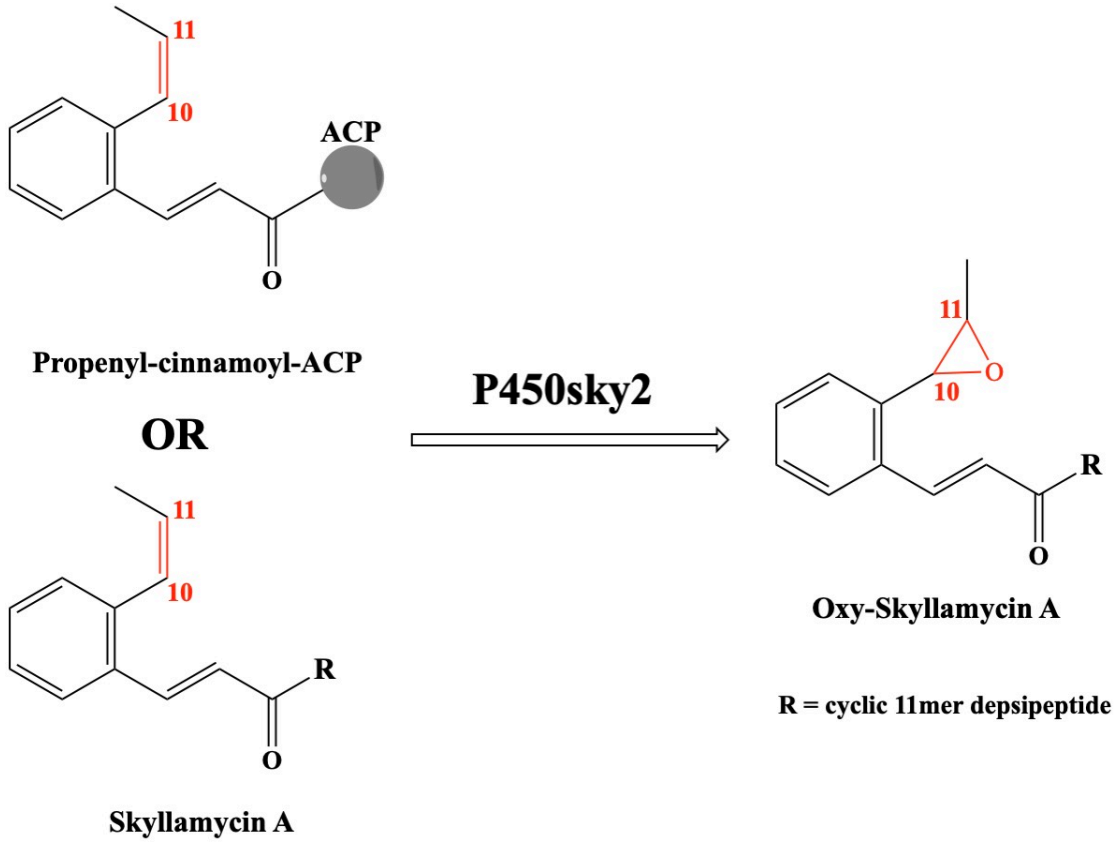


**Figure 3.5** P450sky2 reaction. The substrate can be skyllamycin A or an early intermediate like propenyl-cinnamoyl-ACP.

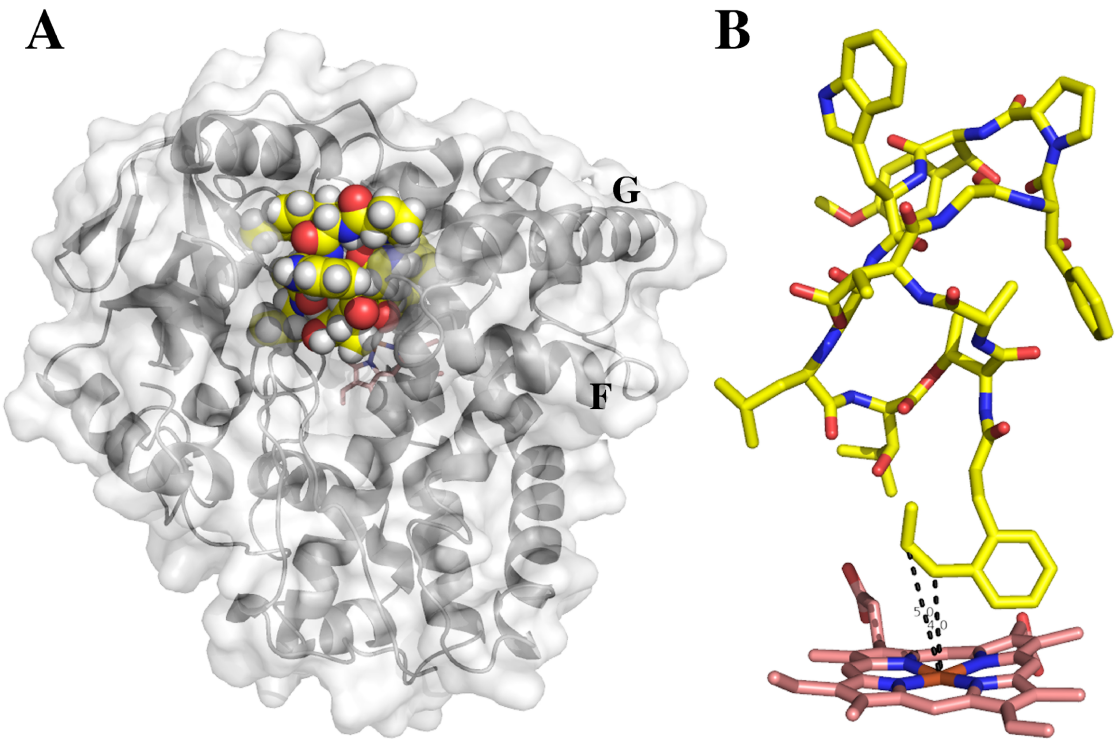


**Figure 3.6** Skyllamycin A modelled into the P450sky2 structure. (A) P450sky2 exhibits a wide active site cavity in which skyllamycin A (spheres) can be readily docked. (B) Distance between heme iron and modeled C10-C11 of skyllamycin A is 4 Å and 5 Å, respectively.

## CONCLUSION

Our collaborators determined the structure of oxy-skyllamycin, a new skyllamycin from the amphotericin B producer, *S. nodosus*. This is the sixth naturally occurring skyllamycin to be identified and could be named skyllamycin F. However, it is yet to be determined how the epoxidation of cinnamoyl chain changes the biological activity of the molecule.

This work also reveals the structure and function of P450sky2 as an epoxide-forming enzyme. Molecular modelling indicates that skyllamycin A can associate with the P450 in a pose that orientates its propenyl substituent towards the heme co-factor. This suggests that

direct epoxidation of the peptide-linked propenyl-cinnamate may be the mechanism for the formation of oxy-skyllamycin A .

Naturally occurring CYP119 from *Sulfolobus acidocaldarius* and other engineered P450s catalyse epoxidation of several substituted styrenes with high enantiomeric selectivity.[32-34] The P450sky2 structure is the first for a P450 that forms a C10-C11 epoxide in a substituted cinnamoyl chain. This should help with protein engineering to design epoxidases that act on substituted styrene to form chiral epoxides. This is useful for synthesis of valuable pharmaceuticals and fine chemicals.

**REFERENCES**


1. Bae, M.; Kim, H.; Moon, K.; Nam, S. J.; Shin, J.; Oh, K. B.; Oh, D. C., Mohangamides A and B, new dilactone-tethered pseudo-dimeric peptides inhibiting Candida albicans isocitrate lyase. *Org Lett* **2015,** *17* (3), 712-5.

2. Hashimoto, M.; Hayashi, K.; Murai, M.; Fujii, T.; Nishikawa, M.; Kiyoto, S.; Okuhara, M.; Kohsaka, M.; Imanaka, H., WS9326A, a novel tachykinin antagonist isolated from Streptomyces violaceusniger no. 9326. II. Biological and pharmacological properties of WS9326A and tetrahydro-WS9326A (FK224). *J Antibiot (Tokyo)* **1992,** *45* (7), 1064-70.

3. Karim, M. R. U.; In, Y.; Zhou, T.; Harunari, E.; Oku, N.; Igarashi, Y., Nyuzenamides A and B: Bicyclic Peptides with Antifungal and Cytotoxic Activity from a Marine-Derived Streptomyces sp. *Org Lett* **2021,** *23* (6), 2109-2113.

4. Liu, Q.; Liu, Z.; Sun, C.; Shao, M.; Ma, J.; Wei, X.; Zhang, T.; Li, W.; Ju, J., Discovery and Biosynthesis of Atrovimycin, an Antitubercular and Antifungal Cyclodepsipeptide Featuring Vicinal-dihydroxylated Cinnamic Acyl Chain. *Org Lett* **2019,** *21* (8), 2634-2638.

5. Omura, S.; Van der Pyl, D.; Inokoshi, J.; Takahashi, Y.; Takeshima, H., Pepticinnamins, new farnesyl-protein transferase inhibitors produced by an actinomycete. I. Producing strain, fermentation, isolation and biological activity. *J Antibiot (Tokyo)* **1993,** *46* (2), 222-8.

6. Sun, C.; Yang, Z.; Zhang, C.; Liu, Z.; He, J.; Liu, Q.; Zhang, T.; Ju, J.; Ma, J., Genome Mining of Streptomyces atratus SCSIO ZH16: Discovery of Atratumycin and Identification of Its Biosynthetic Gene Cluster. *Org Lett* **2019,** *21* (5), 1453-1457.

7. Um, S.; Park, S. H.; Kim, J.; Park, H. J.; Ko, K.; Bang, H. S.; Lee, S. K.; Shin, J.; Oh, D. C., Coprisamides A and B, new branched cyclic peptides from a gut bacterium of the dung beetle Copris tripartitus. *Org Lett* **2015,** *17* (5), 1272-5.

8. Yu, Z.; Vodanovic-Jankovic, S.; Kron, M.; Shen, B., New WS9326A congeners from Streptomyces sp. 9078 inhibiting Brugia malayi asparaginyl-tRNA synthetase. *Org Lett* **2012,** *14* (18), 4946-9.

9. Zhu, J.; Zhang, S.; Zechel, D. L.; Paululat, T.; Bechthold, A., Rational Design of Hybrid Natural Products by Utilizing the Promiscuity of an Amide Synthetase. *ACS Chem Biol* **2019,** *14* (8), 1793-1801.

10. Toki, S.; Agatsuma, T.; Ochiai, K.; Saitoh, Y.; Ando, K.; Nakanishi, S.; Lokker, N. A.; Giese, N. A.; Matsuda, Y., RP-1776, a novel cyclic peptide produced by Streptomyces sp., inhibits the binding of PDGF to the extracellular domain of its receptor. *J Antibiot (Tokyo)* **2001,** *54* (5), 405-14.

11. Navarro, G.; Cheng, A. T.; Peach, K. C.; Bray, W. M.; Bernan, V. S.; Yildiz, F. H.; Linington, R. G., Image-based 384-well high-throughput screening method for the discovery of skyllamycins A to C as biofilm inhibitors and inducers of biofilm detachment in Pseudomonas aeruginosa. *Antimicrob Agents Chemother* **2014,** *58* (2), 1092-9.

12. Yang, Z.; Sun, C.; Liu, Z.; Liu, Q.; Zhang, T.; Ju, J.; Ma, J., Production of Antitubercular Depsipeptides *via* Biosynthetic Engineering of Cinnamoyl Units. *J Nat Prod* **2020,** *83* (5), 1666-1673.

13. Shi, J.; Liu, C. L.; Zhang, B.; Guo, W. J.; Zhu, J.; Chang, C. Y.; Zhao, E. J.; Jiao, R. H.; Tan, R. X.; Ge, H. M., Genome mining and biosynthesis of kitacinnamycins as a STING activator. *Chem Sci* **2019,** *10* (18), 4839-4846.

14. Pohle, S.; Appelt, C.; Roux, M.; Fiedler, H. P.; Sussmuth, R. D., Biosynthetic gene cluster of the non-ribosomally synthesized cyclodepsipeptide skyllamycin: deciphering unprecedented ways of unusual hydroxylation reactions. *J Am Chem Soc* **2011,** *133* (16), 6194-205.

15. Schubert, V.; Di Meo, F.; Saaidi, P. L.; Bartoschek, S.; Fiedler, H. P.; Trouillas, P.; Sussmuth, R. D., Stereochemistry and conformation of skyllamycin, a non-ribosomally synthesized peptide from Streptomyces sp. Acta 2897. *Chemistry* **2014,** *20* (17), 4948-55.

16. Giltrap, A. M.; Haeckl, F. P. J.; Kurita, K. L.; Linington, R. G.; Payne, R. J., Total Synthesis of Skyllamycins A-C. *Chemistry* **2017,** *23* (60), 15046-15049.

17. Giltrap, A. M.; Haeckl, F. P. J.; Kurita, K. L.; Linington, R. G.; Payne, R. J., Synthetic Studies Toward the Skyllamycins: Total Synthesis and Generation of Simplified Analogues. *J Org Chem* **2018,** *83* (13), 7250-7270.

18. Uhlmann, S.; Sussmuth, R. D.; Cryle, M. J., Cytochrome p450sky interacts directly with the nonribosomal peptide synthetase to generate three amino acid precursors in skyllamycin biosynthesis. *ACS Chem Biol* **2013,** *8* (11), 2586-96.

19. Haslinger, K.; Brieke, C.; Uhlmann, S.; Sieverling, L.; Sussmuth, R. D.; Cryle, M. J., The structure of a transient complex of a nonribosomal peptide synthetase and a cytochrome P450 monooxygenase. *Angew Chem Int Ed Engl* **2014,** *53* (32), 8518-22.

20. Yu, J.; Song, J.; Chi, C.; Liu, T.; Geng, T.; Cai, Z.; Dong, W.; Shi, C.; Ma, X.; Zhang, Z.; Ma, X.; Xing, B.; Jin, H.; Zhang, L.; Dong, S.; Yang, D.; Ma, M., Functional Characterization and Crystal Structure of the Bifunctional Thioesterase Catalyzing Epimerization and Cyclization in Skyllamycin Biosynthesis. *ACS Catalysis* **2021,** *11* (18), 11733-11741.

21. Sweeney, P.; Murphy, C. D.; Caffrey, P., Exploiting the genome sequence of Streptomyces nodosus for enhanced antibiotic production. *Appl Microbiol Biotechnol* **2016,** *100* (3), 1285-1295.

22. Lee, N.; Kim, W.; Hwang, S.; Lee, Y.; Cho, S.; Palsson, B.; Cho, B. K., Thirty complete Streptomyces genome sequences for mining novel secondary metabolite biosynthetic gene clusters. *Sci Data* **2020,** *7* (1), 55.

23. Kabsch, W., Xds. *Acta Crystallogr D Biol Crystallogr* **2010,** *66* (Pt 2), 125-32.

24. Battye, T. G.; Kontogiannis, L.; Johnson, O.; Powell, H. R.; Leslie, A. G., iMOSFLM: a new graphical interface for diffraction-image processing with MOSFLM. *Acta Crystallogr D Biol Crystallogr* **2011,** *67* (Pt 4), 271-81.

25. Winn, M. D.; Ballard, C. C.; Cowtan, K. D.; Dodson, E. J.; Emsley, P.; Evans, P. R.; Keegan, R. M.; Krissinel, E. B.; Leslie, A. G.; McCoy, A.; McNicholas, S. J.; Murshudov, G. N.; Pannu, N. S.; Potterton, E. A.; Powell, H. R.; Read, R. J.; Vagin, A.; Wilson, K. S., Overview of the CCP4 suite and current developments. *Acta Crystallogr D Biol Crystallogr* **2011,** *67* (Pt 4), 235-42.

26. McCoy, A. J.; Grosse-Kunstleve, R. W.; Adams, P. D.; Winn, M. D.; Storoni, L. C.; Read, R. J., Phaser crystallographic software. *J Appl Crystallogr* **2007,** *40* (Pt 4), 658-674.

27. Adams, P. D.; Afonine, P. V.; Bunkoczi, G.; Chen, V. B.; Echols, N.; Headd, J. J.; Hung, L. W.; Jain, S.; Kapral, G. J.; Grosse Kunstleve, R. W.; McCoy, A. J.; Moriarty, N. W.; Oeffner, R. D.; Read, R. J.; Richardson, D. C.; Richardson, J. S.; Terwilliger, T. C.; Zwart, P. H., The Phenix software for automated determination of macromolecular structures. *Methods* **2011,** *55* (1), 94-106.

28. Allen, E. E.; Bartlett, D. H., FabF is required for piezoregulation of cis-vaccenic acid levels and piezophilic growth of the deep-Sea bacterium Photobacterium profundum strain SS9. *J Bacteriol* **2000,** *182* (5), 1264-71.

29. Fujishiro, T.; Shoji, O.; Nagano, S.; Sugimoto, H.; Shiro, Y.; Watanabe, Y., Crystal structure of H2O2-dependent cytochrome P450SPalpha with its bound fatty acid substrate: insight into the regioselective hydroxylation of fatty acids at the alpha position. *J Biol Chem* **2011,** *286* (34), 29941-50.

30. Han, S.; Pham, T.-V.; Kim, J.-H.; Lim, Y.-R.; Park, H.-G.; Jeong, D.; Yun, C.-H.; Chun, Y.-J.; Kang, L.-W.; Kim, D., Structural insights into the binding of lauric acid to CYP107L2 from Streptomyces avermitilis. *Biochemical and Biophysical Research Communications* **2017,** *482* (4), 902-908.

31. Kells, P. M.; Ouellet, H.; Santos-Aberturas, J.; Aparicio, J. F.; Podust, L. M., Structure of cytochrome P450 PimD suggests epoxidation of the polyene macrolide pimaricin occurs *via* a hydroperoxoferric intermediate. *Chem Biol* **2010,** *17* (8), 841-51.

32. Li, A.; Liu, J.; Pham, S. Q.; Li, Z., Engineered P450pyr monooxygenase for asymmetric epoxidation of alkenes with unique and high enantioselectivity. *Chemical Communications* **2013,** *49* (98), 11572-11574.

33. Zhao, P.; Chen, J.; Ma, N.; Chen, J.; Qin, X.; Liu, C.; Yao, F.; Yao, L.; Jin, L.; Cong, Z., Enabling highly (R)-enantioselective epoxidation of styrene by engineering unique non-natural P450 peroxygenases. *Chemical Science* **2021,** *12* (18), 6307-6314.

34. Zhang, C.; Liu, P. X.; Huang, L. Y.; Wei, S. P.; Wang, L.; Yang, S. Y.; Yu, X. Q.; Pu, L.; Wang, Q., Engineering P450 Peroxygenase to Catalyze Highly Enantioselective Epoxidation of cis-β-Methylstyrenes. *Chemistry–A European Journal* **2016,** *22* (31), 10969-10975.

# Chapter 4

# Unexpected Differences between Two Closely Related Bacterial P450 Camphor Monooxygenases

## SUMMARY

The bacterial cytochrome P450cam catalyzes the oxidation of D-camphor to 5-*exo*-hydroxycamphor as the first step in the oxidative assimilation of camphor as a carbon/energy source. CYP101D1 is another bacterial P450 that catalyzes the same reaction. A third P450 (P450tcu) has recently been discovered that has ≈86% sequence identity to P450cam as well as very similar enzymatic properties. P450tcu, however, exhibits three unusual features not found in P450cam. First, we observe product in at least two orientations in the X-ray structure that indicates that, unlike the case for P450cam, X-ray-generated reducing equivalents can drive substrate hydroxylation *in crystallo*. We postulate, on the basis of molecular dynamics simulations, that greater flexibility in P450tcu enables easier access of protons to the active site and, together with X-ray driven reduction, results in $O_2$ activation and substrate hydroxylation. Second, the characteristic low-spin to high-spin transition when camphor binds occur immediately with P450cam but is very slow in P450tcu. Third, isothermal titration calorimetry shows that in P450cam substrate binding is entropically driven with a $\Delta H$ of >0 while in P450tcu with a $\Delta H$ of <0 with a more modest change in $-T\Delta S$. These results indicate that despite nearly identical structures and enzymatic properties, these two P450s exhibit quite different properties most likely related to differences in conformational dynamics.

## INTRODUCTION

Cytochrome P450s are best known for catalyzing the oxidation of unactivated C–H bonds to give the corresponding alcohol.[1] The most well-studied P450 is CYP101A1 (P450cam) that catalyzes the oxidation of D-camphor to 5-*exo*-hydroxycamphor, the first step in the oxidative assimilation of camphor as an energy/carbon source in *Pseudomonas putida*. While serving as a paradigm for understanding the structural and mechanistic properties of P450s, P450cam exhibits certain mechanistic features that are not shared by many other P450s. The most important is the strict requirement for its own $Fe_2S_2$ ferredoxin redox partner, Pdx, in the second electron transfer.[2] Many P450s, but not P450cam, can utilize foreign redox partners as donors of the second electron. We now know that Pdx plays an "effector" role by binding to P450cam and switching the enzyme to a more open conformation[3-6] that establishes the proton relay network required for $O_2$ activation.[4] This level of specificity for a protein redox partner, however, is not shared by other camphor monooxygenases. For example, CYP101D1 catalyzes exactly the same reaction as P450cam with a similar rate and coupling efficiency, but unlike P450cam, it can utilize foreign redox partners.[7, 8]

Structural differences around the critical active site Asp residue required in the $O_2$ activation proton relay network help to explain this difference. In P450cam, the critical Asp (Asp251) is tied up *via* salt bridges to Lys178 and Arg186 residues (Figure 4.1). The binding of Pdx results in structural changes that break these salt bridges, thereby freeing Asp251 to serve its catalytic function. In CYP101D1, Lys178 is replaced with Gly180 and the critical Asp259 is ion paired with only Arg188. In addition, Asp259 in CYP101D1 occupies two conformations.[7] The one fewer salt bridge and multiple conformations indicate that Asp259 is not as rigidly held in place as P450cam

Asp251, and as a result, binding of a specific redox partner is not required for establishing the proton relay network in CYP101D1.

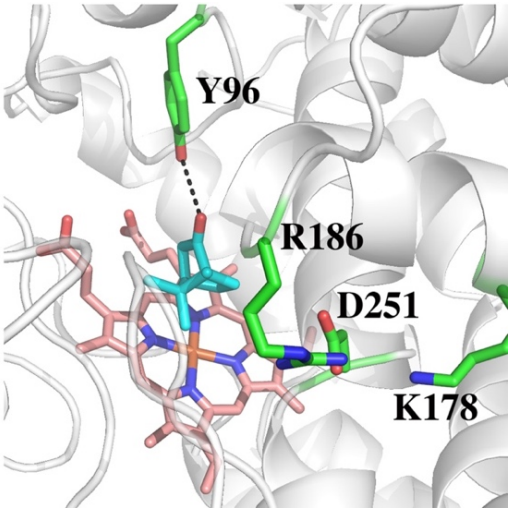


**Figure 4.1** Active site of P450cam highlighting the salt bridges among Asp251, Arg186, and Lys178. CYP101D1 is very similar except the homologue to Lys178 is a Gly.

Recently, a third camphor monooxygenase has been discovered in *Pseudomonas* sp. strain TCU-HL1, which utilizes borneol as an energy/carbon source.[9] The first step in the assimilation of borneol is its oxidation to camphor and, subsequently, to 5-*exo*-hydroxycamphor by a P450cam-like monooxygenase, which we termed "P450tcu". Tsang et al. showed that *Pseudomonas* sp. has the genes that encode a P450cam-like camphor oxidation system, including the camC gene (THL1_4171 UniProt gene sequence) that encodes a P450.[9] Amino acid sequence comparisons (Figure 4.2) show that P450cam shares ≈86% identity with P450tcu but only 45% with CYP101D1. Given that CYP101D1 and P450cam exhibit quite different properties, we undertook this comparative study to investigate enzymatic behaviors of P450cam and P450tcu to better understand structure–function relationships in camphor monooxygenases. Here we present structural, enzymatic, and biochemical characterizations of P450tcu.


**Figure 4.2** Sequence alignment of CYP101D1, P450tcu and P450cam.

## EXPERIMENTAL PROCEDURE

### *Protein Expression and Purification*

Gene sequences that encode P450tcu and Pdxtcu were obtained from the UniProt database. Synthetic genes encoding these two proteins were codon optimized for expression in *Escherichia coli* (GeneScript, Inc.). The P450tcu gene was subcloned into pET28a (NdeI and BamHI) with a

thrombin-cleavable N-terminal six-His tag. The Pdxtcu gene was subcloned into pET17b (NdeI and EcoRI). Both plasmids were transformed into *E. coli* BL21(DE3) cells separately.

For P450tcu, transformed cells were grown in 1 L of Luria-Bertani (LB) broth containing kanamycin at 37 °C. When the culture reached an $OD_{600}$ of 0.8–1.0, the temperature was decreased to 25 °C and the cells were induced with 1 mM isopropyl 1-thio-d-galactopyranoside. Sixteen hours after induction, cells were harvested by centrifugation and cell pellets were resuspended in lysis buffer containing 50 mM $KP_i$ (pH 7.4) and 100 mM sodium chloride. This was followed by sonication and centrifugation at 4 °C. The supernatant was loaded on a Ni-IMAC column. The column was washed with lysis buffer containing 40 mM imidazole. Elution buffer containing 50 mM $KP_i$ (pH 7.4), and 200 mM imidazole was used to elute the protein. The eluted protein was mixed with thrombin (20 units of thrombin/mg of P450tcu) to cleave the His tag and then dialyzed overnight against 50 mM $KP_i$ (pH 7.4) at 4 °C. After dialysis, ammonium sulfate was added to reach 32% saturation and the solution was centrifuged at 14,000 rpm for 1 h at 4 °C. The supernatant was loaded on a phenyl sepharose column, and protein was eluted with a 32% to 0% gradient of ammonium sulfate. The protein fractions were pooled, concentrated, and passed through a gel filtration Superdex 75 column equilibrated in 50 mM $KP_i$ (pH 7.4) to achieve better purity.

Cells transformed with the Pdxtcu plasmid were grown in 1 L of LB medium containing ampicillin at 37 °C. The temperature was decreased to 25 °C when the $OD_{600}$ reached 1. Cells were harvested after 40 h, and cell pellets were resuspended in lysis buffer containing 10 mM $KP_i$ (pH 7.4) and 1 mM DTT. After sonication and centrifugation at 4 °C, the supernatant was loaded on a Q-sepharose column and washed with lysis buffer. The protein was eluted using a linear gradient from 0 to 500 mM KCl in 50 mM $KP_i$ (pH 7.4) and 1 mM DTT. The protein fractions were pooled, concentrated,

and further purified on a Sephacryl S-200 HR column using 50 mM $KP_i$ and 1 mM DTT as the buffer. Putidaredoxin reductase (Pdr) was expressed and purified using a previously published protocol.[10]

***Enzyme Assays***

Camphor hydroxylation activity was determined by measuring NADH oxidation[11] at 25 °C by monitoring the change in absorbance at 340 nm with an extinction coefficient of 6.22 $mM^{-1}$ $cm^{-1}$. The initial mixture consisted of 0.5 μM P450tcu, 5 μM Pdxtcu, 0.5 μM Pdr, and 200 μM NADH in 50 mM $KP_i$ (pH 7.4). Reactions were initiated by the addition of 200 μM D-camphor. The NADH oxidation rate was determined as the difference in the rate before and after the addition of D-camphor.

The coupling efficiency in P450 reactions is the ratio of NADH oxidized to product formed. In a 100% coupled P450 system, one NADH molecule is oxidized per product molecule formed. To determine the coupling efficiency, the reaction was allowed to proceed such that a known amount of NADH was oxidized. After the completion of the reaction, 500 μM cineole was added as an internal standard, and the mixture was subjected to organic extraction using dichloromethane. This organic layer was then analyzed by GC-MS to estimate product formation.[12]

***Isothermal Titration Calorimetry (ITC)***

All experiments were performed on a MicroCal PEAQ-ITC instrument using a previously published protocol.[13] The concentration of substrate-free and substrate-bound P450tcu was measured using an $\varepsilon_{418}$ of 115 $mM^{-1}$ $cm^{-1}$ and an $\varepsilon_{392}$ of 100 $mM^{-1}$ $cm^{-1}$, respectively. The Pdxtcu concentration was measured at 455 nm using an extinction coefficient of 5.9 $mM^{-1}$ $cm^{-1}$.

***Oxy Complex Stability***

The stability of the oxy–P450tcu complex was determined at 23 °C by stopped flow spectroscopy using an Applied Photophysics SX.18MV instrument. The buffer used in these experiments contained 50 mM $KP_i$ (pH 7.4) and 1 mM D-camphor. P450tcu was degassed and purged with nitrogen, followed by reduction with a minimal amount of sodium dithionite. Reduced P450tcu was mixed in a 1:1 (v:v) ratio against oxygen-purged buffer in the absence and presence of a 2-fold excess of oxidized Pdxtcu to observe the formation and decay of the oxy complex. The concentrations of P450tcu and Pdxtcu before mixing were 9 μM and 18 μM, respectively.

***Crystallization***

The hanging drop vapor diffusion method was used to grow P450tcu crystals. The reservoir solution contained 50–100 mM Bis-Tris (pH 6.5), 100 mM $MgCl_2 \cdot 6H_2O$, and 15–20% (w/v) PEG 3350. Drops (2 μL) of 20 mg/mL P450tcu [in 50 mM $KP_i$ (pH 7.4) with 1 mM D-camphor] were mixed with 2 μL drops of the reservoir solution and equilibrated against 500 μL of the reservoir solution at room temperature. The crystals were flash-frozen using liquid nitrogen with Paratone®N (Hampton Research) as a cryoprotectant. Diffraction data were collected at the Stanford Synchrotron Radiation Lightsource beamline 12-2. MOSFLM[14] or XDS[15] was used to index and integrate the raw data, and Aimless[16] used for scaling. The structure was determined by molecular replacement with Phaser[17] and P450cam as a search model (PDB: 5CP4). Phenix was used to carry out further refinements.[18]

***Computational Methods***

Molecular dynamics (MD) simulations were carried out by Prof. Thomas L. Poulos. Experimental details can be found in the published paper.[19]

## RESULTS AND DISCUSSION

### *Substrate and Redox Partner Binding*

Camphor binding results in a low-spin to high-spin spectral change in both P450cam and P450tcu. However, the high-spin transition in P450cam occurs immediately upon camphor addition but is very slow with a half-life of 25 min (Figure 4.3) in P450tcu. This indicates that P450tcu undergoes a very slow structural change required to switch the heme from low- to high-spin. Association of camphor with P450cam was previously measured by isothermal titration calorimetry (ITC), which showed that this process is entropically driven ($\Delta H > 0$).[13] With P450tcu, camphor binding gave the opposite result, with a $\Delta H$ of <0 (Figure 4.4 and Table 4.1). Despite this difference, the $\Delta G$ values of binding derived from the obvious thermograms are similar (Table 4.1).

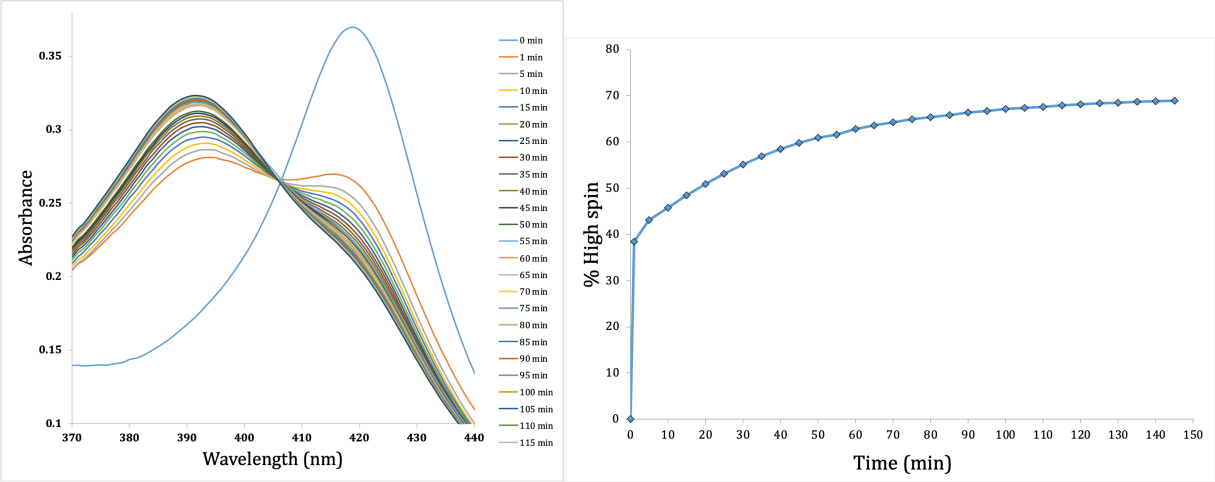


**Figures 4.3** Spectral data of time dependent spin shift.

**Table 4.1** Isothermal Titration Calorimetry of substrate binding to P450cam and P450tcu

| | **ΔH (kcal/mol)** | **-TΔS (kcal/mol)** | **ΔG (kcal/mol)** | **$K_D$ (μM)** |
|---|---|---|---|---|
| $^{13}$P450cam | 2.13± 0.09 | -10.2 | -8.09 | 1.2 ±0.4 |
| P450tcu | -2.77 ±0.04 | -5.63 | -8.40 | 0.702± 0.098 |

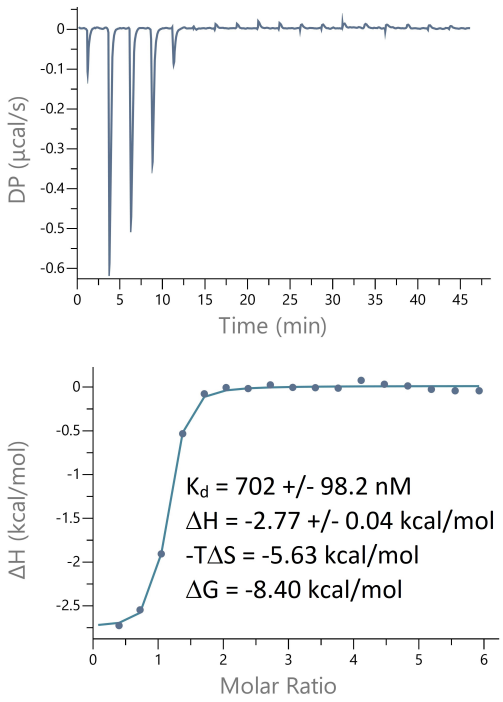


**Figure 4.4** Isothermal titration calorimetry of camphor binding to P450tcu.

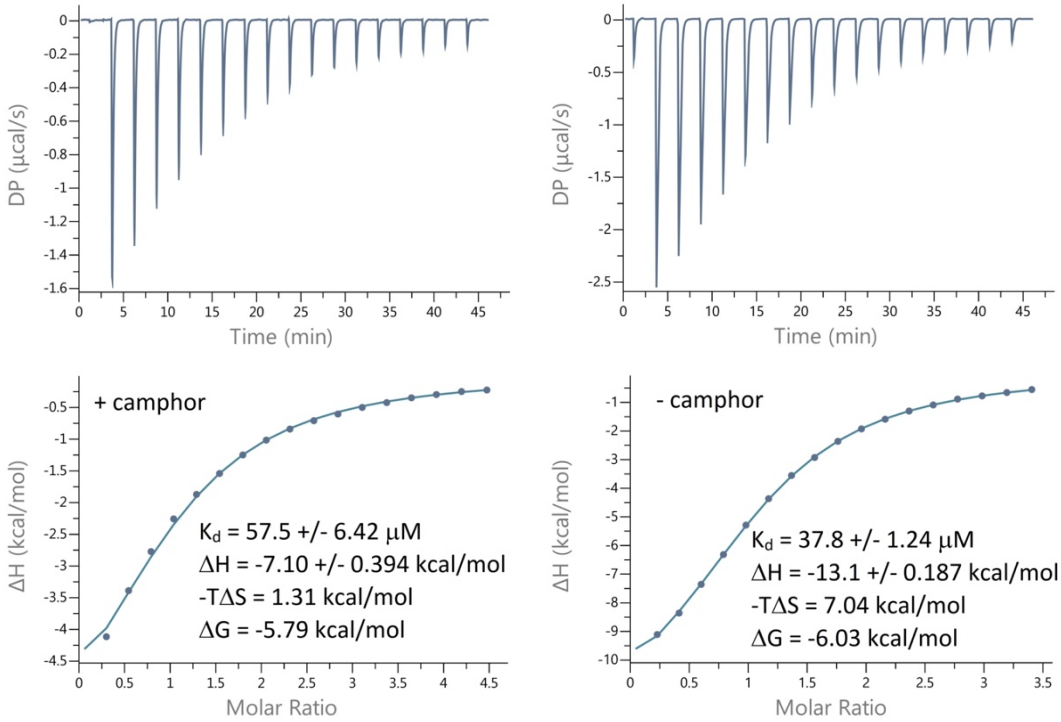


**Figure 4.5** ITC thermograms for Pdxtcu binding to P450tcu measured in the presence (left) and absence (right) of D-camphor. Similar to the P450cam–Pdx pair, Pdxtcu has a higher binding affinity for an open (or substrate-free) form of P450tcu.

ITC can also be used to investigate redox partner interactions. Previously, we demonstrated that Pdx binds more tightly to substrate-free P450cam,[20] which is consistent with the notion that Pdx shifts P450cam toward the more open low-spin state. As shown in Figure 4.5, Pdxtcu also binds more tightly to substrate-free P450tcu.

Another important feature is the destabilizing effect of Pdx on the ferrous P450cam–dioxygen (P450cam–oxy) complex. The P450cam–oxy complex is quite stable ($t_{1/2}$ = 25 min) at 4 °C, yet its stability decreases by ∼150-fold when oxidized Pdx is bound.[21] Pdxtcu has a similar effect and increases the decay of the P450tcu–oxy complex by ∼140-fold at 23 °C (Figure 4.6). Again, this finding suggests Pdxtcu shifts P450tcu to a more open state that, in the absence of electron transfer, exposes the oxy complex to bulk solvent and disrupts the local stabilizing H-bonding network. In summary, the effect of Pdxtcu on P450tcu closely parallels with what was observed with the P450cam–Pdx complex and suggests that oxidized Pdxtcu binds more tightly to substrate-free P450tcu and destabilizes the P450tcu–oxy complex.

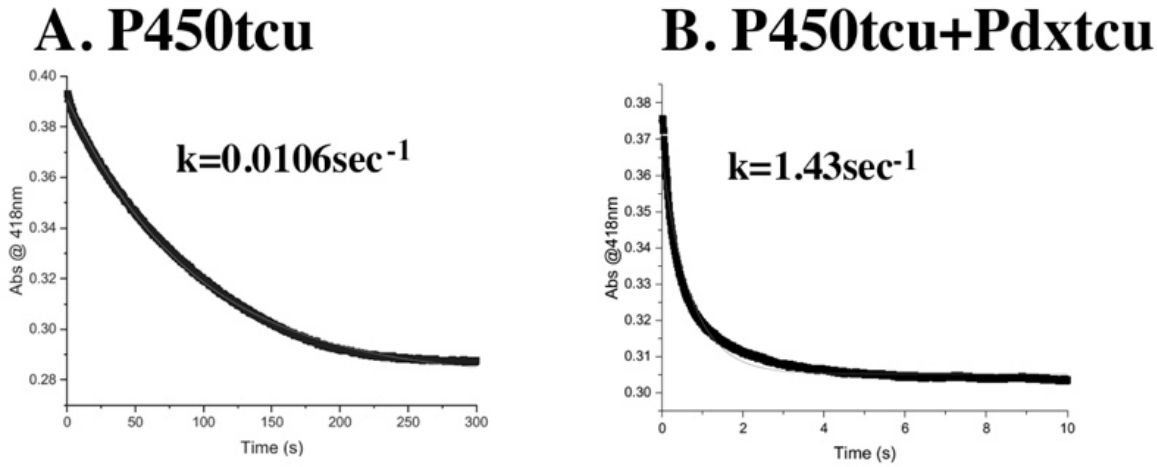


**Figure 4.6** Decomposition of the P450tcu–oxy complex in the presence and absence of 2 equivalents of Pdxtcu. Similar to the P450cam–Pdx redox pair,[21] the binding of oxidized Pdxtcu substantially increases the rate of decay of the P450tcu–oxy complex.

***Enzymatic Characterization***

In Table 4.2, we compare enzymatic activities of P450tcu and P450cam. The coupling efficiency is the ratio of NADH oxidized to product molecule formed. In a fully coupled P450 reaction, 100% of NADH-derived electrons are utilized for the substrate oxidation, with one NADH molecule required for one product molecule formed.

**Table 4.2** Enzymatic Characterization of P450tcu. $k_{cat}$ was determined by the rate of NADH oxidation. % coupling efficiency is the ratio of NADH oxidized to product formed. Pdx is the native redox partner for P450cam while Pdxtcu is the native redox partner for P450tcu. Arx is the redox partner for CYP101D1, and Pdx Δ106 is Pdx with the C-terminal Trp106 removed. Pdr is the native reductase of P450cam and was used for all the reactions.

| Enzyme | Redox partner | $k_{cat}$ ($min^{-1}$) | % Coupling efficiency |
|---|---|---|---|
| P450tcu | Pdx | 758±30 | ~93 |
| P450tcu | Pdxtcu | 624±13 | ~95 |
| P450cam | Pdx | 913±20 | ~95 |
| P450cam | Pdxtcu | 621±21 | ~95 |
| P450tcu | Arx | [1]ND | ND |
| P450tcu | Pdx Δ106 | ND | ND |

[1]ND=not detectable

As shown in Table 4.2, the P450tcu and P450cam monooxygenase systems have similar camphor oxidase activities (624 and 913 $min^{-1}$, respectively) and coupling efficiency (~95%). We also tested the ability of non-natural redox partners to support P450tcu catalysis. The CYP101D1 redox partner, Arx, cannot support P450cam or P450tcu catalysis. In contrast, the P450cam redox partner, putidaredoxin (Pdx), supports P450tcu and Pdxtcu, the ferredoxin from the P450tcu system, supports P450cam catalysis. Moreover, as shown previously for P450cam,[22, 23] removal of the C-terminal Trp106 eliminates P450tcu activity. As noted earlier, Pdx plays an essential effector role in P450cam by shifting P450cam to a more open state that triggers the formation of a proton relay network required for $O_2$ activation.[4] Trp106 provides important nonbonded contacts with P450cam that favor the more open conformation.[4] Given the similarity of P450tcu and P450cam

in redox partner selectivity, and the importance of Pdx Trp106 for functional activity, it is very likely that binding of Pdxtcu to P450tcu results in structural changes similar to those observed for P450cam redox partner binding.

**Table 4.3** Crystallographic Data Collection and Refinement Statistics

| **Parameter** | **P450tcu** |
|---|---|
| PDB entry | 6WPL |
| Space group | P $2_1$ $2_1$ $2_1$ |
| Unit cell | 35.42 56.993 189.373 90 90 90 |
| Resolution range (Å) | 34.82 – 2.097 (2.172 – 2.097) |
| Multiplicity | 2.0 (2.0) |
| Completeness (%) | 95.64 (82.55) |
| Number of unique reflections | 22980 (1878) |
| $R_{sym}$ *or* $R_{merge}$ | 0.0882 (0.6425) |
| $R_{pim}$ | 0.0882 (0.6425) |
| $I/\sigma(I)$ | 4.93 (2.42) |
| *B* factor (mean) (Å$^2$) | 24.81 |
| $R_{work}$ | 0.1934 (0.2424) |
| $R_{free}$ | 0.2468 (0.3128) |
| Root-mean-square deviation for bonds (Å) | 0.008 |
| Root-mean-square deviation for angles (deg) | 1.07 |
| Ramachandran favored (%) | 96.53 |
| Ramachandran allowed (%) | 2.72 |
| Ramachandran outliers (%) | 0.74 |

Values in the () are for the highest resolution shell.

***Crystal Structure of P450tcu***

Sequence comparisons among three camphor monooxygenases (P450cam, P450tcu, and CYP101D1) are shown in Figure 4.2. Given the 86% sequence identity between P450cam and P450tcu, it is not surprising that the 2.1 Å crystal structure of P450tcu (Table 4.3) is very similar to the P450cam structure with a root-mean-square deviation among the Cα atoms of ~0.36 Å. Figure 4.7 highlights the location of sequence differences. Differences are scattered throughout the molecule and located primarily on the surface of the protein with no differences in the active

site near the substrate (Figure 4.7). The closest difference to the active site is ≈11 Å from the camphor. There was, however, one striking difference. In camphor bound P450cam, the substrate is well-ordered, with no signs of product formation. In P450tcu, the bound ligand is partially disordered, and the fitting indicates that it is a product, hydroxycamphor, rather than the substrate, camphor. Moreover, as shown in Figure 4.8, the product can fit into the electron density in two different orientations. In the first one, the product hydroxyl group extends down toward the iron, which is very similar to what was observed when P450cam crystals were soaked with the product.[24] However, when modeled in this substrate-like orientation, the extra density clearly indicates at least one additional orientation. This undoubtedly means that hydrated electrons, generated by the synchrotron X-ray beam, can drive substrate hydroxylation in P450tcu but not in wild type P450cam.

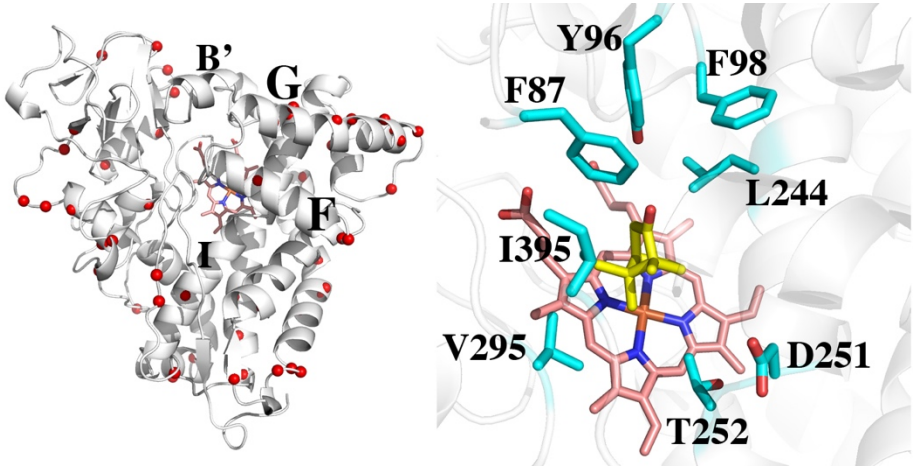


**Figure 4.7** Ribbon diagram of P450tcu with the location of sequence differences between P450tcu and P450cam highlighted as red spheres. A majority of the differences are located on or near the surface of the protein. The active site residues near the camphor are identical in both enzymes.

The product has been observed in WT P450cam in the P450–Pdx complex, where P450cam is locked in the open conformation,[4] and in a P450cam mutant where an ion pair to the essential Asp251 is disrupted.[13] Upon the Pdx-induced shift to a more open conformation, the Asp251-mediated salt bridges in P450cam are broken, thereby enabling solvent protons to protonate the

iron-linked $O_2$ molecule.[13] P450tcu has the same set of salt bridges, and there is no obvious structural basis for these salt bridges to be weaker than in P450cam (Figure 4.1). We therefore turned to MD simulations to probe possible dynamical difference between P450tcu and P450cam that are not evident in crystal structures.

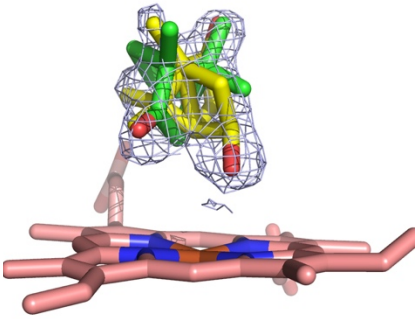

**Figure 4.8** $2F_o - F_c$ electron density map contoured at 1.0 σ. The density is consistent with a product molecule occupying two different orientations. The yellow molecule is in the productive binding mode.

***Molecular Dynamics***

Each P450 was subjected to ten 100 ns MD simulations using the same energy-minimized starting structures but different starting velocities. The overall relative flexibility can be assessed by examining temperature or *B* factors of Cα atoms. The only regions of substantial difference are located in surface loop regions. More revealing are the computed *B* factors of key regions of the active site. As shown in Table 4.4, camphor, Tyr96, and Asp251 all have much larger *B* factors in P450tcu than in P450cam. In addition, the H-bond between Tyr96 and the camphor carbonyl O atom is more stable in P450cam. In the ten 100 ns MD runs (a total of 50000 snapshots), the distance between the Tyr96 hydroxyl group and camphor carbonyl oxygen atom remains <3.0 Å 89% of the time, while in P450tcu, it is shorter than this distance only 62% of the time. Greater flexibility also is reflected in the crystallographic *B* factors. In P450tcu, the average side chain *B* factors for Tyr96 and Asp251 are 53% and 21%, respectively, higher than the

average *B* factor for all Cα atoms. In P450cam, the average *B* factor is within 2% of being the same as Cα atoms for Asp251 while for Tyr96 it is ~15% lower. This greater dynamic flexibility in P450tcu is consistent with easier access of protons to the active site, which results in $O_2$ activation and substrate hydroxylation in P450tcu but not in P450cam.

**Table 4.4** B factors (Å$^2$) computed from MD simulations.[a]

| | **camphor** | **Tyr96** | **Asp251** |
|---|---|---|---|
| **P450cam** | 55.5 | 22.2 | 10.5 |
| **P450tcu** | 73.9 | 61.9 | 19.4 |

[a]B factors were computed using 50,000 snapshots obtained from 10 100ns MD runs.

We also employed Mole2 (https://mol.upol.cz/), which computationally locates channels and pores in protein structures. As shown in Figure 4.9, P450cam and P450tcu display substantial differences in channels that connect the active site to the surface of the protein. Both contain the opening between helices F and G that provides the primary entry point for substrate into the active site and is the region that experiences the largest movement between the open and closed states. P450tcu, however, has more solvent accessible channels that can potentially provide additional access of solvent protons to the active site, which helps to explain why the product forms *in crystallo*.

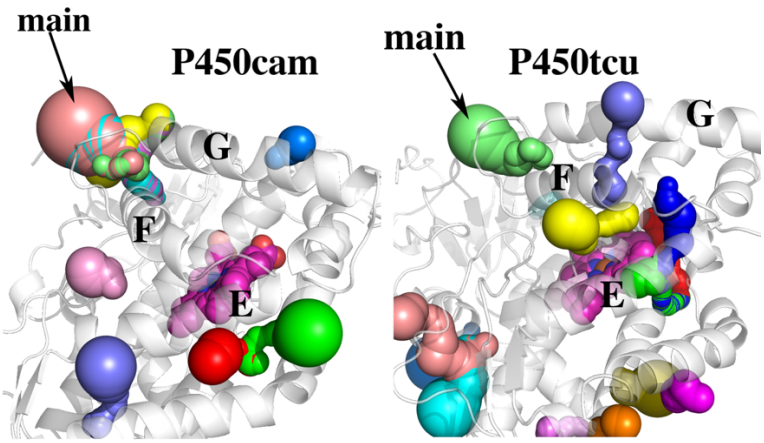


**Figure 4.9** Solvent access channels found by Mole2 in P450cam and P450tcu. The colored tubes represent channels that can be accessed by a solvent probe. Both contain the same main access channels between helices F and G. P450tcu, however, has more channels connecting the surface to the active site.

## CONCLUSION

Thus far, P450tcu is the closest homologue to the well-studied P450cam. With ≈86% sequence identity, it is not surprising that P450tcu and P450cam have very similar structures, enzymatic properties, and selectivity for redox partners. Even so, there are striking differences between these proteins. First, there is a large difference in the thermodynamics of camphor binding, which is entropically driven in P450cam with a $\Delta H$ of >0 and a $-T\Delta S$ of <0. In P450tcu, $\Delta H < 0$ and there is more of a balance between $\Delta H$ and $-T\Delta S$ and thus, camphor binding is favored both enthalpically and entropically.

Related to thermodynamic differences is the slow low- to high-spin conversion when P450tcu binds camphor. One possible model for explaining these differences is provided in Figure 4.10.

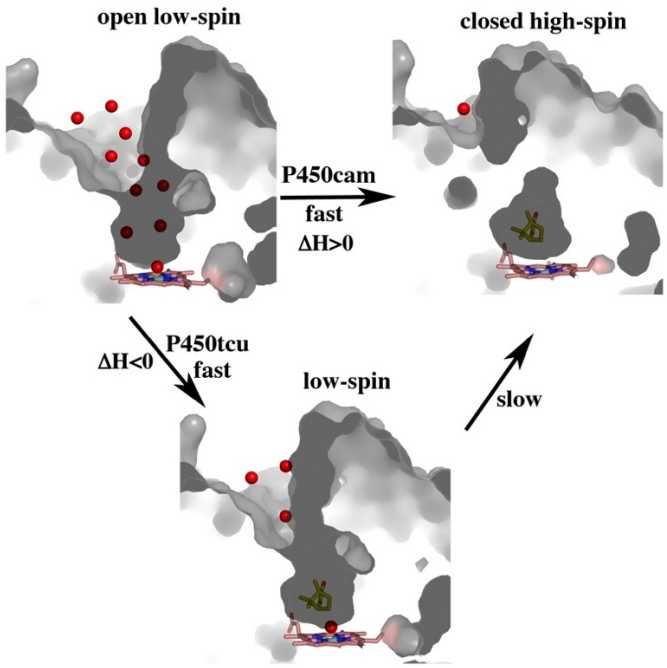


**Figure 4.10** Possible model for the binding of camphor to P450cam and P450tcu. The models are surface representations of the open, closed, and intermediate states with the camphor as yellow sticks and water molecules as red spheres, one of which is coordinated to the heme iron. In P450cam, camphor binds to the active site, resulting in a rapid low- to high-spin transition and desolvation of the active site. This is the process measured by ITC giving a $\Delta H$ of >0. In P450tcu, ITC measures an initial rapid binding to the open form possibly resulting in a partially closed state giving a mix of low- and high-spin states. This is followed by a slow transition to the closed high-spin state observed in the crystal structure.

With P450cam the binding of camphor, closing of the active site and dehydration of the active site to give the low- to high-spin transition occur simultaneously. With P450tcu, camphor binds to the active site in a rapid process that does not result in a complete low- to high-spin shift followed by a slower change resulting in a conversion to ≈70% high-spin. The possibility that camphor can bind in the active site but not fully displace the iron water ligand has been observed in the crystal structure of another camphor monooxygenase, CYP101D2.[25] Therefore, in P450cam, ITC measures binding to the active site together with the processes involved in full conversion to the high-spin state while with P450tcu ITC measures binding to the active site prior to the changes required for conversion to the high-spin state. This further suggests that with P450tcu ITC measures primarily the initial substrate–protein interactions ($\Delta H < 0$) together with at least partial desolvation of the substrate and active site ($-T\Delta S < 0$). With P450cam, ITC also includes protein structural changes involved in the low- to high-spin transition. This can help to improve our understanding of why with P450cam $\Delta H > 0$ because included in this $\Delta H$ is not only protein–substrate interactions but also displacement of the water ligand ($\Delta H > 0$) together with various protein changes associated with the open to closed transition. These findings, however, are at odds with the generally accepted view that P450cam activity is tightly associated with a full low- to high-spin transition. This clearly is not the case given that P450tcu is very efficient, yet the low- to high-spin change is slow on the time scale of catalysis. This simple picture of a fully high-spin P450 as a requirement for efficient catalysis is no longer adequate. We now know, however, that P450cam is far more dynamic than initially thought and samples stable conformational states that result in the formation of a new active site access channel, substantial restructuring of the active site, and *cis/trans* isomerization of prolines 89 and 105,[26-28] all of which are influenced by the redox partner. This provides a more complex view of the conformational dynamics under turnover

conditions where P450cam is associated with Pdx as opposed to the simple low-spin to high-spin transition of an isolated P450.

One final difference is that we observe product in the P450tcu active site because of X-ray-driven substrate hydroxylation. In contrast, no product has been observed in crystal structures of wild type ferric P450cam in the absence of its redox partner. This means that synchrotron-generated hydrated electrons promote substrate hydroxylation in ferric P450tcu but not in ferric P450cam. Previous studies have shown that the ability to form product in the X-ray beam is associated with a loosening of the active site access channel by weakening or disrupting the Asp251 ion pairs (Figure 4.1). Disruption of the salt bridges enables solvent protons to access the active site more readily, which, in turn, enables $O_2$ activation *in crystallo*.[7, 13] This implies that P450tcu might experience larger dynamic motions that enable proton access to the active site *in crystallo*. This view is supported by MD simulations, a comparison of crystallographic *B* factors, and the additional solvent channels found in P450tcu that together underscore dynamical differences between these two P450s. In summary, our results show that despite sharing ≈86% sequence identity and nearly identical crystal structures and enzymatic properties, P450tcu and P450cam exhibit substantial differences in physical properties most likely related to differences in conformational dynamics. These results also strengthen the view that P450s must retain a level of flexibility not only consistent with substrate binding and product egress but also to enable the operation of a proton relay network required for $O_2$ activation.

**REFERENCES**


1. Poulos, T. L., Heme enzyme structure and function. *Chem Rev* **2014,** *114* (7), 3919-62.

2. Lipscomb, J. D.; Sligar, S.; Namtvedt, M.; Gunsalus, I., Autooxidation and hydroxylation reactions of oxygenated cytochrome P-450cam. *Journal of Biological Chemistry* **1976,** *251* (4), 1116-1124.

3. Hiruma, Y.; Hass, M. A.; Kikui, Y.; Liu, W. M.; Olmez, B.; Skinner, S. P.; Blok, A.; Kloosterman, A.; Koteishi, H.; Lohr, F.; Schwalbe, H.; Nojiri, M.; Ubbink, M., The structure of the cytochrome p450cam-putidaredoxin complex determined by paramagnetic NMR spectroscopy and crystallography. *J Mol Biol* **2013,** *425* (22), 4353-65.

4. Tripathi, S.; Li, H.; Poulos, T. L., Structural basis for effector control and redox partner recognition in cytochrome P450. *Science* **2013,** *340* (6137), 1227-30.

5. Lee, Y. T.; Wilson, R. F.; Rupniewski, I.; Goodin, D. B., P450cam visits an open conformation in the absence of substrate. *Biochemistry* **2010,** *49* (16), 3412-9.

6. Liou, S. H.; Mahomed, M.; Lee, Y. T.; Goodin, D. B., Effector Roles of Putidaredoxin on Cytochrome P450cam Conformational States. *J Am Chem Soc* **2016,** *138* (32), 10163-72.

7. Batabyal, D.; Poulos, T. L., Crystal structures and functional characterization of wild-type CYP101D1 and its active site mutants. *Biochemistry* **2013,** *52* (49), 8898-906.

8. Yang, W.; Bell, S. G.; Wang, H.; Zhou, W.; Hoskins, N.; Dale, A.; Bartlam, M.; Wong, L. L.; Rao, Z., Molecular characterization of a class I P450 electron transfer system from Novosphingobium aromaticivorans DSM12444. *J Biol Chem* **2010,** *285* (35), 27372-27384.

9. Tsang, H. L.; Huang, J. L.; Lin, Y. H.; Huang, K. F.; Lu, P. L.; Lin, G. H.; Khine, A. A.; Hu, A.; Chen, H. P., Borneol Dehydrogenase from Pseudomonas sp. Strain TCU-HL1

Catalyzes the Oxidation of (+)-Borneol and Its Isomers to Camphor. *Appl Environ Microbiol* **2016,** *82* (21), 6378-6385.

10. Sevrioukova, I. F.; Li, H.; Poulos, T. L., Crystal structure of putidaredoxin reductase from Pseudomonas putida, the final structural component of the cytochrome P450cam monooxygenase. *J Mol Biol* **2004,** *336* (4), 889-902.

11. Sevrioukova, I. F.; Hazzard, J. T.; Tollin, G.; Poulos, T. L., Laser flash induced electron transfer in P450cam monooxygenase: putidaredoxin reductase-putidaredoxin interaction. *Biochemistry* **2001,** *40* (35), 10592-600.

12. Churbanova, I. Y.; Poulos, T. L.; Sevrioukova, I. F., Production and characterization of a functional putidaredoxin reductase-putidaredoxin covalent complex. *Biochemistry* **2010,** *49* (1), 58-67.

13. Batabyal, D.; Richards, L. S.; Poulos, T. L., Effect of Redox Partner Binding on Cytochrome P450 Conformational Dynamics. *J Am Chem Soc* **2017,** *139* (37), 13193-13199.

14. Battye, T. G.; Kontogiannis, L.; Johnson, O.; Powell, H. R.; Leslie, A. G., iMOSFLM: a new graphical interface for diffraction-image processing with MOSFLM. *Acta Crystallogr D Biol Crystallogr* **2011,** *67* (Pt 4), 271-81.

15. Kabsch, W., Xds. *Acta Crystallogr D Biol Crystallogr* **2010,** *66* (Pt 2), 125-32.

16. Winn, M. D.; Ballard, C. C.; Cowtan, K. D.; Dodson, E. J.; Emsley, P.; Evans, P. R.; Keegan, R. M.; Krissinel, E. B.; Leslie, A. G.; McCoy, A.; McNicholas, S. J.; Murshudov, G. N.; Pannu, N. S.; Potterton, E. A.; Powell, H. R.; Read, R. J.; Vagin, A.; Wilson, K. S., Overview of the CCP4 suite and current developments. *Acta Crystallogr D Biol Crystallogr* **2011,** *67* (Pt 4), 235-42.

17. McCoy, A. J.; Grosse-Kunstleve, R. W.; Adams, P. D.; Winn, M. D.; Storoni, L. C.; Read, R. J., Phaser crystallographic software. *J Appl Crystallogr* **2007,** *40* (Pt 4), 658-674.

18. Adams, P. D.; Afonine, P. V.; Bunkoczi, G.; Chen, V. B.; Echols, N.; Headd, J. J.; Hung, L. W.; Jain, S.; Kapral, G. J.; Grosse Kunstleve, R. W.; McCoy, A. J.; Moriarty, N. W.; Oeffner, R. D.; Read, R. J.; Richardson, D. C.; Richardson, J. S.; Terwilliger, T. C.; Zwart, P. H., The Phenix software for automated determination of macromolecular structures. *Methods* **2011,** *55* (1), 94-106.

19. Murarka, V. C.; Batabyal, D.; Amaya, J. A.; Sevrioukova, I. F.; Poulos, T. L., Unexpected Differences between Two Closely Related Bacterial P450 Camphor Monooxygenases. *Biochemistry* **2020,** *59* (29), 2743-2750.

20. Hollingsworth, S. A.; Batabyal, D.; Nguyen, B. D.; Poulos, T. L., Conformational selectivity in cytochrome P450 redox partner interactions. *Proc Natl Acad Sci U S A* **2016,** *113* (31), 8723-8.

21. Glascock, M. C.; Ballou, D. P.; Dawson, J. H., Direct observation of a novel perturbed oxyferrous catalytic intermediate during reduced putidaredoxin-initiated turnover of cytochrome P-450-CAM: probing the effector role of putidaredoxin in catalysis. *J Biol Chem* **2005,** *280* (51), 42134-41.

22. Sligar, S. G.; Debrunner, P. G.; Lipscomb, J. D.; Namtvedt, M. J.; Gunsalus, I. C., A role of the putidaredoxin COOH-terminus in P-450cam (cytochrome m) hydroxylations. *Proc Natl Acad Sci U S A* **1974,** *71* (10), 3906-10.

23. Kuznetsov, V. Y.; Poulos, T. L.; Sevrioukova, I. F., Putidaredoxin-to-cytochrome P450cam electron transfer: differences between the two reductive steps required for catalysis. *Biochemistry* **2006,** *45* (39), 11934-44.

24. Li, H.; Narasimhulu, S.; Havran, L. M.; Winkler, J. D.; Poulos, T. L., Crystal structure of cytochrome P450cam complexed with its catalytic product, 5-exo-hydroxycamphor. *Journal of the American Chemical Society* **1995,** *117* (23), 6297-6299.

25. Yang, W.; Bell, S. G.; Wang, H.; Zhou, W.; Bartlam, M.; Wong, L. L.; Rao, Z., The structure of CYP101D2 unveils a potential path for substrate entry into the active site. *Biochem J* **2011,** *433* (1), 85-93.

26. Follmer, A. H.; Mahomed, M.; Goodin, D. B.; Poulos, T. L., Substrate-Dependent Allosteric Regulation in Cytochrome P450cam (CYP101A1). *J Am Chem Soc* **2018,** *140* (47), 16222-16228.

27. Follmer, A. H.; Tripathi, S.; Poulos, T. L., Ligand and Redox Partner Binding Generates a New Conformational State in Cytochrome P450cam (CYP101A1). *J Am Chem Soc* **2019,** *141* (6), 2678-2683.

28. OuYang, B.; Pochapsky, S. S.; Dang, M.; Pochapsky, T. C., A functional proline switch in cytochrome P450cam. *Structure* **2008,** *16* (6), 916-23.

# FINAL CONCLUSIONS

Heme proteins are omnipresent in the biosphere and perform a diverse array of functions from oxygen storage and transport to drug detoxification. The protein architecture that harbors the protoporphyrin IX is able to fine tune the diversification of the reactions. To understand this structure-function relationship, we explored two heme enzymes – NOS and cytochrome P450s.

bNOS produced NO protects Gram-positive bacteria like MRSA and *Bacillus anthracis* from antibiotic and host-induced oxidative stress. Inhibiting bNOS will weaken the bacteria and make it susceptible to the antibiotics. The main hiccup in developing bNOS inhibitors is its structural homology with three mammalian isoforms. The mNOS generated NO acts as a signaling molecule and inhibiting mNOS can lead to serious side effects. Hence, our aim is to selectively target bNOS over mNOS to weaken the bad bugs. To achieve this, we collaborated with the Silverman lab at the Northwestern University to design and synthesize inhibitors and we screen these inhibitors using X-ray crystallography and biochemical assays.

Based on the past works of our collaboration on bNOS, a series of novel double-headed inhibitors were developed and screened. The idea is to target both the active and the pterin site at the same time to specifically target bNOS over mNOS. Crystal structures of bNOS bound to inhibitors prove the hypothesis of double heads binding to both active and pterin site. We also found that these inhibitors bind to eNOS as well as bNOS rendering them not selective. However, they show selectivity for nNOS over eNOS, suggesting that these inhibitors can be repurposed as nNOS inhibitors to treat neurodegenerative disorders. This emphasizes that the newer generation of inhibitors need to specifically target only the pterin site of bNOS. One possibility is to develop

double-headed inhibitors where each head binds to the pterin pocket of each monomer of bNOS homodimer and renders the enzyme inactive.

We then moved on to study a fascinating class of heme enzymes – cytochromes P450. P450s play an important role in xenobiotic detoxification and natural product biosynthesis. Natural products are an essential class of molecules that have a variety of biological activates, antibiotic being one of them. We structurally characterized two P450s, NysL and P450sky2, involved in late-stage oxidation in the biosynthesis of antibiotics, nystatin and skyllamycin, respectively. Understanding the structure-function relationship will help to shed light on the nuances required for regio- and stereo-selective oxidation. In closely related macrolide oxidizing P450s, NysL, AmphL and PimD, the back wall of the active site where the hemiketal and the mycosamine ring binds controls the substrate burial in the active site and hence the oxidation pattern. This will further the knowledge required to engineer biocatalysts to develop newer generations of antibiotics and other chemical products. P450sky2 is the first structure of a P450 involved in epoxidation of a substituted cinnamoyl chain. The wide-open active site of P450sky2 can easily fit in large molecules such as skyllamycin A. Based on this, P450sky2 can be engineered to epoxidate bulky molecules with cinnamoyl side chain or act on substituted styrenes to form chiral epoxides which is useful for development of beneficial pharmaceuticals.

The last chapter focuses on a detailed characterization of a camphor monooxygenase, P450tcu. A comparison was drawn with a closely related, extensively studied of another camphor monooxygenase, P450cam. They share about 86% sequence identity and still exhibit quite different properties due to differences in conformational dynamics. This reinstates the fact that P450s are more flexible/dynamic compared to simple transition from low-spin to high-spin states.